View metadata, citation and similar papers at core.ac.uk
brought to you by CORE
provided by ScholarBank@NUS

DESIGN AND PERFORMANCE ANALYSIS OF EFFICIENT WIRELESS SYSTEMS

WANG PEIJIE

NATIONAL UNIVERSITY OF SINGAPORE

2011

DESIGN AND PERFORMANCE ANALYSIS OF EFFICIENT WIRELESS SYSTEMS

WANG PEIJIE

(*M.Sc., National University of Singapore*)

A THESIS SUBMITTED

FOR THE DEGREE OF DOCTOR OF PHILOSOPHY

DEPARTMENT OF ELECTRICAL AND COMPUTER ENGINEERING

NATIONAL UNIVERSITY OF SINGAPORE

2011

Dedications:

To my family

Acknowledgment

It is my great pleasure to take this opportunity to express my sincere thanks to everyone who has supported me during my PhD study.

First and foremost, my utmost gratitude and appreciation go to my supervisor, Professor Kam Pooi-Yuen for his encouragement, guidance and support in all aspects of my research working. I am deeply stimulated by his enthusiasm and expertise on scientific research. It has been a great honor for me to work under his supervision throughout the past four years. Those precious working experiences with him and knowledge he has taught me, are the priceless treasures enriching my life.

My sincere thanks also go to my colleagues in the ECE-I2R Wireless Communications Lab for their warm friendship. I would like to give my special and grateful thanks to Wu Mingwei and Cao Le for their stimulating discussions in research. Many thanks go to Zhu Yonglan, Lin Xuzheng, Yuan Haifeng, Zhang Jianwen, Kang Xin, Chen Qian, He Jun, Jiang Jinhua and Siow Hong Lin, Eric.

I am grateful to Ghasem Naddaf, Dong Xiangxu, Han Mingding, Eu Zhi Ang and Prof. Tham Chen-Khong, for producing works together.

I also would like to thank my friends, Li Lin, Peng Yafeng, Zhang Hao and Li Ti, who have made my life enjoyable and always full of interesting things.

I am forever indebted to my parents for their endless love and support. Last but not least, I owe my deepest gratitude to my girlfriend Liang Xi. Her love and support lead me to where I am today.

Finally, the support of Singapore MoE AcRF Tier 2 Grant T206B2101 in the form of a research scholarship is gratefully

acknowledged.

Contents

Summary

Driven by the rapidly increasing demand on mobile wireless communication systems, many promising technologies for fast and reliable transmissions over wireless channels have been developed in the past decades. A key issue that most of these works have addressed is to mitigate signal fading. The fading is caused by the inherent, time-varying attribute of a wireless medium, and has a detrimental effect on the reliability of received wireless signals. To combat fading, one effective approach is known as transmitter power control with channel state information (CSI) feedback. We use the bit error outage probability (BEOP) as a new performance measure to design an actual feedback power control system for specific modulation formats, and develop the BEOP-based power control law at the transmitter. Compared with the traditional design, which is based on the average bit error probability (ABEP), the new BEOP-based law provides much more reliable instantaneous quality of service by sacrificing only a little in the ABEP performance. Our design also addresses the effect of imperfect CSI, which has not been considered in previous works.

Another efficient approach that has been widely used nowadays to achieve reliable transmissions is space diversity. By exploiting the broadcast nature of a wireless medium and allowing terminals to cooperatively transmit information through relaying, cooperative relay systems allow single-antenna users to gain benefits from space diversity through relay cooperation. We consider receiver design for a decode-and-forward (DF) relay system with one source, one destination and L multiple relays. Our key contribution is to derive the maximal likelihood (ML)

receiver at the destination with imperfect CSI at all receiving nodes. The derived ML receiver applies to an arbitrary M-ary quadrature amplitude modulation. It is important to note that our receiver result shows that for optimum detection at the destination, the instantaneous information of the source-relay link is required, and this information is summarized as the decoding error probability at the relay. For simplicity, we analyze the ML receiver with binary phase shift keying, and provide several suboptimum receivers. In performance analysis, we arrive at some closed-form results for the ABEP performance of the destination receivers for both a single relay system and a multiple relay system. We prove that for a DF relay system, the destination receiver using the instantaneous decoding error probabilities at the relays achieves full diversity.

The effect of imperfect CSI is a main issue addressed in our research. In practice, the availability of CSI to a wireless system has a crucial effect on the system performance. Therefore, we also devote some effort to CSI acquisition using the least-mean-square (LMS) adaptive filter. We propose a control parameter-free step-size adjustment algorithm for the tap-weight coefficients adaptation of an LMS adaptive filter. When applied to channel estimation, simulation results show the performance advantage of the new algorithm over the existing step-size adjustment algorithms under different wireless channel environments.

List of Tables

List of Figures

Abbreviations

ABEP	Average Bit Error Probability
AF	Amplify-and-Forward
ARQ	Automatic Repeat Request
ASSA	Automatic Step-Size Adjustment
AWGN	Additive White Gaussian Noise
A-ML	Averaged Maximum Likelihood
A-PL	Averaged Piecewise Linear
BEF	Bandwidth Expansion Factor
BEOP	Bit Error Outage Probability
BEOPR	Bit Error Outage Probability at the Receiver
BEOPT	Bit Error Outage Probability at the Transmitter
BEP	Bit Error Probability
BFSK	Binary Frequency Shift Keying
BPSK	Binary Phase Shift Keying
CDF	Cumulative Distribution Function
CRC	Cyclic Redundancy Check
CSI	Channel State Information
CSIR	Channel State Information at the Receiver
CSIT	Channel State Information at the Transmitter
CWSD	Clipped Weighed Slope-Detector
C-MRC	Cooperative Maximum Ratio Combining
DBPSK	Differential Binary Phase Shift Keying

DF	Decode-and-Forward
FSS	Fixed Step-Size
IBEP	Instantaneous Bit Error Probability
ISEP	Instantaneous Symbol Error Probability
i.i.d.	independent and identically distributed
i.n.d.	independent and non-identically distributed
LMS	Least-Mean-Square
MAP	Maximum A Posteriori
MGF	Moment Generating Function
MIMO	Multiple-Input/Multiple-Output
MISO	Multiple-Input/Single-Output
ML	Maximum Likelihood
MMSE	Minimum Mean-Square Error
MRC	Maximum Ratio Combining
MSE	Mean-Square Error
NLMS	Normalized Least-Mean-Square
PDF	Probability Density Function
PL	Piecewise Linear
PSAM	Pilot Symbol Assisted Modulation
QAM	Quadrature Amplitude Modulation
QoS	Quality of Service
QPSK	Quadrature Phase Shift Keying
SIMO	Single-Input/Multiple-Output
SISO	Single-Input/Single-Output
SNR	Signal-to-Noise Ratio
SR	Selection Relaying
ST	Space-Time
WSD	Weighed Slope-Detector

Notations

In this thesis, scalar variables are written as plain lower-case letters, vectors as bold-face lower-case letters, and matrices as bold-face upper-case letters. Some further used notations and commonly used acronyms are listed in the following:

a	plain lower-case to denote scalars
$\mathbf{a}$	boldface lower-case to denote column vectors
$\mathbf{A}$	boldface upper-case to denote matrices
$\mathbf{I}_N$	the $N \times N$ identity matrix
$(\cdot)^T$	the transpose operation
$(\cdot)^*$	the conjugate operation
$(\cdot)^H$	the conjugate transpose operation
$(\cdot)^{-1}$	the inversion operation
$\mathbb{E}[\cdot]$	the statistical expectation operation
$\Re(\cdot)$	the real part of the argument
$\mathrm{erfc}(\cdot)$	the complementary error function
$\exp(\cdot)$	the exponential function
$\ln(\cdot)$	the natural logrithm
$\mathrm{sgn}(\cdot)$	the signum function
$u(\cdot)$	the unit step function
$\dot{\delta}(\cdot)$	the Dirac delta function
$\Gamma(\cdot,\cdot)$	the upper incomplete gamma function
$W(\cdot)$	the *Lambert W function*

$J_m(\cdot)$	the m-th order Bessel function of the first kind
$I_m(\cdot)$	the m-th order modified Bessel function of the first kind
$Q(\cdot,\cdot)$	the first-order Marcum Q-function

Chapter 1

Introduction

In wireless communications, information is transmitted over time-varying channels, which causes severe fluctuations of the amplitude of the received signal. The fluctuation, known as fading [1], significantly degrades the reliability of transmission links, and has become the key challenge for enhancing system performance. Fostered by the dramatically increasing demand for mobile wireless communication systems, a great deal of work has gone into the development of efficient technologies for transmission over fading channels.

One approach to perform reliable communications over fading channels is achieved by a class of channel-adaptive methods. These schemes exploit the current state of the channel at the transmitter side to optimize the transmitted signal by systematically modifying some transmitter parameters, e.g., power, rate, modulation type. The current state of the channel, commonly referred to as the instantaneous channel state information (CSI), is acquired at the transmitter through feedback. A system employing feedback always uses a low data rate stream on the reverse side of the forward link to offer reliable transmission to the transmitter. By employing channel-adaptive signaling, it yields large improvements in almost any performance metric. From the information theoretic point of view, it has been shown that with perfect CSI at the transmitter, the capacity of the fading channels is significantly improved [2–4]. More practical works have taken into consideration of the imperfect

CSI, which is generally known as limited feedback [5]. From a design point of view, the design of channel-adaptive communication systems is always formulated as an optimization problem, where the purpose is to optimize some performance metric, subject to some systematic constraints. In particular, a power-adaptive transmission system for fading channels is designed to adapt the transmitted power to match the current state of the channel. Most of the works on the design or analysis of power-adaptive transmission systems are information theoretic works, where performance limits in terms of capacity and information outage are under consideration. On the design of practical systems, the works are quite limited. Hayes [6] first solved the optimal power control problem for a binary system over a Rayleigh fading multipath channel with the assumption of a noiseless and delayless feedback channel. It shows that the average bit error probability (ABEP) of the system is significantly reduced compared with a non-feedback system for the same average power. A few more works toward the design of practical systems, can be found in [7–10]. All these works design the power law based on the ABEP as a performance measure, and they show that power-adaptive systems offer a significant gain over the constant-power systems in reducing the ABEP. While the effect of imperfect CSI at the transmitter (CSIT) has been widely considered in information theoretic research, it remains unaddressed in the design of a practical feedback system.

Another key idea that has been widely used to achieve reliable transmissions is space diversity. It is realized by means of multiple-antenna transmissions or multi-node cooperative communications. Operating on the space domain, space diversity techniques are widely recognized as an effective means in combating signal fading in wireless communications. The philosophy is that by exploiting the low probability of concurrence of deep fades in all the diversity channels, the reliability of the end-to-end transmission is enhanced. This kind of diversity is of particular interest as it can be readily combined with time or frequency diversity. Due to size and cost limitations, multiple antennas may not be supportable on many

wireless terminals. To relax such a restriction, cooperative relay communication systems are introduced to allow single-antenna users to gain benefits from space diversity. By exploiting the broadcast nature of the wireless medium and allowing terminals to cooperatively transmit information through relaying, cooperative relay communication systems achieve space diversity through relay cooperation. Various relaying protocols have been proposed to gain the benefit from relay cooperation, e.g. amplify-and-forward (AF), decode-and-forward (DF), selection relaying (SR) [11]. As the SR protocol can employ either AF or DF relays, to distinguish the terms, when talking about the AF or the DF protocol solely, it refers to relaying without selection. Among those protocols, the DF protocol is recognized as the most practical relaying strategy. In comparison, the AF relaying protocol requires additional, expensive analog processing at the relays, and the SR protocol is usually accompanied by interaction from a high layer. It has been shown that relay transmission incorporating error control codes can significantly improve the overall performance. However, in analysis, to isolate the diversity gain achieved through relaying from the coding gain, an uncoded data stream is always used.

In evaluating the performance of digital communication systems, the ABEP is commonly used as the performance measure. In wireless communications, the transmitted signal is perturbed by an unknown, time-varying, multiplicative, complex fading gain. This fading gain causes severe fluctuations of the received signal power, and tremendously distorts the reliability of transmissions. As is known, the ABEP is obtained by averaging the instantaneous bit error probability (IBEP) over the distribution of the fading gain [12]. Therefore, the ABEP as a performance measure does not reflect the instantaneous quality of service (QoS) experienced by the user. For high-data rate transmission, a short duration of deep fade may go across a large number of data bits and cause erroneous receptions of them. In such a case, the ABEP as a performance measure becomes meaningless. As has been pointed out in [13], the bit error outage probability (BEOP) is a more useful performance measure for high-data rate transmission over time-varying fading

channels. It is defined as the probability of the IBEP exceeding a QoS-specified IBEP threshold. It monitors the instantaneous QoS experienced by the user. The BEOP reflects, in the long term, the fraction of received bits that have IBEP exceeding the IBEP threshold. As a new dimension in performance evaluation of wireless communication systems, many existing technologies can be reconsidered from the viewpoint of the BEOP. For example, [14] examines the performance of the packet automatic-repeat-request (ARQ) scheme with packet-error-outage-probability QoS measure. The packet error outage probability is defined in a similar way to the BEOP.

In our work, we use the BEOP as a new performance measure to design a feedback power control system, and we have arrived at some good results. Comparing to the existing designs using the ABEP as the performance measure, the BEOP-based feedback power control provides a much more reliable instantaneous QoS by sacrificing only a little in the ABEP performance. For cooperative relay communication systems, the examination of the BEOP is more complicated, as it covers the joint of the instantaneous QoS of all source-relay and relay-destination links. Due to lack of time, we put it as a future work. Here, we are more concerned about some unsolved fundamental problems regarding to DF relay systems. We will introduce these problems in detail in the next section. Another main issue we have addressed in our research is the effect of imperfect CSI to wireless communications. The most widely-used assumption of perfect CSI, provides a benchmark for system design and performance analysis. However, as many works have shown, the degree of available CSI significantly affects the performance of wireless communication systems. Thus, the imperfect CSI is a serious issue that needs to be considered in the design and performance analysis of actual communication systems. Noting the importance of the CSI, we also devote some effort to CSI acquisition. The CSI is commonly obtained by pilot-symbol-assisted channel estimation [15], where the channel model and its parameters are required for a minimum mean-square error (MMSE) estimation of the CSI. However, in many practical cases, the wireless

channel model is unknown, or even if the model is given, its parameters may not be known. For that reason, We propose an effective adaptive algorithm for CSI acquisition.

1.1 Motivation of the Work

1.1.1 Feedback Power Control

By adapting the transmitter power to match the current state of the channel, power control is a promising technology in mitigating the signal fading in wireless communications. Most of the works on power control study the performance limits of communication systems in terms of ergodic capacity or information outage probability [2–4]. The performance limits of systems having limited CSI and/or delay and noise on the feedback channel have been well investigated, e.g. [16–19]. Besides these information theoretic researches, it is of great importance to design practically realizable feedback power control systems for specific modulation formats and examine their end-to-end performance. Unfortunately, research in this area is quite limited, and has been put away for a long time in the literature. In [6], Hayes first solved the optimal power control problem for a binary system over a Rayleigh fading multipath channel with a noiseless and delayless feedback channel. With perfect CSI, the power law is set such that the ABEP at the receiver is minimized subject to a constraint on the average transmitted power. The optimum transmit power is implicitly given as a function of the CSI. It shows that the ABEP is significantly reduced compared with a non-feedback system for the same average power. A few more works can be found in [7–10].

All these limited existing works on the design of actual feedback power control systems use the ABEP as the performance measure. For transmission over fading channels, the ABEP is obtained by averaging the IBEP over the distribution of the fading, and therefore it cannot reflect the instantaneous depth of fade experienced by the user. For high data-rate transmission, a short duration of deep fade may

cause thousands of erroneous received data bits. In such a case, the ABEP as a performance measure becomes meaningless. As has been pointed out in [13], to reflect the instantaneous QoS, the BEOP is a more useful measure. The bit error outage (BEO) event is defined as the event that the IBEP exceeds an IBEP threshold. The BEOP reflects, in the long term, the fraction of the received bits that have IBEP exceeding the IBEP threshold. From the viewpoint of QoS assurance, it is meaningful to set an upper limit on the BEOP to ensure that in the long term, less than a certain fraction of received bits would have IBEP exceeding the IBEP threshold.

Motivated by the importance of BEOP and its advantage over the ABEP as a QoS measure, we propose a BEOP-based power control law for single-input/single-output (SISO) transmission. It can be straightforwardly extended to the single-input/multiple-output (SIMO) case. The extension to the multiple-input/single-output (MISO) case or the multiple-input/multiple-output (MIMO) case is more involved. For a start, we only consider the SISO case for simplicity. We use a Rayleigh channel model as the probability density function (PDF) of its channel fading gain provides good tractability for performance analysis. Basically, the BEOP-based power control law adjusts the transmitted power according to the variations of the channel such that the BEOP at the receiver is always kept within some threshold. This threshold is a system-designed value depending on what level of QoS is required. By applying the BEOP-based law, the instantaneous QoS can be guaranteed.

Another motivation for our work is the issue of imperfect CSI for an actual system. Although the effect of imperfect CSI has been widely considered in information theoretic research of feedback systems, it remains unaddressed in the design of actual feedback systems. In a practical feedback power contol system, since the transmitted power is adjusted according to the CSI obtained, it is expected that the imperfect CSI has a considerable effect on the performance. In those existing works, it is commonly assumed that the perfect CSI is obtained at the receiver, and

is then fed back to the transmitter through a noiseless and delayless feedback channel to provide the CSIT. More intuitively, this implies that before each bit is sent out, the transmitter has already perfectly known the channel that the bit is going to pass through. It is clear that this genie-aided channel model does not apply to practical transmissions. Nevertheless, the assumption of perfect CSI enables us to access the elegance of feedback power control systems. For a more practical consideration, the design of feedback power control systems should incorporate imperfect CSI at both the receiver side and the transmitter side. Our practical system model offers a general framework to study the issue of imperfect CSI for an actual feedback system.

1.1.2 Receiver Design and Performance Analysis of DF Relay Communication Systems

Transmitting signals through multiple relays is a way to obtain the space diversity and is effective in mitigating the signal fading. Generally, a relay employs one of the two relaying protocols, namely, AF and DF [11]. Comparing to the AF protocol which requires additional, expensive analog processing at the relay, the DF protocol can be directly employed by most of the current wireless networks without redeploying the existing wireless terminals. As an extension, the SR protocol [11] selects those relays that meet certain requirements to forward the source information to the destination via either AF or DF. The relay selection is usually accompanied by interaction from a high layer. We note that many of the current works on the SR protocol have drawn the conclusion that the DF protocol (without relay selection) does not achieve full diversity, while the SR protocol does. This is a misleading claim as we will show later. The cause for this misleading claim is that all the existing works attempting to analyze the maximum likelihood (ML) detector for a DF relay system, fall into the analysis of a suboptimum detector which utilizes the statistical information of the source-relay link for detection at the destination. In fact, the optimum (ML) detector at the destination for a DF relay system utilizes the instantaneous instead of the statistical information of the

source-relay link. In [20], this point has been shown for a DF single relay system with coherent binary transmission. The instantaneous information of interest is simply summarized as the IBEP at the relay. Unfortunately, the importance of using the IBEP at the relay is not emphasized in [20].

As is known, the complexity of analyzing the ML detector for a DF relay system increases exponentially as the number of relays increases. To avoid to study the complex optimum (ML) detector, some works have proposed suboptimum detectors [21–24] to approximate the ML detector. To the best of our knowledge, for a coherent DF relay system, the ML detector has only been derived in [20] for a single relay case with binary phase shift keying (BPSK) modulation. The ML detector for a multiple relay system with general M-ary quadrature amplitude modulation (M-QAM) remains unsolved.

Driven by the need of the ML detector in the most general form, from which we can fairly assess the performance of the DF relaying protocol (without relay selection), we study the fundamental issue of ML receiver design, and derive the ML detector for a multiple relay system with general M-QAM. From our receiver result, we point out and emphasize the importance of retaining the instantaneous information of the source-relay link for the detection at the destination. This point has been overlooked in many works on DF relay systems.

Moreover, we note that all the existing receiver designs for DF relay systems assume perfect CSI at the relay and at the destination. As has been mentioned, the effect of imperfect CSI is an important issue that should be covered in the design of actual systems. This motivates us to consider the receiver design based on a practical system model with channel estimation.

Although it has been shown that relay transmission incorporating error control codes can significantly improve the overall performance, to isolate the diversity gain achieved through relaying from the coding gain, our design and analysis use uncoded data streams. Next, we consider the performance analysis of the ML detector for a general DF relay system.

As has been mentioned above, in the attempt to analyze the ML detector, all the previous works actually analyzed a suboptimum detector which uses the statistical information of the source-relay link for detection at the destination. The use of this statistical information, of course, simplifies the performance analysis of the ABEP. However, it is noted that the penalty of using the statistical information is a loss in the achievable diversity order, which is quite undesirable for the design of a multiple relay communication system. Moreover, so far, the exact performance analysis for a DF relay system with the ML detector, is limited to a single relay or a two-relay case. Reference [23] has noted the importance of using the instantaneous information of the source-relay link for detection at the destination, and it considers a multiple relay system. However, in [23], the bit error probability (BEP) is only analyzed from the diversity point of view, where extremely high signal-to-noise ratio (SNR) is assumed. Motivated by these facts, we analyze the performance of a multiple relay system with the ML detector at the destination which utilizes the instantaneous information of the source-relay link, and we provide exact, closed-form results. We confine ourselves to the analysis with BPSK, as the ML detector for higher order modulations is fairly complex. The consideration of imperfect CSI builds our work on a more practical basis. Our analysis covers a single relay system, as well as a multiple relay system with an arbitrary number of relays.

1.1.3 Fast Adaptive Algorithm for CSI Acquisition

As has been noted in our works on the feedback power control and the DF relay systems, the CSI is a critical information that determines the system performance. In fact, in coherent detection for transmission over fading channels, an accurate acquisition of the instantaneous CSI is a crucial requirement. Therefore, we devote some effort to CSI acquisition. In many works involving theoretical analysis of transmissions over fading channels, the perfect CSI is a common assumption. It greatly simplifies the analysis and helps develop an insightful view of those promising techniques. However, in practice, the perfect CSI is of course, unknown to the

receiver. Therefore, channel estimation must be carried out to provide a degraded version of the perfect CSI, i.e., the imperfect CSI.

One of the most popular CSI-acquisition model used for analytical purpose utilizes a Wiener filter for weighting the received pilot information to form the MMSE estimate of the true CSI. The implementation of a Wiener filter with optimum filter tap-weight coefficients requires the statistics of the fading environment. However, in wireless communication systems, especially when the communication terminals are mobile, the statistics of the environment may change from time to time. In addition, the communication terminals are sometimes required to work in a completely unknown environment. Under such cases, the exact statistical information of the environment is not available. Therefore, filters employing weight-adaptive algorithms have to be used to approximate the performance of the Wiener filter in an iterative manner.

Among those weight-adaptive algorithms, the least-mean-square (LMS) algorithm is one of the most popular and has been widely used for its robustness and simplicity. For LMS adaptive filters, the convergence behavior of the weights is controlled by a step-size parameter. As is well-known, for LMS adaptive filters, a variable step-size is superior to a fixed step-size (FSS) as the former can respond to a changing environment and more importantly, it can provide a fast rate of convergence at the beginning of the adaptation process, and arrive at a small steady-state mean-square error (MSE) when the adaptive algorithm converges. A common feature of the existing variable step-size algorithms for the weights adaptation of LMS adaptive filters is that preset control parameters are required to enhance their performance, and those parameters are always chosen from extensive simulations or from experience, which is undesirable for practical use.

Parameter-free step-size adjustment algorithms that avoid the tedious process of parameter chosen is highly desired, especially in those applications with time-varying or space-varying environments. Motivated by the demand of robust and fast acquisition of the CSI, we develop the automatic step-size adjustment (ASSA)

algorithm for the weights adaptation of the LMS adaptive filter. Unlike all the existing step-size algorithms that require control parameters, the ASSA algorithm is truly control parameter-free. The LMS adaptive filter employing the ASSA algorithm can be used for effective CSI acquisition, when the optimum Winer filter is not available.

1.2 Main Results and Contributions

1.2.1 Feedback Power Control

As has been addressed in Section 1.1.1, all the limited existing works on the feedback power control in a practical system [6–10] commonly use the ABEP as the performance measure for power adaptation. By noting the importance of the BEOP and its advantage over the ABEP as a QoS measure, we propose to use the BEOP as a new performance measure in the design of a feedback system. To bring up our idea, we first assume perfect CSIT and perfect CSI at the receiver (CSIR), and they are identical. This is a common assumption in all existing works on actual feedback systems. We propose the BEOP-based power control law where the transmitted power is adjusted according to the variations of the channel such that the BEOP is kept within some QoS-specified threshold. It ensures that in the long term, less than a certain fraction of received bits would have IBEP exceeding some IBEP threshold. Therefore, the instantaneous QoS is guaranteed.

The BEOP-based power control law indicates that instead of the full information of the channel fading gain, only the magnitude of the channel fading gain is required at the transmitter for power adaptation. This has also been pointed out in [6] for the ABEP-based power control law. In practice, this observation helps the feedback system reduce the size of the feedback information.

Considering the BEOP-based power control scheme in more detail, if perfect CSIT is available, we can always adjust the transmitted power such that no outage event appears, i.e., the IBEP is always less than the IBEP threshold. However,

practically, the transmitter power is usually limited to some peak value. When the channel is very weak, it may happen that the power needed for an outage-free transmission exceeds the peak transmitter power. In such a case, an outage happens. From this point of view, the QoS-specified BEOP threshold indicates how much the peak transmitter power is required to ensure the BEOP at the receiver being no more than that QoS-specified BEOP threshold.

The effect of imperfect CSI is an overlooked issue in the design of a feedback power control system. So far, no works on the design or analysis of actual feedback power control systems have considered the imperfect CSI case. As a more practical consideration, we build up a system model where the information is transmitted in packets. The channel is assumed to be block-faded and all the symbols inside a packet undergo the same fading. Each packet contains pilot symbols for channel estimation purpose. The number of pilots that can be added is determined by the maximal allowable bandwidth expansion factor (BEF) of the system. Upon receiving a packet, the CSI is obtained at the receiver with estimation errors. In addition, a future CSI is predicted at the receiver and fed back to the transmitter to provide the CSIT through a feedback link. We assume that the feedback link is noiseless and the complete information of the predicted future CSI can be fed back. The advance in time of the predicted CSI should capture the processing delay at the receiver and the propagation delay on the feedback channel. In other words, it must ensure that when the predicted CSI arrives at the transmitter, the packet corresponding to that future CSI has not been sent out yet. Therefore, it is easy to understand that for the same packet, its CSIT and CSIR are different, or say, decorrelated due to the delay. This is a practical and general model for the design and performance analysis of actual feedback systems. Based on this model, we develop both the ABEP-based and the BEOP-based power control laws for the imperfect CSI case.

For both the ABEP-based and the BEOP-based power control laws, we derive explicit ABEP and BEOP results under perfect CSI and under imperfect CSI, respectively. From these results, it is found that for each power law, the performance

loss due to channel estimation errors is very large. However, there remains a significant gain over a non-feedback system. Under either perfect CSI or imperfect CSI, the BEOP-based law shows a remarkable gain over the ABEP-based law in terms of BEOP, and sacrifices only a little in the ABEP performance. Therefore, the BEOP-based power control law provides an attractive solution for instantaneous QoS assurance for communications over fading channel. Our design and analysis of the ABEP-based and the BEOP-based power control laws are generalized for both BPSK and quadrature phase shift keying (QPSK) modulations.

1.2.2 Receiver Design and Performance Analysis of DF Relay Communication Systems

Receiver Design

We consider a general, uncoded DF relay system with one source, one destination and L multiple relays, and we assume $L + 1$ orthogonal channels available. The source communicates with the destination and all the relays using one channel. All the L relays communicate with the destination using the remaining L channels. We derive the ML detector at the destination with an arbitrary M-QAM. It shows the optimum diversity combining strategy for the reception of signals from L independent, non-identically distributed (i.n.d.) links, and the reliability of each link is different due to the decoding errors at each relay. The only reference on the ML detector for a coherent DF relay system is [20], which only considers a single relay case with BPSK under perfect CSI. Our derived ML detector can be specialized to [20]'s result easily.

It is important to note that our receiver result clearly shows that for optimum detection at the destination, the instantaneous information of the source-relay link is required and this information is summarized as the instantaneous decoding error probability at the relay. In many previous works, this instantaneous decoding error probability has been replaced by its average, i.e., the average decoding error

probability at the relay. The loss of the instantaneous information of the source-relay link for detection at the destination would significantly degrade the system performance, and therefore, should be avoided in the design of high-performance receivers. Moreover, it is worth noting that only the instantaneous decoding error probability at the relay needs to be forwarded to the destination, instead of the complete channel fading gain of the source-relay link.

Our derived detector generalizes both perfect and imperfect CSI scenarios. For the imperfect CSI scenario, we assume blockwise static channel for packet transmission. Pilot symbols are inserted into a data packet for channel estimation purpose. The number of pilots can be added is determined by the maximal BEF of the system. Our work is the first one that builds a general DF multiple relay system on a solid, practical channel estimation model.

Due to the complexity of the ML detector for higher order modulations, we confine ourself to study the ML detector with BPSK modulation. In this case, the contribution of the relay to the ML detector is summarized as a nonlinear function. For ease of implementation and analysis, we provide a batch of suboptimum detectors to approximate the ML detector. As has been mentioned earlier, one common way that has been widely used in many works is to replace the IBEP at the relay by its average. To distinguish, we term the ML detector using the ABEP at the relay as the averaged-ML (A-ML) detector for short. Although it is not suitable, the traditional maximum ratio combining (MRC) can be used as a suboptimum detector for a multiple relay system for its simplicity. The MRC simply assumes that the relay makes no decision errors, and it combines all the received signals in the traditional way of diversity reception. We find an intuitional improvement on the traditional MRC, which takes into consideration of the decoding errors at the relay to some extent. We term it as the weighted slope-detector (WSD). The WSD approximates the nonlinear function of the ML detector with a straight line whose slope is affected by the IBEP at the relay. Furthermore, we propose a clipped WSD (CWSD), which is similar to the classic piecewise linear (PL) detector but with a

different slope. The PL approximation to the ML detector is firstly proposed in [25]. Here, we emphasize that in [25], the originally proposed PL detector uses the ABEP at the relay for detection. Our receiver result shows that the IBEP at the relay should be used, even for the PL detector. The WSD or the CWSD provides marginal improvement on the MRC or the PL detector, respectively. In the WSD, the CWSD and the PL detector, the IBEP at the relay can also be replaced by the ABEP at the relay, which results in further approximations to the ML detector. We term them as averaged-WSD (A-WSD), averaged-CWSD (A-CWSD) and averaged-PL (A-PL) detector for short.

Table 1.1: Summary of the ML detector and its approximations for a DF relay system

Optimum	ML detector	
	MRC	
	(use IBEP at the relay)	(use ABEP at the relay)
		A-ML
Suboptimum	WSD	A-WSD
	CWSD	A-CWSD
	PL	A-PL

For clarification, we summarize different detectors mentioned above for a DF relay system in Table 1.1. We emphasize that the optimum detector refers to the ML detector. All the other forms of its approximations are referred to as suboptimum detectors.

Performance Analysis

As has been mentioned in Section 1.1.2, in the attempt to analyze the ML detector, all the existing works study a suboptimum detector which uses the ABEP at the

relay to replace the IBEP at the relay. More specifically, they all examined the performance of the A-PL detector, and is with the assumption of perfect CSI. Therefore, those results and observations are quite limited.

In our analysis, we first consider a single relay system. Referring to Table 1.1 for different names of detectors, we derive closed-form conditional BEP conditioned on the IBEP at the relay, for the WSD, the CWSD, and the PL detector. It is noted that in those derived conditional BEP results, by replacing the IBEP at the relay with its average, it gives the ABEP of the A-WSD, the A-CWSD and the A-PL detector, respectively. Among those conditional BEP results, the conditional BEP of the PL detector provides the most tractability. Therefore, we further obtain a closed-form, approximate ABEP of the PL detector. We emphasize that although being an approximation, this obtained ABEP is for the PL detector which utilizes the IBEP at the relay. It shows that for a single relay system, a diversity order of 2, i.e., full diversity, can be achieved. Those previous results on the ABEP of the A-PL detector show a loss of diversity, and lead to the misleading claim that DF relay systems cannot achieve full diversity.

To analyze the performance of the ML detector, we first derive the conditional BEP conditioned on the IBEP at the relay. This conditional BEP result contains integrals. Again, it is noted that in the derived conditional BEP, by replacing the IBEP at the relay with its average, it gives the ABEP of the A-ML detector. To arrive at a closed-form conditional BEP of the ML detector for further analysis, we apply an equivalent approximation to that which has been used in [26]. The use of this approximation results in that the obtained closed-form, approximate, conditional BEP of the ML detector amounts to the conditional BEP of the PL detector. Therefore, the obtained results for the PL detector applies to the ML detector as approximate results.

Considering a multiple relay system with an arbitrary number of relays, the exact conditional BEP or ABEP of the PL detector cannot be obtained in general. For that reason, we derive closed-form Chernoff upper bounds on the ABEPs of the

A-PL and the PL detectors, respectively. The obtained Chernoff bounds enable us to deduce the diversity order of a DF multiple relay system. These results proof conclusively that the destination detector utilizing the IBEP at the relay achieves full diversity. In contrast, the averaged destination detector utilizing the ABEP at the relay suffers a loss of diversity.

By comparing the performance under perfect CSI and under imperfect CSI, we examine the performance loss due to channel estimation errors. It is found that channel estimation errors do not change the slope of the BEP curves, i.e., the diversity order remains unchanged.

1.2.3 Fast Adaptive Algorithm for CSI Acquisition

Arising from the two topics we have studied, it is seen that CSI acquisition plays a crucial rule in the develoment of these advanced technologies to mitigate the detrimental effects of fading. For analytical purpose, a Wiener filter-based channel acquisition model is popular for its simplicity, accuracy, and tractability. As has been addressed in Section 1.1.3, the implementation of a Wiener filter with optimum filter tap-weight coefficients may be impossible due to the lack of environmental statistics. The LMS adaptive filter offers a simple and robust solution to this problem. Driven by the demand of truly control parameter-free step-size adjustment algorithms, we propose the ASSA algorithm for the tap-weight coefficients adaptation of an LMS adaptive filter. The LMS adaptive filter employing the ASSA algorithm can be used for effective CSI acquisition, when the optimum Winer filter is not available. The most significant feature that distinguishes the ASSA algorithm from any other existing variable step-size algorithms is that the ASSA algorithm does not require any preset control parameters. When applied to channel estimation, simulation results show the performance advantage of the ASSA algorithm over the existing step-size adjustment algorithms under different wireless channel environments.

The proposed ASSA algorithm serves as a fundamental contribution to the step-size adjustment for the tap-weight coefficients adaptation of LMS adaptive

filters. It is expected to be applicable to other cases where LMS adaptive filters are employed, e.g., system identification, channel equalization. In our work, we confine ourselves to the use of the ASSA algorithm for CSI acquisition purpose only.

1.3 Organization of the Thesis

The rest of the thesis is organized as follows.

In Chapter 2, we review some previous works that are related to our work.

In Chapter 3, we propose the BEOP-based power control law. For both the ABEP-based and the BEOP-based power control laws, we develop them for the imperfect CSI case. The ABEP and the BEOP of both laws are derived explicitly. Using these results, we compare the performance of different power control laws.

In Chapter 4, we derive the ML detector of a general, uncoded DF multiple relay system with an arbitrary M-QAM, and the receiver result generalizes both perfect and imperfect CSI scenarios. We further propose the WSD, the CWSD and also show the traditional MRC in a DF relay system. Those suboptimum detectors can be viewed as byproducts of the derived ML detector.

In Chapter 5, we analyze the BEP performance of the ML detector and its approximations with BPSK modulation, which are shown in Chapter 4. Simulations are used to validate our derivations. The diversity order of the DF relay system is analyzed using the numerical and simulation results.

In Chapter 6, we propose the ASSA algorithm, which is used for the tap-weight coefficients adaptation of an LMS adaptive filter. Simulations are used to show the performance of the ASSA algorithm.

Finally, we summarize our work in Chapter 7, and point out a number of future research directions.

Chapter 2

Literature Review

In this chapter, we conduct a comprehensive literature review to the existing works that are related to our research. For the feedback power control topic, we focus on the review of the limited works on the feedback power control for practically realizable systems, and also introduce some of the important results on feedback communications from information theoretic research. For relay communication systems, we summarize many of the current results on the receiver design and performance analysis of DF relay systems. For the topic on fast adaptive algorithms, we review the Wiener filter, the LMS algorithm and a few of its popular step-size adjustment schemes.

2.1 Feedback Communications over Fading Channels

Feedback communications provide a way of utilizing the CSI of the forward channel at the transmitter side. By modifying the transmitted signal according to the variations of the channel, channel-adaptive signalling considerably improves the system performance compared with non-feedback communication systems. Feedback has an impact in many areas such as design of control systems and source coding. As a branch of channel-adaptive communications, the power-adaptive transmission with

feedback has been widely studied in the literature. Power-adaptive transmission is realized by means of power control at the transmitter.

2.1.1 Information Theoretic Results

From the information theoretic point of view, [2] shows that power control with perfect CSIT significantly improves the capacity of fading channels. Reference [3] considers a block-fading Gaussian channel. Assuming perfect CSIR and perfect CSIT, [3] solves for the optimum transmit power that minimizes the information outage probability for a fixed-rate coding system under different power constraints at the transmitter. Recently, the transmit power control topic has been extended to the MIMO communication system. In [4], the information outage probability of block-fading, additive white Gaussian noise (AWGN) channels with multiple antennas under an input power constraint is derived. Coding scheme that is designed to minimize the information outage probability has also be investigated in [4]. For more practical considerations, a large number of works examine the performance limits of feedback systems having limited CSI and/or delay and noise on the feedback channel. For example, [16] proposes practical design of power-adaptive systems with differential binary phase shift keying (DBPSK) modulation for ABEP minimization over flat fading channels using finite optimal policies under short-term and long-term power constraints, respectively. In [16], the instantaneous received SNR is assumed to be known to the receiver and a quantized version of this SNR is fed back to the transmitter to provide the CSIT. In addition, the finite optimal policy, which is referred to a finite number of different transmission modes, is used to reflect the limitations of the transmitter and the feedback channels. Reference [17] considers a fixed-rate system, where power control is used to minimize the outage probability. In [17], only partial CSIR and partial CSIT are available, and the resources used for estimation and feedback are counted as part of the total available resources. More works can be found in [18, 19, 27–30], where different kinds of limited feedback information are examined under different situations. A comprehensive overview of

the limited feedback issue can be found [5], where most of the relevant works up to that time is summarized.

2.1.2 Feedback Power Control in Practical Systems

Most of the works on power control aim to identify the performance limits of communication systems in terms of ergodic capacity or information outage probability. On the other hand, it is of great importance to examine the end-to-end performance of practically realizable feedback power control systems for specific modulation formats. Commonly, power control schemes are designed in a way that the ABEP is minimized subject to some systematic constraints. In [6], Hayes first solved the optimal power control problem for a binary system over a Rayleigh fading multipath channel with a noiseless and delayless feedback channel. With perfect CSIT, the power law is set such that the ABEP at the receiver is minimized subject to a constraint on the average transmitted power. The optimum transmit power is implicitly given as a function of the CSI. It shows that the ABEP is significantly reduced compared with a non-feedback system for the same average power. In [7] and [8], power and rate control are considered at the same time to minimize the ABEP at the receiver subject to constraints on the average power and average rate. Both [7] and [8] demonstrate the superiority of a feedback system over a non-feedback system in reducing the ABEP. Using pilot tone signalling to provide the CSI for detection, [9] obtains the optimal power law which minimizes the ABEP. A more recent work [10] derives the optimal power law that minimizes the ABEP subject to both average and peak power constraints for BPSK signalling over the Rayleigh fading channel. Comparing to the comprehensive works from the viewpoint of information theory, researches on the end-to-end performance of power control systems are quite limited.

2.2 Relay Communication Systems

Multiple relay communication systems have received extensive attention from scholars in the past a few years for its efficiency in offering space diversity in wireless communications. The topic of relay communication systems contains a large number of issues from all aspects of a conventional digital communication system. In this section, we first briefly introduce the relaying protocols for multiple relay communication systems and discuss issues on performance analysis. Then, we focus on summarizing the current results on the receiver design and performance analysis of coherent DF relay systems, which are related to our work. In the following descriptions, unless otherwise specified, we refer to a relay system as a system with the source-destination link available.

2.2.1 Relaying Protocols and Performance Analysis Issues

Generally, a relay employs one of the two relaying protocols, namely, AF and DF [11]. In the AF protocol, each relay that receives a signal from the source forwards an amplified version of this signal to the destination. In the DF protocol, upon receiving a source message, each relay decodes the source message, and generates a copy of that source message as an output to destination. At the destination, a final decision is made based on all the received signals from the source as well as from the relays. As an extension of the basic AF and DF protocols, the SR protocol [11] selects those relays that meet certain requirements to forward the source information to the destination. Commonly, those requirements can be an SNR threshold of an AF relay or an error probability threshold of a DF relay [31–36]. Besides AF and DF, a relay can also transmit a compressed and quantized version of the past received signals to the destination, and this protocol is known as the compress-and-forward (CF) protocol [37–39]. The main drawback of the CF protocol is its relatively high complexity, and this limits its development for practical use. Performance analysis shows that relay communication systems offer great performance improvement over the traditional non-relaying systems from various perspectives.

From information theoretic point of view, the performance analysis of relay communication systems refers to analyze the performance limits, e.g., capacity, achievable rates and information outage probability [11, 37, 39–43]. Here, we focus on the discussion on end-to-end performance analysis of real implementable relay communication systems. We also mention that for a relay system, the two most common encoding strategies are simple uncoded or repetition coding, and space-time (ST) coding [44–47]. While ST coding provides additional gain from relay cooperation at the expense of increasing system complexity, the implementation of simple uncoded or repetition coding is straightforward, and the performance gain achieved by using the uncoded transmission is from information relaying solely. The performance of an uncoded relay system has been widely studied under different relaying protocols.

Compared with a general, uncoded DF relay system, a general, uncoded AF relay system is easier to analyze, as the performance of the latter one can be circumvented by examining the equivalent, end-to-end SNR of the source-relay-destination path at the destination. Reference [48] evaluates the performance of a two-hop, AF single relay system without the source-destination link. It is worth noting that in [48], the average received SNR at the destination (or say, the equivalent, end-to-end SNR of the source-relay-destination path) is expressed as the *harmonic mean* of two exponential random variables. These two exponential random variables denote the SNRs of the source-relay and the relay-destination links, respectively. In [48], the moment generating function (MGF) of the *harmonic mean* of two exponential random variables is derived. Therefore, the MGF of the average received SNR at the destination is known. With this MGF result, [48] shows that the symbol error probability of the relay system with various M-ary modulations can be easily obtained using the famous MGF-based method [49]. The above-mentioned equivalent, end-to-end SNR-based approach is very popular in evaluating the performance of a general AF relay system [50, 51]. The performance of a general, uncoded DF relay system will be discussed in detail

after we review the receiver design for DF relay systems.

2.2.2 Receiver Design for DF Relay Systems

For coherent DF relay systems, as the relay can make decision errors, the traditional MRC which is optimum for diversity reception of equally-probable transmitted signals, is not suitable.

Reference [20] shows the optimum (ML) detector structure for a DF single relay system with coherent binary transmission. As it is shown in [20], the ML detector contains a nonlinear function that captures the effect of decoding errors at the relay. The nonlinear function is clipped by a term that is related to the IBEP of decoding the source message at the relay. As the decoding error probability at the relay increases, the contribution of the source-relay-destination link to the ML detector is reduced. In [25], it shows a general detector structure with either coherent or noncoherent binary frequency shift keying (BFSK) modulation for a DF multiple relay system. The authors of [25] called their detector the ML detector. However, it should be noted that this detector is not truly optimum, as it uses the ABEP at the relay instead of the IBEP. The contribution of each source-relay-destination link amounts to a similar nonlinear function that has been shown in [20]. In the error performance analysis, to ease the difficulty brought by the nonlinear function, [25] proposes a PL function that closely approximates the original nonlinear function. The authors of [25] termed the detector with the PL approximation as the PL detector. However, since ABEP at the relay is used instead of the IBEP by the destination detector, [25] actually proposes the A-ML and the A-PL detectors for coherent BFSK, and only analyzes the A-PL detector. Like some other works, e.g., [26] and [52], [25] fails to see the fact that the ML detector uses the IBEP at the relay, instead of its average.

As is known, the complexity of analyzing the ML detector for a DF relay system increases exponentially as the number of relays increases. To simplify the performance analysis of a DF relay system, some works have proposed suboptimum

detectors [21–24] to approximate the ML detector. In [21] and [22], a destination detector termed as the λ-MRC is derived to approximate the ML detector with BPSK modulation. The optimal value of the parameter λ has to be found through numerical search. In [23], a suboptimum detector termed as the cooperative MRC (C-MRC) is proposed for a general multiple-relay, multi-hop system with general constellations. The C-MRC improves on the traditional MRC such that the weights for weighting the received signals from different relays are modified. For each source-relay-destination path, the modified weight is selected to capture the quality of both source-relay and relay-destination links. Reference [24] proposes a suboptimum detector for a single relay system with M-ary pulse amplitude modulation and M-QAM. In [24], the ML decision rule is approximated using the max-log approximation [53].

The performance analysis of the above detectors will be discussed next.

2.2.3 Performance Analysis of DF Relay Systems

Unlike that for an AF relay system, for a DF relay system, as the relay can make decision errors, the equivalent, end-to-end SNR of the source-relay-destination link is hard to obtain. Therefore, the performance of a DF relay system cannot be evaluated using the popular MGF-based method. In fact, in many works, it has been demonstrated that the exact performance analysis of DF relay systems is much more complicated than that of AF relay systems.

In [20], the ABEP performance of the ML detector is studied by simply assuming that the relay always decodes correctly and using large SNR approximations. In [25], the ABEP of the A-PL detector with coherent and noncoherent BFSK is obtained in a closed form. The PL approximation is widely used in the performance analysis of ML detection for DF relay systems with binary modulations. Using high-SNR approximations, [25] shows that full diversity order is not achieved by the A-PL detector. In [54] and [55], the ABEP of the A-PL detector for a single relay system with BPSK is obtained in an integral form. It is

noted that [54] and [55] assume real channel fading coefficients, which is not common for practical fading channels. Reference [26] aims to solve the exact ABEP of the A-ML detector for a DF single relay system with BPSK. To arrive at a closed-form result, [26] uses approximations in its analysis, which results in that the obtained ABEP for the A-ML detector amounts to the ABEP of the A-PL detector. For a DF multiple relay system, [26] obtains the ABEP of the A-PL detector by using an approximation based on the central limit theorem. Similar to that in [25], due to the use of the averaged detector (uses the ABEP at the relay instead of the IBEP), a loss in the diversity order is reported in [26]. The authors of [26] extended their work to DF MIMO relay channels in [56]. Reference [57] obtains the exact ABEP of the A-PL detector for a DF two-relay system with BPSK. The analysis is done using a contour integral approach for evaluating the Gil-Pelaez integral [58] involving the characteristic function of the decision variable. In [52], closed-form ABEPs of the A-PL detector for both a DF single relay system and a DF two-relay system is respectively obtained with binary signalling including noncoherent BFSK, coherent BFSK and coherent BPSK. The ABEP results for a single relay system in [52] amounts to those in [25] and [26] for different modulation formats, respectively, by properly manipulating the terms. It is noted that the method used in [52] in deriving the ABEP is different from that in [25] or [26]. As can be seen, those works [25,26,52,54,55,57] analyze the performance of the A-PL or the A-ML detector in which the ABEP at each relay is used for detection at the destination. Although their performance is more tractable than that of the ML or the PL detector where the IBEP at each relay is used, the A-ML or the A-PL detector suffers a loss in the diversity gain. This is quite undesired for the design of spatial diversity systems.

The C-MRC [23] retains the instantaneous information of the source-relay link. For a single relay system with BPSK modulation, [23] shows the conditional BEP of the destination detector conditioned on all the instantaneous SNRs of all links. Due to the complexity of the conditional BEP result, it is difficult to obtain the exact ABEP. Therefore, an upper bound on the conditional BEP is obtained instead.

Based on this result, it shows that the diversity order of a single relay system is two, i.e., full diversity is achieved. For higher order constellations, [23] uses high-SNR approximations to show that the C-MRC achieves full diversity. Using simulations, [23] also shows that the C-MRC performs better than an SR system, in which the relays are assumed to equip cyclic redundancy check (CRC) and only forward those correctly decoded messages. It is noted that all the BEP curves in [23] are drawn from simulations, as no exact ABEP results are obtained.

Table 2.1: Summary of current works on coherent, uncoded DF relay systems

	ML	PL	A-ML, A-PL	Others (Suboptimum)
Single relay system	[20]		[25,26,52,54,55]	[21–24]
Multiple relay system			[25,26,52,57]	[23]

In Table 2.1, we summarize the current works on coherent, uncoded DF relay systems. As can be seen, the ML detector for a DF relay system with multiple relays remains unaddressed. In addition, [20] only considers binary modulations. For general constellations, proposals on suboptimum detectors can be found in [23] and [24].

2.2.4 Multiple Relay Systems with Imperfect CSI

It is noted that in all the aforementioned works, perfect CSI is assumed for coherent detections. For practical considerations, it is necessary to study the detections under imperfect CSI. In the literature, many works have done the analysis of relay systems with AF relays (with or without relay selection) under imperfect CSI, e.g., [59–66]. In contrast, the attempt to analyze relay systems with DF relays is quite limited. A few examples can be found in [67–69], and all of them involves relay selection.

As far as we are concerned, no works have considered a general, uncoded DF relay system with imperfect CSI from either receiver design or performance analysis point of view.

2.3 LMS Adaptive Filters

For the purpose of CSI acquisition in an unknown wireless environment, adaptive filters can be used. In this section, we provide a survey on the LMS adaptive filter. We first briefly review the Wiener filter and the LMS as well as the normalized LMS (NLMS) algorithms [70]. Then, we turn to review some popular variable step-size schemes for the LMS and the NLMS algorithms, respectively.

2.3.1 Wiener Filter

A Wiener filter is designed based on the MSE criterion, i.e., the filter coefficients are optimized in the sense that the mean-square value of the estimation error is minimized. Given the autocorrelation function of the input sequence and the cross-correlation between the input sequence and the desired sequence, the optimum filter tap-weight coefficients of a discrete Wiener filter can be solved from the Winer-Hopf equation [70]. Consider in general an N-tap filter, with the weight vector $\mathbf{w}(n)$ at time point n denoted by

$$\mathbf{w}(n) = [w_1(n) \;\; w_2(n) \;\; ... \;\; w_N(n)]^T. \tag{2.1}$$

Let $\{x(n)\}$ be the input sequence and $\mathbf{x}(n) = [x(n) \;\; x(n-1) \;\; ... \;\; x(n-N+1)]^T$ be its vector representation containing the immediate past N samples of $\{x(n)\}$. The filter output $y(n) = \mathbf{w}^H(n)\mathbf{x}(n)$ aims to follow a desired signal $d(n)$, and the estimation error $e(n)$ is defined as

$$e(n) = d(n) - y(n). \tag{2.2}$$

The autocorrelation matrix of the input vector $\mathbf{x}(n)$ and the cross-correlation between $\mathbf{x}(n)$ and $d(n)$ are denoted, respectively, by

$$\mathbf{R} = \mathbb{E}\left[\mathbf{x}(n)\mathbf{x}^H(n)\right], \tag{2.3}$$

and

$$\mathbf{p} = \mathbb{E}\left[\mathbf{x}(n)d^*(n)\right]. \tag{2.4}$$

The optimum weight vector is solved from the Winer-Hopf equation, and is denoted by

$$\mathbf{w}_o = \mathbf{R}^{-1}\mathbf{p}. \tag{2.5}$$

Here, it should be noted that $\mathbf{w}_o$ is not time-varying. The MMSE of the estimation process is given by

$$2V^2 = \mathbb{E}\left[|d(n)|^2\right] - \mathbf{w}_o^H\mathbf{R}\mathbf{w}_o. \tag{2.6}$$

From the above, it is noted that the implementation of the Wiener filter requires the knowledge of $\mathbf{R}$ and $\mathbf{p}$, which is statistical information that may be unavailable in practice. When the statistical information is unknown, iterative adaptive algorithms can be used to approximate the performance of the Wiener filter in an iterative manner. Among those iterative algorithms, the LMS algorithm is widely used for its robustness and simplicity. We will briefly review it in the following subsection.

2.3.2 The LMS and the NLMS Algorithms

In the LMS algorithm, the filter tap-weight coefficients are updated in a manner such that the squared instantaneous estimation error is minimized. This results in a time-varying tap-weight vector which is iteratively updated as [71]

$$\mathbf{w}(n+1) = \mathbf{w}(n) + \mu e(n)\mathbf{x}(n). \tag{2.7}$$

Here, μ is a step-size parameter that controls the trade-off between the rate of convergence and the steady-state MSE of the LMS algorithm. It is a very important

parameter that needs to be carefully chosen. If the μ is chosen large, the algorithm converges fast to the steady-state MSE. However, once the steady-state MSE is achieved, the adaptive algorithm cannot learn any more. On the contrary, if the μ is chosen small, the algorithm converges slower but leading to a smaller steady-state MSE, which also means that the estimation performed by the filter is more accurate. To compromise the rate of convergence and the steady-state MSE, a variable step-size is desired. The basic idea of using a variable step-size comes from the facts that a large step-size at the beginning of the adaptation is capable of speeding up the convergence; and when the filter coefficients are about to converge, a small step-size is necessary for a low steady-state MSE. In the literature, many variable step-size schemes have been proposed, and they are shown to be more efficient than the FSS LMS algorithm.

As a special extension of the LMS algorithm with a variable step-size, the NLMS algorithm is designed to compensate the *gradient noise amplification* [70] problem caused by the LMS algorithm. The NLMS algorithm uses a time-varying step-size that is inversely proportional to the signal level at the filter input. The tap-weight vector is updated as

$$\mathbf{w}(n+1) = \mathbf{w}(n) + \frac{\hat{\mu}}{\mathbf{x}^T(n)\mathbf{x}(n)} e(n)\mathbf{x}(n), \tag{2.8}$$

where $\hat{\mu}$ is a parameter to be chosen and $\hat{\mu}/\mathbf{x}^T(n)\mathbf{x}(n)$ is the actual step-size. A more reliable implementation of the NLMS algorithm in practice requires the assistance of a regularization parameter ε, and it results in the ε-NLMS algorithm [70] with the improved step-size $\hat{\mu}/(\mathbf{x}^T(n)\mathbf{x}(n)+\varepsilon)$. Although having the tap-weight adaptation equations in a similar form (and differing only in the choice of the step-size), LMS-type algorithms are usually not compared with NLMS-type algorithms. In the literature, it has been shown that NLMS-type algorithms provide a potentially faster rate of convergence [70, 72, 73]. However, it should be noted that additional computational complexity is required by the NLMS algorithm in computing $\hat{\mu}/\mathbf{x}^T(n)\mathbf{x}(n)$, which is N additions, N multiplications and 1 division. In the NLMS algorithm, the parameter $\hat{\mu}$ or ε, or even both of them, can be adjusted

according to some rules to further improve its performance. We categorize these extensions into variable step-size schemes for the NLMS algorithm, and review some of the popular ones along with the variable step-size schemes for the LMS algorithm in the next section.

2.3.3 Variable Step-Size Algorithms

The popularity of the LMS algorithm drives the development of many efficient variable step-size schemes, some of which have received extensive attention. Here, we briefly revisit a few popular variable step-size schemes for the LMS algorithm and the NLMS algorithm, respectively.

In [74], the signs of the gradient terms in updating the weight vector are continuously monitored, based on which, the step-size is increased if the number of consecutive identical signs exceeds a specified threshold, and similarly, the step-size is decreased if the number of consecutive sign changes exceeds another specified threshold. Reference [75] proposes and analyzes the gradient adaptive step-size (GASS) algorithm, where the squared estimation error is reduced at each iteration. As can be seen, a initial value of the step-size, $\mu(0)$, and a constant ρ are the two parameters that control the convergence. Reference [76] proposes to directly update the step-size according to the square of the instantaneous estimation error. The process is controlled by two parameters, namely, α and γ. In the simulations of [76], these two parameters have been chosen differently for different cases. Reference [77] improves on the work of [76] by using a time-averaged estimate of the error, instead of the instantaneous error. Besides the two parameters α and γ that have appeared in [76], [77] introduces a new control parameter β in generating the estimate of the autocorrelation between two adjacent errors. The authors of [77] had shown that the new algorithm that they call the modified variable step-size (MVSS) LMS algorithm outperforms the algorithm in [76], especially in a noisy environment. In [78], a kurtosis of the estimation error is defined, based on which the step-size is updated. The computation of the kurtosis requires the statistics of the estimation error. In

addition, a control parameter α needs to be adjusted to enhance the performance.

Considering variable step-size schemes for the NLMS-type algorithms, following a procedure similar to that in [75], [79] applies a normalized gradient adaptive descent algorithm to the $\hat{\mu}$ in (2.8), and arrives at the variable step-size NLMS (VSS-NLMS) algorithm. In [79], no regularization is performed, i.e., $\varepsilon = 0$, and it is noted that an initial value of $\hat{\mu}$ (in [79], it is referred to as μ_0) and an additional constant ρ are to be set for the algorithm to work properly. Instead of adjusting $\hat{\mu}$, [80] proposes to update ε according to a generalized normalized gradient descent algorithm. In [80], a parameter ρ controls the learning rate of the algorithm, and $\rho = 0.15$ is used as a typical value in the simulations. Reference [81] proposes a robust regularization method where a sign function is applied to the derived gradient descent term in [80], and by using the typical setting of $\rho = 0.15$, it shows an improvement over the method of [80] in terms of steady-state MSE. Variations and enhancements on the LMS or the NLMS algorithms are also developed for the use in some special environments, or for some specific applications, where variable step-sizes are also desired, and thus gives rise to a large number of different algorithms [82–89].

It is noted that a common feature of all the above-mentioned step-size adjustment algorithms is that preset control parameters are required, and of course, the choice of these parameters would greatly affect the performance of these algorithms. So far, these control parameters are always chosen from extensive simulations or from experience. To obviate the tedious process of choosing appropriate parameters, parameter-free algorithms are desired. Reference [90] presents a nonparametric variable step-size NLMS (NPVSS-NLMS) algorithm which aims to reduce the impact of the noise present in the desired response $d(n)$. In its case, $d(n)$ is corrupted by a system noise. When setting the power of this noise to zero, the NPVSS-NLMS algorithm reduces to the conventional NLMS algorithm. To the best of our knowledge, no parameter-free algorithms in the true sense have been introduced in the literature.

Chapter 3

Feedback Power Control for the Rayleigh Channel

By exploiting the CSIT, a feedback power control system yields large performance improvements over a non-feedback system. We propose to use the BEOP as a new performance measure in the design of a feedback power control system. Compared with the traditional performance measure, i.e., the ABEP, the BEOP is a more meaningful measure for high-data rate transmission over fading channels. We propose the BEOP-based power control law where the transmitted power is adjusted according to the variations of the channel such that the BEOP is kept within some QoS-specified threshold. It ensures that in the long term, less than a certain fraction of received bits would have IBEP exceeding some IBEP threshold. Therefore, the instantaneous QoS is guaranteed. Based on a practical system model with channel estimation and prediction, we develop the traditional ABEP-based power control law and the new BEOP-based power control law. The effect of imperfect CSI has been an overlooked issue in the literature of design and performance analysis of an actual feedback power control system. For both the ABEP-based and the BEOP-based power control laws, we derive explicit ABEP and BEOP results. The BEOP-based law shows a remarkable gain over the ABEP-based law in terms of BEOP, and sacrifices only a little in the ABEP performance.

3.1 Introduction

By adapting the transmitter power to match the current state of the channel, power control is a promising technology in mitigating the signal fading in wireless communications. Most of the works on power control study the performance limits of communication systems in terms of ergodic capacity or information outage probability [2–4]. While information theoretic research is important, it is of great use to design practically realizable feedback power control systems for specific modulation formats and examine their end-to-end performance. Unfortunately, as has been summarized in Section 2.1.2, research in this area is quite limited. All those existing works [6–10] on the design of practical feedback power control systems use the ABEP as the performance measure. For transmission over fading channels, the ABEP is obtained by averaging the IBEP over the distribution of the fading, and therefore, it cannot reflect the instantaneous depth of fade experienced by the user. For high data-rate transmission, a short duration of deep fade may cause thousands of erroneous received data bits. In such a case, the ABEP as a performance measure becomes meaningless. As has been pointed out in [13], to reflect the instantaneous QoS, the BEOP is a more useful measure. The BEO event is defined as the event that the IBEP exceeds an IBEP threshold. The BEOP reflects, in the long term, the fraction of the received bits that have IBEP exceeding the IBEP threshold. From the viewpoint of QoS assurance, it is meaningful to set an upper limit on the BEOP to ensure that in the long term, less than a certain fraction of received bits would have IBEP exceeding the IBEP threshold.

Motivated by the importance of BEOP and its advantage over ABEP as a QoS measure, we propose to use the BEOP as a new performance measure in the design of a feedback power control system. To bring up our idea, we first assume perfect CSIT and perfect CSIR, and they are identical. This is a common assumption in all existing works on actual feedback systems. We propose the BEOP-based power control law where the transmitted power is adjusted according to the variations of the channel such that the BEOP is kept within some QoS-specified threshold. As a

more practical consideration, we build up a system model with channel estimation and channel prediction at the receiver, and develop both the traditional ABEP-based power control law and the BEOP-based power control law for the imperfect CSI case. For both laws, we derive explicit ABEP and BEOP results under perfect CSI and under imperfect CSI, respectively. These results show that for each power law, the performance loss due to channel estimation errors is very large. However, there remains a significant gain over a non-feedback system. The BEOP-based law shows a remarkable gain over the ABEP-based law in terms of BEOP, and sacrifices only a little in the ABEP performance. Therefore, the BEOP-based power control law provides an attractive solution for instantaneous QoS assurance in communications over fading channels.

The rest of this chapter is organized as follows. In Section 3.2, we describe the system model, where the imperfect CSI scenario is discussed in detail. In Sections 3.3, 3.4 and 3.5, we discuss the design and analysis of power control laws under perfect CSI. From Section 3.6 to Section 3.8, we extend the study to the imperfect CSI case. Numerical results are presented in Section 3.9. Finally, Section 3.10 concludes the chapter.

3.2 System Model

We consider SISO transmission over the frequency-nonselective Rayleigh block-fading channel with CSI feedback from the receiver to the transmitter. The message is sent in packets with uncoded BPSK or QPSK. The fading is assumed to be constant over the duration of one packet, and we assume a packet length of N symbols. The packet length that fits the block-wise static channel assumption is determined by the coherence time of the channel and the available bandwidth. For the purpose of power control, we assume a fixed transmission rate R and a fixed symbol duration T. Therefore, the control on the transmitted power is equivalent to the control on the transmitted energy. Let $x(k)$ denote the symbol sent at time

point k. The received signal in the k-th symbol interval $kT \leq t \leq (k+1)T$ is

$$y(k) = E_s^{1/2} h_l x(k) + n(k), \tag{3.1}$$

where E_s is the transmitted energy per symbol. The channel fading coefficient of the l-th packet is denoted by h_l, and is complex Gaussian distributed with mean zero and autocorrelation function $E[h_{l+m}h_l^*] = 2\sigma^2 R(m)$, where $2\sigma^2$ is the variance and $R(m)$ is the correlation coefficient of the fading process at a time difference of m. Assuming Jake's Doppler spectrum, we have $R(m) = J_0(2\pi f_D T m)$ with $f_D T$ being the normalized Doppler frequency and $J_0(\cdot)$ denoting the Bessel function of the first kind of order zero. The $n(k)$ denotes the AWGN, which is complex Gaussian distributed with mean zero and variance N_0.

We consider both the perfect CSI case and the imperfect CSI case, and introduce them separately in the following.

3.2.1 Perfect CSI

Upon receiving a source packet, the receiver is assumed to be able to obtain the exact h_l, i.e., perfect CSIR is available. The complete h_l is then fed back to the transmitter through a noiseless feedback channel. We assume that the feedback channel changes slowly such that the CSIT is exactly the same as the CSIR. Although this genie-aided feedback is not practical, it provides a theoretically analyzable model, and shows the best performance that a feedback system can achieve. This perfect CSI model is commonly used in all existing works on actual feedback systems [6–10].

3.2.2 Imperfect CSI

For the imperfect CSI case, channel estimation is required at the receiver to obtain an estimate of the CSI for coherent detection. Here, we use pilot symbols for channel estimation. We assume that a packet consists of N_d data symbols prefixed by N_p pilot symbols to form a packet of length N, i.e., $N = N_p + N_d$. Let E_p be the energy per pilot symbol and E_d be the energy per data symbol. The received signal has

been shown in (3.1), where $E_s = E_d$ for data symbols and $E_s = E_p$ for pilot symbols. The total packet energy is given by $E_{\text{pkt}} = N_p E_p + N_d E_d$. For the purpose of power control, we assume that E_p does not change according to the channel variation, and denote the average energy per data symbol by E_d^{ave}. If the packet energy is fixed, we cannot adjust E_p and E_d^{ave} freely, as it will affect the system performance. For that reason, we define a power allocation factor ξ, such that $N_p E_p = \xi N_d E_d^{\text{ave}}$. The ξ determines the power allocation between the data symbols and the pilot symbols for a given fixed total packet energy. Without loss of generality, we also assume that N_p and N_d are fixed. In a practical system, the number of pilots that can be added to a data packet is determined by the maximal BEF of the system. Compared with the perfect CSI case, due to the use of pilots, the efficiency of data transmission is reduced. The effective average transmitted energy per data symbol is denoted by

$$E_d^{\text{eff-ave}} = \frac{E_{\text{pkt}}}{(1+\xi)N}. \tag{3.2}$$

Upon receiving a source packet, the receiver estimates the CSI using the pilot information. In addition, a future CSI is predicted and fed back to the transmitter through a noiseless feedback channel to provide the CSIT. We assume that the feedback link is noiseless and the complete information of the predicted CSI can be fed back. The advance in time of the predicted CSI should capture the processing delay at the receiver and the propagation delay on the feedback channel. In other words, it must ensure that when the predicted CSI arrives at the transmitter, the packet corresponding to that future CSI has not been sent out yet. Therefore, it is easy to understand that for the same packet, its CSIT and CSIR are different, or say, decorrelated due to the delay.

In the next subsection, we discuss the channel estimation/prediction issue in detail.

3.2.3 Channel Estimation and Prediction using Pilots

At the receiver, the received pilot signals are fed into a Wiener filter to obtain the MMSE estimate of the channel. To distinguish from data symbols, we denote the

transmitted pilot symbol and the received pilot signal by $x_p(k)$ and $p(k)$, respectively. Without loss of generality, we assume $x_p(k) = 1$.

Channel Estimation

At the receiver, the channel fading coefficient h_l is estimated using the received pilot signals gathered from the current l-th as well as the immediate past L_e packets. Let

$$\mathbf{p} = [\mathbf{p}_0 \quad \mathbf{p}_1 \quad \cdots \quad \mathbf{p}_{L_e}]^T, \tag{3.3}$$

where

$$\mathbf{p}_i = [p(l-i+1) \quad p(l-i+2) \quad \cdots \quad p(l-i+N_p)]^T, \ i = 0, 1, ..., L_e \tag{3.4}$$

denotes the received pilot signals in the past i-th packet. Note that $i = 0$ refers to the current l-th packet. The MMSE estimate of h_l can be represented as [70, eq.(2.1)]

$$\hat{h}_{l|l} = \mathbf{w}_o^T \mathbf{p}. \tag{3.5}$$

Here, $\mathbf{w}_o$ is the optimum tap-weight vector of the $(L_e+1)N_p$-th order Wiener filter and can be obtained by using [70, eq.(2.36)], as

$$\mathbf{w}_o = \mathbf{R}^{-1}\mathbf{v}, \tag{3.6}$$

where $\mathbf{R}$ is the autocorrelation matrix of $\mathbf{p}$, and $\mathbf{v}$ is the cross correlation between h_l and $\mathbf{p}$. The $\mathbf{R}$ can be expressed as

$$\mathbf{R} = \begin{bmatrix} \mathbf{R}_0 & \mathbf{R}_1 & \cdots & \mathbf{R}_{L_e} \\ \mathbf{R}_1 & \mathbf{R}_0 & \cdots & \mathbf{R}_{L_e-1} \\ \vdots & \vdots & \vdots & \vdots \\ \mathbf{R}_{L_e} & \mathbf{R}_{L_e-1} & \cdots & \mathbf{R}_0 \end{bmatrix} + N_0 \mathbf{I}_{(L_e+1)N_p \times (L_e+1)N_p}, \tag{3.7}$$

where

$$\mathbf{R}_i = R(i) E_p 2\sigma^2 \begin{bmatrix} 1 & 1 & \cdots & 1 \\ 1 & 1 & \cdots & 1 \\ \vdots & \vdots & \vdots & \vdots \\ 1 & 1 & \cdots & 1 \end{bmatrix}, i = 0, 1, ..., L_e \tag{3.8}$$

is an $N_p \times N_p$ matrix, and $\mathbf{I}_{(L_e+1)N_p \times (L_e+1)N_p}$ denotes an $(L_e+1)N_p \times (L_e+1)N_p$ identity matrix. The vector $\mathbf{v}$ can be expressed as

$$\mathbf{v} = [\mathbf{v}_0 \quad \mathbf{v}_1 \quad \cdots \quad \mathbf{v}_{L_e}]^T, \tag{3.9}$$

where

$$\mathbf{v}_i = R(i)\sqrt{E_p}2\sigma^2[1 \quad 1 \quad \cdots \quad 1]^T, \ i = 0, 1, ..., L_e, \tag{3.10}$$

and is of the length N_p. The estimation error is denoted by $\hat{e}_{l|l}$, and is a complex Gaussian random variable with mean zero and variance $2V^2$. The $2V^2$ is known as the MMSE of the estimation process, and can be obtained by using [70, eq.(2.49)], as

$$2V^2 = 2\sigma^2 - \mathbf{v}^T\mathbf{R}^{-1}\mathbf{v}. \tag{3.11}$$

The h_l can be expressed as

$$h_l = \hat{h}_{l|l} + \hat{e}_{l|l}. \tag{3.12}$$

It is noted that $\hat{h}_{l|l}$ is a complex Gaussian random variable with mean zero and variance $2\lambda^2 = 2\sigma^2 - 2V^2$.

Channel Prediction

Besides estimation of the current channel, a future channel is also predicted at the receiver and fed back to the transmitter to provide the CSIT. Due to the processing time at the receiver and the propagation delay on the feedback channel, from the viewpoint of the transmitter, the prediction is based on the received pilot signals from past received packets with a delay. Assuming this delay is a multiple of the packet duration NT, i.e., DNT, where D is a positive integer, and the pilot signals from the past L_p consecutive packets are used, the pilot information for predicting h_l can be represented by the vector

$$\mathbf{p}' = [\mathbf{p}_D \quad \mathbf{p}_{D+1} \quad \cdots \quad \mathbf{p}_{D+L_p-1}]^T, \tag{3.13}$$

where $\mathbf{p}_i,\ i = D, D+1, ..., D+L_p-1$ has been defined in (3.4). Note that $D = 1$ refers to the case that no feedback delay is incurred. For a practical consideration which takes into account both the processing time and the feedback delay, it requires that $D \geq 2$. The MMSE prediction of h_l is denoted by

$$\tilde{h}_{l|l-D} = \mathbf{w}_o'^T \mathbf{p}'. \tag{3.14}$$

The optimum filter tap-weight vector $\mathbf{w}_o'$ is given by

$$\mathbf{w}_o' = \mathbf{R}'^{-1}\mathbf{v}', \tag{3.15}$$

where

$$\mathbf{R}' = \begin{bmatrix} \mathbf{R}_0 & \mathbf{R}_1 & \cdots & \mathbf{R}_{L_p-1} \\ \mathbf{R}_1 & \mathbf{R}_0 & \cdots & \mathbf{R}_{L_p-2} \\ \vdots & \vdots & \vdots & \vdots \\ \mathbf{R}_{L_p-1} & \mathbf{R}_{L_p-2} & \cdots & \mathbf{R}_0 \end{bmatrix} + N_0 \mathbf{I}_{L_pN_p \times L_pN_p}, \tag{3.16}$$

and

$$\mathbf{v}' = [\mathbf{v}_D \quad \mathbf{v}_{D+1} \quad \cdots \quad \mathbf{v}_{D+L_p-1}]^T. \tag{3.17}$$

The prediction error is denoted by $\tilde{e}_{l|l-D}$, which is a complex Gaussian random variable with mean zero and variance

$$2V'^2 = 2\sigma^2 - \mathbf{v}'^T \mathbf{R}'^{-1}\mathbf{v}'. \tag{3.18}$$

The $2V'^2$ is also known as the MMSE of the channel prediction process. The h_l can be expressed as

$$h_l = \tilde{h}_{l|l-D} + \tilde{e}_{l|l-D}. \tag{3.19}$$

It is noted that $\tilde{h}_{l|l-D}$ is a complex Gaussian random variable with mean zero and variance $2\lambda'^2 = 2\sigma^2 - 2V'^2$.

The Relationship Between Channel Estimation and Prediction

From (3.12) and (3.19), we have

$$\hat{h}_{l|l} = \tilde{h}_{l|l-D} + \tilde{e}_{l|l-D} - \hat{e}_{l|l}. \tag{3.20}$$

It is noted that according to the principle of orthogonality in Wiener filtering [70], $\hat{h}_{l|l-1}$ and $\hat{e}_{l|l-1}$ are uncorrelated, and $\tilde{h}_{l|l-D}$ and $\tilde{e}_{l|l-D}$ are uncorrelated. If $\mathbf{p}$ and $\mathbf{p}'$ have overlap, any two of the four terms in (3.20) are correlated except for those two orthogonal pairs mentioned above. In the following, we derive the conditional distribution of $\hat{h}_{l|l}$ conditioned on $\tilde{h}_{l|l-D}$. Later, this distribution will be used for performance analysis at the receiver side of the feedback system.

First, we revisit *Lemma* 3.1 of [91]. It states that if X and Y are jointly Gaussian circularly symmetric complex random variables with means $\mathbb{E}[X] = 0$, $\mathbb{E}[Y] = 0$ and variances σ_X^2, σ_Y^2, the covariance $\mu_{XY} = \mathbb{E}[XY^*]$ is shown to be a real number. Conditioned on X, Y is a conditional Gaussian random variable with conditional mean

$$\mathbb{E}[X|Y] = \rho_{XY}\frac{\sigma_X}{\sigma_Y}Y, \tag{3.21}$$

and conditional variance

$$\mathrm{Var}[X|Y] = \sigma_X^2(1-\rho_{XY}^2), \tag{3.22}$$

where the normalized covariance ρ_{XY} is defined as

$$\rho_{XY} = \frac{\mu_{XY}}{\sigma_X\sigma_Y}. \tag{3.23}$$

Using the above results, conditioned on $\tilde{h}_{l|l-D}$, the conditional mean and variance of $\hat{h}_{l|l}$ are given, respectively, by

$$\mathbb{E}[\hat{h}_{l|l}|\tilde{h}_{l|l-D}] = \left(1 - \frac{\mathbb{E}[\hat{e}_{l|l}\tilde{h}_{l|l-D}^*]}{2\lambda'^2}\right)\tilde{h}_{l|l-D}, \tag{3.24}$$

and

$$\begin{aligned}\mathrm{Var}[\hat{h}_{l|l}|\tilde{h}_{l|l-D}] &= \mathrm{Var}[\tilde{e}_{l|l-D}|\tilde{h}_{l|l-D}] + \mathrm{Var}[\hat{e}_{l|l}|\tilde{h}_{l|l-D}] - 2\mathbb{E}[\tilde{e}_{l|l-D}\hat{e}_{l|l}|\tilde{h}_{l|l-D}] \\ &\quad +2\mathbb{E}[\tilde{e}_{l|l-D}|\tilde{h}_{l|l-D}]\mathbb{E}[\hat{e}_{l|l}|\tilde{h}_{l|l-D}].\end{aligned} \tag{3.25}$$

If the errors $\tilde{e}_{l|l-D}$ and $\hat{e}_{l|l}$ are very small, we can assume that they are uncorrelated, i.e.,

$$\mathbb{E}[\tilde{e}_{l|l-D}\hat{e}_{l|l}] = E[\tilde{e}_{l|l-D}]E[\hat{e}_{l|l}]. \tag{3.26}$$

Therefore, the conditional variance can be expressed as

$$\mathrm{Var}[\hat{h}_{l|l}|\tilde{h}_{l|l-D}] = 2V'^2 + 2V^2\left(1 - \frac{(\mathbb{E}[\hat{e}_{l|l}\tilde{h}^*_{l|l-D}])^2}{2V^2 2\lambda'^2}\right). \tag{3.27}$$

Let $s = |\mathbb{E}[\hat{h}_{l|l}|\tilde{h}_{l|l-D}]|$ and $2\Omega^2 = \mathrm{Var}[\hat{h}_{l|l}|\tilde{h}_{l|l-D}]$. Conditioned on $\tilde{h}_{l|l-D}$, $|\hat{h}_{l|l}|^2$ is conditionally noncentral chi-square distributed with the PDF

$$p_{|\hat{h}_{l|l}|^2|\tilde{h}_{l|l-D}}(x|\tilde{h}_{l|l-D}) = \frac{1}{2\Omega^2}\exp\left(-\frac{x+s^2}{2\Omega^2}\right) I_0\left(\sqrt{x}\frac{s}{\Omega^2}\right) u(x), \tag{3.28}$$

where $u(\cdot)$ is the unit step function and $I_0(\cdot)$ is the modified Bessel function of the first kind of order zero. The conditional cumulative distribution function (CDF) of $|\hat{h}_{l|l}|^2$ can be represented as

$$F_{|\hat{h}_{l|l}|^2|\tilde{h}_{l|l-D}}(x|\tilde{h}_{l|l-D}) = 1 - Q\left(\frac{s}{\Omega}, \frac{\sqrt{x}}{\Omega}\right), \tag{3.29}$$

where $Q(a,b)$ is the first-order Marcum Q-function defined as

$$Q(a,b) = \int_b^\infty x\exp\left(-\frac{x^2+a^2}{2}\right) I_0(ax)dx, a \geq 0, b \geq 0. \tag{3.30}$$

It is also noted that conditioned on $\tilde{h}_{l|l-D}$, $|\hat{h}_{l|l}|$ is conditionally Rician distributed with the PDF

$$p_{|\hat{h}_{l|l}||\tilde{h}_{l|l-D}}(x|\tilde{h}_{l|l-D}) = \frac{x}{\Omega^2}\exp\left(-\frac{x^2+s^2}{2\Omega^2}\right) I_0\left(\frac{xs}{\Omega^2}\right), \tag{3.31}$$

and the CDF

$$F_{|\hat{h}_{l|l}||\tilde{h}_{l|l-D}}(x|\tilde{h}_{l|l-D}) = 1 - Q\left(\frac{s}{\Omega}, \frac{x}{\Omega}\right). \tag{3.32}$$

The Rician K-factor is represented as

$$K = \frac{s^2}{2\Omega^2}. \tag{3.33}$$

From the above point of view, transmission over the Rayleigh channel in the feedback system is equivalent to transmission over the Rician channel with the line-of-sight component $\tilde{h}_{l|l-D}$.

A Simplified Channel Estimation/Prediction Model

We consider here a simplified model of the channel estimation/prediction, where we only utilize the received pilot signals from one packet. In this case, an explicit relationship between the MMSE for estimation/predition and the N_pE_p can be obtained.

For channel estimation, to estimate h_l, the received pilot signals from the current l-th packet are used, and we have

$$\mathbf{R} = \mathbf{R}_0 + N_0\mathbf{I}_{N_p\times N_p} \tag{3.34}$$

and

$$\mathbf{v} = R(0)\sqrt{E_p}2\sigma^2[1 \quad 1 \quad \cdots \quad 1]^T. \tag{3.35}$$

Therefore, the variance of the estimation error $\hat{e}_{l|l}$ can be explicitly obtained as

$$2V^2 = \frac{2\sigma^2}{1+\frac{N_pE_p2\sigma^2}{N_0}}. \tag{3.36}$$

The variance of the estimate $\hat{h}_{l|l}$ is thus given by

$$2\lambda^2 = \frac{N_pE_p(2\sigma^2)^2}{N_pE_p2\sigma^2+N_0}. \tag{3.37}$$

For channel prediction, to predict h_l, the received pilot signals from the past D-th packet are used, and we have

$$\mathbf{R}' = \mathbf{R}_0 + N_0\mathbf{I}_{N_p\times N_p} \tag{3.38}$$

and

$$\mathbf{v}' = R(D)\sqrt{E_p}2\sigma^2[1 \quad 1 \quad \cdots \quad 1]^T. \tag{3.39}$$

Therefore, the variance of the prediction error $\tilde{e}_{l|l-D}$ is obtained as

$$2V'^2 = \frac{(1-R(D)^2)N_pE_p(2\sigma^2)^2+N_02\sigma^2}{N_pE_p2\sigma^2+N_0}, \tag{3.40}$$

and the variance of the predicted channel $\tilde{h}_{l|l-D}$ is given by

$$2\lambda'^2 = \frac{R(D)^2N_pE_p(2\sigma^2)^2}{N_pE_p2\sigma^2+N_0}. \tag{3.41}$$

These simplified results with explicit expressions are useful to analytical purpose.

3.3 BEP and BEOP of A Feedback System with Perfect CSI

In a feedback system with power control, the transmitted energy is some function of the CSI. This function is to be determined based on different power control strategies. Here, we obtain general expressions of the IBEP, the ABEP and the BEOP for a feedback system with perfect CSI.

With the assumption of perfect CSI, the transmitter is assumed to have the complete knowledge of the CSI of the forward channel. Therefore, the obtained performance measures at the transmitter are identical to those at the receiver. For coherent detection of equally likely symbol points, the IBEP can be represented as

$$F(\alpha|h_l) = \frac{1}{2}\text{erfc}\left(\frac{E_s|h_l|^2\cos^2\alpha}{N_0}\right)^{1/2}, \tag{3.42}$$

where α is some angle, and note that E_s is the transmitter energy to be chosen. With Gray mapping, $\alpha = 0$ and $\alpha = \pi/4$ refer to BPSK and QPSK modulations, respectively [92]. The ABEP is obtained as

$$F(\alpha) = \int_0^\infty \frac{1}{2}\text{erfc}\left(\frac{E_s x\cos^2\alpha}{N_0}\right)^{1/2} p_{|h_l|^2}(x)dx, \tag{3.43}$$

where

$$p_{|h_l|^2}(x) = \frac{1}{2\sigma^2}\exp\left(-\frac{1}{2\sigma^2}x\right)u(x) \tag{3.44}$$

is the PDF of $|h|^2$. The BEOP, according to its definition, is the probability

$$P_{\text{out}}(\alpha) \;=\; P\left(F(\alpha|h_l) > \varepsilon\right), \tag{3.45}$$

where ε is the IBEP threshold, which is a QoS-specified parameter that can be adjusted according to different QoS requirements. Keeping in mind that for a feedback system, the transmitted energy E_s is some value to be determined according to h_l. Therefore, now we cannot get an explicit result of the ABEP or the BEOP. However, for a non-feedback system, since E_s is fixed, the ABEP and the BEOP can

be explicitly evaluated using the distribution of h_l, and the results are, respectively, given by

$$F(\alpha) = \frac{1}{2}\left(1 - \sqrt{\frac{E_s 2\sigma^2 \cos^2\alpha}{N_0 + E_s 2\sigma^2 \cos^2\alpha}}\right), \tag{3.46}$$

and

$$P_{\text{out}}(\alpha) = 1 - \exp\left(-\frac{N_0 C}{E_s 2\sigma^2 \cos^2\alpha}\right), \tag{3.47}$$

where

$$C = \left(\text{erfc}^{-1}(2\varepsilon)\right)^2 \tag{3.48}$$

can be viewed as a constant related to a given IBEP threshold ε. In a feedback system, explicit results for the ABEP or the BEOP can only be obtained after the transmitted energy E_s is determined.

In the following two sections, we explore different power control laws with perfect CSI.

3.4 ABEP-based Power Control with Perfect CSI

In [6], Hayes has proposed a power control law to minimize the ABEP for the reception of binary modulated signals, subject to a constraint on the average transmitted power. Here, we generalize Hayes's work with both BPSK and QPSK modulations, and also analyze the outage performance.

3.4.1 Design of the Power Law

Our purpose is to minimize (3.43) subject to a constraint on the average transmitted power, or the average transmitted energy. The minimization problem whose solution gives the optimum transmitted energy is described as

$$\begin{aligned} \underset{E_s}{\text{minimize}} \quad F(\alpha) &= \int_0^\infty \frac{1}{2}\text{erfc}\left(\frac{E_s x \cos^2\alpha}{N_0}\right)^{1/2} p_{|h_l|^2}(x)dx \\ \text{subject to} \quad E_s^{\text{ave}} &= \int_0^\infty E_s p_{|h_l|^2}(x)dx, \end{aligned} \tag{3.49}$$

where E_s^{ave} denotes the specified average energy per symbol. Using the method of Lagrange multipliers [6, 10], we form an auxiliary function

$$\begin{aligned} L &= F(\alpha) + \mu\left(\int_0^\infty E_s p_{|h_l|^2}(x)dx - E_s^{\text{ave}}\right) \\ &= \int_0^\infty \left[\frac{1}{2}\text{erfc}\left(\frac{E_s x\cos^2\alpha}{N_0}\right)^{1/2} + \mu E_s\right] p_{|h_l|^2}(x)dx - \mu E_s^{\text{ave}}, \end{aligned} \tag{3.50}$$

where μ is the Lagrange multiplier. It is noted that L is minimized if $\frac{1}{2}\text{erfc}\left(\frac{E_s x\cos^2\alpha}{N_0}\right)^{1/2} + \mu E_s$ is minimized for every single realization of $x = |h_l|^2$. Let

$$L_{\text{ins}} = \frac{1}{2}\text{erfc}\left(\frac{E_s|h_l|^2\cos^2\alpha}{N_0}\right)^{1/2} + \mu E_s. \tag{3.51}$$

We have

$$\frac{d}{dE_s}L_{\text{ins}} = -\frac{1}{2\sqrt{\pi}}\exp\left(-\frac{E_d|h_l|^2\cos^2\alpha}{N_0}\right)E_s^{-1/2}\left(\frac{|h_l|^2\cos^2\alpha}{N_0}\right)^{1/2} + \mu. \tag{3.52}$$

It can be shown that $\frac{d^2}{dE_s^2}L_{\text{ins}} > 0$. Therefore, solving $\frac{d}{dE_d}L_{\text{ins}} = 0$ for E_s gives the optimal E_s that minimizes L_{ins}, and the solution is

$$E_s = \frac{W\left(\frac{1}{8\pi\mu^2}\left(\frac{2|h_l|^2\cos^2\alpha}{N_0}\right)^2\right)}{\left(\frac{2|h_l|^2\cos^2\alpha}{N_0}\right)}, \tag{3.53}$$

where $W(\cdot)$ is the *Lambert W function*, which is defined as the function that satisfies the equation

$$W(z)e^{W(z)} = z. \tag{3.54}$$

Substituting (3.44) and (3.53) into (3.49), we have

$$E_s^{\text{ave}} = \int_0^\infty \frac{W\left(\frac{1}{8\pi\mu^2}\left(\frac{2x\cos^2\alpha}{N_0}\right)^2\right)}{\left(\frac{2x\cos^2\alpha}{N_0}\right)}\frac{1}{2\sigma^2}e^{-\frac{1}{2\sigma^2}x}dx. \tag{3.55}$$

From (3.55), it is seen that for any given E_s^{ave}, μ can be numerically solved. Substituting the solved μ into (3.53) gives the optimum transmitted energy E_s that minimizes $F(\alpha)$. Eq. (3.53) is recognized as the transmitted power law.

We observe from (3.53) that the transmitted energy E_s is a function of $|h_l|^2$. This means that only the magnitude of the channel fading gain needs to be fed back from the receiver to the transmitter. This has also been mentioned in [6]. Actually, as we will see, for the purpose of power control, this is a general case. In practice, this observation helps the feedback system reduce the size of feedback information.

3.4.2 Performance Analysis

ABEP

The ABEP is easily obtained by substituting (3.44) and (3.53) into (3.43), and is explicitly given by

$$F(\alpha)=\int_0^{\infty}\frac{1}{2}\mathrm{erfc}\left(\frac{W\left(\frac{1}{8\pi\mu^2}\left(\frac{2x\cos^2\alpha}{N_0}\right)^2\right)}{2}\right)^{1/2}\frac{1}{2\sigma^2}e^{-\frac{1}{2\sigma^2}x}dx. \tag{3.56}$$

BEOP

Using (3.45), the BEOP is given by

$$\begin{aligned}P_{\text{out}}(\alpha) &= P\left(F(\alpha|h_l)>\varepsilon\right)\\ &= P\left(\frac{1}{2}\mathrm{erfc}\left(\frac{E_s|h_l|^2\cos^2\alpha}{N_0}\right)^{1/2}>\varepsilon\right).\end{aligned} \tag{3.57}$$

Substituting (3.53) into the above and after some manipulation, we obtain the BEOP as

$$P_{\text{out}}(\alpha) = P\left(W\left(\frac{1}{8\pi\mu^2}\left(\frac{2|h_l|^2\cos^2\alpha}{N_0}\right)^2\right)<2C\right). \tag{3.58}$$

To compute (3.58), we introduce the following lemma.

Lemma 3.1 For any real numbers $A\geq 0$ and $B>0$, we have

$$W(A)\leq B \Leftrightarrow A\leq Be^B. \tag{3.59}$$

Proof: The *Lambert W function* can be defined as the inverse function of $A=Be^B$, i.e., $B=W(A)$. It is noted that when $A\geq 0$, $W(A)$ is a monotonically increasing

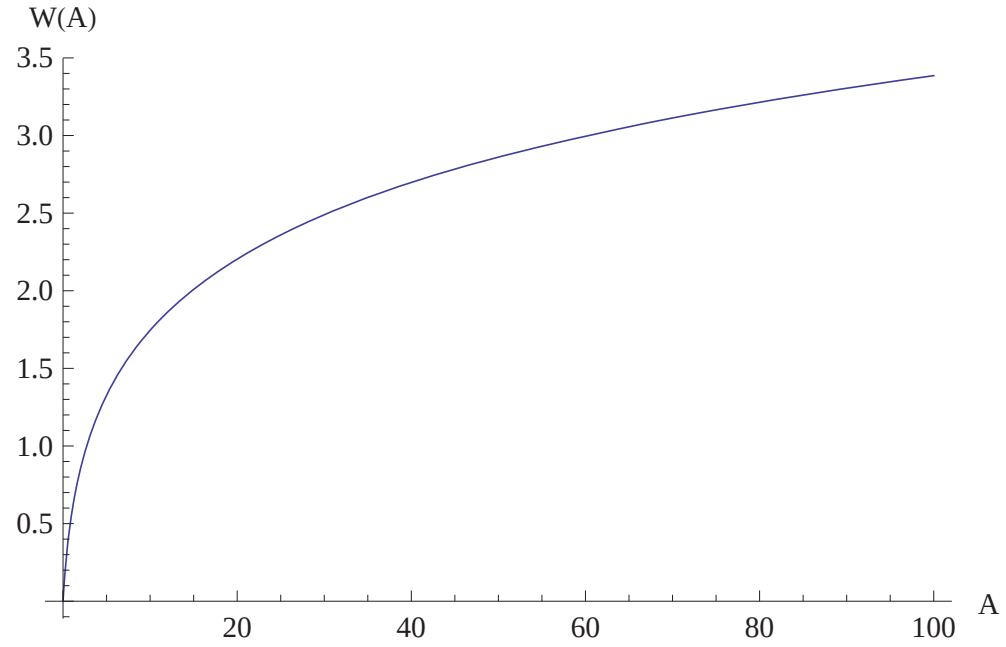

Figure 3.1: Plot of the *Lambert W function* $W(A)$ for $A \geq 0$.

function of A, and $W(A) \geq 0$, as shown in Fig 3.1. Therefore, it is easy to see that for any $A \geq 0$ and $B > 0$, eq.(3.59) stands.

□

Using Lemma 3.1, (3.58) can be further evaluated as

$$\begin{aligned} P_{\text{out}}(\alpha) &= P\left(|h_l|^2 < \frac{N_0}{\cos^2\alpha}\sqrt{4\pi\mu^2 C e^{2C}}\right) \\ &= 1 - \exp\left(-\frac{N_0}{2\sigma^2\cos^2\alpha}\sqrt{4\pi\mu^2 C e^{2C}}\right). \end{aligned} \tag{3.60}$$

We emphasize that μ is chosen from (3.55) for a given E_s^{ave}, and therefore, $P_{\text{out}}(\alpha)$ is a function of E_s^{ave}.

3.5 BEOP-based Power Control with Perfect CSI

In this section, we consider the design of the power control law from the perspective of BEOP with perfect CSI. We propose to choose the transmitted energy such that

the BEOP would not exceed some QoS-specified threshold, say, δ. At the same time, we want the minimum transmitted energy consumption. The BEOP has been defined in (3.45). Substituting (3.42) into (3.45), we rewrite the BEOP as

$$P_{\text{out}}(\alpha) = P\left(E_s|h_l|^2 < \frac{N_0 C}{\cos^2\alpha}\right), \tag{3.61}$$

where C has been defined as $C = \left(\text{erfc}^{-1}(2\varepsilon)\right)^2$, and ε is the IBEP threshold. We note from here that E_s can be adjusted according to $|h_l|^2$ such that $E_s|h_l|^2 = \frac{N_0 C}{\cos^2\alpha}$, i.e., $E_s = \frac{N_0 C}{|h_l|^2\cos^2\alpha}$. If so, the BEOP would be zero with the minimum consumption of energy. However, when h_l tends to zero, E_s tends to infinity. Usually, the transmitter power of a communication system is limited to a certain peak power. When the transmission rate and the symbol duration are fixed, this is equivalent to a limit on the transmitted energy, say, E_{pk}. Therefore, it is straightforward that when the channel adaptive E_s exceeds E_{pk}, $E_s|h_l|^2$ is less than $\frac{N_0 C}{\cos^2\alpha}$, and an outage happens. From this point of view, the obtained BEOP itself is the QoS-specified threshold δ. The BEOP is related to the peak energy constraint E_{pk}, and their relationship indicates how much peak energy is required to ensure the BEOP being no more than the QoS-specified BEOP threshold δ. Based on the above observations, next, we formulate the power law.

3.5.1 Formulation of the Power Law

From the above discussion, the power law under a peak energy constraint E_{pk} is given by

$$E_s = \begin{cases} \frac{N_0 C}{|h_l|^2\cos^2\alpha}, & |h_l|^2 \geq \frac{N_0 C}{E_{\text{pk}}\cos^2\alpha} \\ E_{\text{pk}}, & |h_l|^2 < \frac{N_0 C}{E_{\text{pk}}\cos^2\alpha} \end{cases} \tag{3.62}$$

Again, we note from (3.62) that only the magnitude of h_l is needed for power adjustment at the transmitter. According to the definition of a BEO event, the BEOP of this power law is simply calculated as

$$\begin{aligned} P_{\text{out}}(\alpha) &= P\left(\frac{N_0 C}{|h_l|^2\cos^2\alpha} > E_{\text{pk}}\right) \\ &= 1 - \exp\left(-\frac{N_0 C}{E_{\text{pk}} 2\sigma^2\cos^2\alpha}\right), \end{aligned} \tag{3.63}$$

The IBEP threshold ε, the BEOP threshold δ and the peak transmitter energy $E_{\rm pk}$ are related through

$$1-\exp\left(-\frac{N_0C}{E_{\rm pk}2\sigma^2\cos^2\alpha}\right)=\delta, \tag{3.64}$$

i.e., given ε (or say, C), to keep the BEOP within δ, a minimum peak energy indicated by (3.64) is required. Solving (3.64) for $E_{\rm pk}$, and noting that $C=\left(\text{erfc}^{-1}(2\varepsilon)\right)^2$, we have

$$E_{\rm pk}=\frac{N_0\left(\text{erfc}^{-1}(2\varepsilon)\right)^2}{2\sigma^2\cos^2\alpha\ln(1-\delta)^{-1}}. \tag{3.65}$$

It is clear that as ε decreases or as δ decreases, the required $E_{\rm pk}$ increases. The average energy of this power law is obtained by averaging (3.62) over the distribution of h_l, and we have

$$E_s^{\rm ave} = \int_0^{\frac{N_0C}{E_{\rm pk}\cos^2\alpha}} E_{\rm pk}p_{|h_l|^2}(x)dx+\int_{\frac{N_0C}{E_{\rm pk}\cos^2\alpha}}^{\infty}\frac{N_0C}{x\cos^2\alpha}p_{|h_l|^2}(x)dx. \tag{3.66}$$

The first integral is easy to calculate, and the second integral can be calculated by changing the variable appropriately. The explicit result is given by

$$E_s^{\rm ave} = E_{\rm pk}\left(1-e^{-\frac{N_0C}{E_{\rm pk}2\sigma^2\cos^2\alpha}}\right)+\frac{N_0C}{2\sigma^2\cos^2\alpha}\Gamma\left(0,\frac{N_0C}{E_{\rm pk}2\sigma^2\cos^2\alpha}\right), \tag{3.67}$$

where $\Gamma(a,x)$ denotes the upper incomplete gamma function defined as

$$\Gamma(a,x)\triangleq\int_x^{\infty}t^{a-1}e^{-t}dt. \tag{3.68}$$

3.5.2 ABEP Analysis

The BEOP of the power law described by (3.62) has been shown in (3.63). Substituting (3.62) into (3.43), the ABEP is given by

$$\begin{aligned}F(\alpha) = &\int_0^{\frac{N_0C}{E_{\rm pk}\cos^2\alpha}}\frac{1}{2}\text{erfc}\left(\frac{E_{\rm pk}x\cos^2\alpha}{N_0}\right)^{1/2}p_{|h_l|^2}(x)dx+\\ &\int_{\frac{N_0C}{E_{\rm pk}\cos^2\alpha}}^{\infty}\frac{1}{2}\text{erfc}\,(C)^{1/2}\,p_{|h_l|^2}(x)dx\end{aligned} \tag{3.69}$$

The second integral is easy to calculate, and the result is

$$\int_{\frac{N_0 C}{E_{\rm pk}\cos^2\alpha}}^{\infty} \frac{1}{2}\mathrm{erfc}\,(C)^{1/2}\, p_{|h_l|^2}(x)dx = \varepsilon \exp\left(-\frac{N_0 C}{E_{\rm pk} 2\sigma^2 \cos^2\alpha}\right). \tag{3.70}$$

Denoting the first integral by I, it can be evaluated as follows. Writing the erfc function in its integral form, we have

$$I = \frac{1}{\sqrt{\pi}2\sigma^2}\int_0^{\frac{N_0 C}{E_{\rm pk}\cos^2\alpha}} \int_{\sqrt{\frac{E_{\rm pk} x\cos^2\alpha}{N_0}}}^{\infty} e^{-t^2}dt\; e^{-\frac{1}{2\sigma^2}x}dx \tag{3.71}$$

Letting $y = \sqrt{\frac{E_{\rm pk} x\cos^2\alpha}{N_0}}$ and interchanging the order of integration, we have

$$\begin{aligned} I = \frac{1}{\sqrt{\pi}2\sigma^2}\Bigg(&\int_0^{\sqrt{C}}\int_0^{t} e^{-\frac{1}{2\sigma^2}\frac{N_0}{E_{\rm pk}\cos^2\alpha}y^2}\frac{N_0}{E_{\rm pk}\cos^2\alpha}dy^2\; e^{-t^2}dt + \\ &\int_{\sqrt{C}}^{\infty}\int_0^{\sqrt{C}} e^{-\frac{1}{2\sigma^2}\frac{N_0}{E_{\rm pk}\cos^2\alpha}y^2}\frac{N_0}{E_{\rm pk}\cos^2\alpha}dy^2\; e^{-t^2}dt\Bigg). \end{aligned} \tag{3.72}$$

Simplifying (3.72), we have

$$\begin{aligned} I = \frac{1}{2} - \frac{1}{2}\frac{1}{\sqrt{1+\frac{N_0}{E_{\rm pk}2\sigma^2\cos^2\alpha}}}\left(1-\mathrm{erfc}\left(\sqrt{C\left(1+\frac{N_0}{E_{\rm pk}2\sigma^2\cos^2\alpha}\right)}\right)\right) - \\ \varepsilon\exp\left(-\frac{N_0 C}{E_{\rm pk}2\sigma^2\cos^2\alpha}\right). \end{aligned} \tag{3.73}$$

Letting $\gamma_{\rm pk} = \frac{E_{\rm pk}2\sigma^2\cos^2\alpha}{N_0}$ and substituting (3.70) and (3.73) into (3.69), we finally get

$$F(\alpha) = \frac{1}{2} - \frac{1}{2}\sqrt{\frac{\gamma_{\rm pk}}{1+\gamma_{\rm pk}}}\left(1-\mathrm{erfc}\left(\sqrt{C\left(1+\frac{1}{\gamma_{\rm pk}}\right)}\right)\right). \tag{3.74}$$

In Section 3.4, we reviewed the ABEP-based power law and extended it to the QPSK case. In Section 3.5, we proposed and analyzed the BEOP-based power law. Next, we develop both laws for the imperfect CSI case. We first analyze the BEP and the BEOP in general for a feedback system with imperfect CSI.

3.6 BEP and BEOP of A Feedback System with Imperfect CSI

It is noted that in a feedback system with imperfect CSI, since the CSIR and the CSIT are different, the BEP and the BEOP need to be considered from the receiver side and from the transmitter side, separately.

In the imperfect CSI case, we assume that the transmitted energy per pilot symbol E_p is fixed. Therefore, we only need to adjust the transmitted energy per data symbol E_d. We emphasize that the transmitter can only utilize the CSIT to adjust E_d. When a signal arrives at the receiver, the receiver makes a decision based on the newly obtained CSIR, which is different from the CSIT that has been used to adjust E_d. From the viewpoint of the transmitter, the IBEP is obtained using the predicted channel fading gain $\tilde{h}_{l|l-D}$, and is given by

$$F^{\mathrm{X}}(\alpha|\tilde{h}_{l|l-D}) = \frac{1}{2}\mathrm{erfc}\left(\frac{E_d|\tilde{h}_{l|l-D}|^2\cos^2\alpha}{E_d 2V'^2 + N_0}\right)^{1/2}. \tag{3.75}$$

The superscript X denotes the viewpoint of the transmitter. Averaging (3.75) over the PDF of $|\tilde{h}_{l|l-D}|^2$ gives the ABEP at the transmitter

$$F^{\mathrm{X}}(\alpha) = \int_0^\infty \frac{1}{2}\mathrm{erfc}\left(\frac{E_d x\cos^2\alpha}{E_d 2V'^2 + N_0}\right)^{1/2} p_{|\tilde{h}_{l|l-D}|^2}(x)dx, \tag{3.76}$$

where

$$p_{|\tilde{h}_{l|l-D}|^2}(x) = \frac{1}{2\lambda'^2}e^{-\frac{1}{2\lambda'^2}x}u(x). \tag{3.77}$$

The BEOP at the transmitter is the probability

$$P^{\mathrm{X}}_{\mathrm{out}}(\alpha) \;=\; P\left(F^{\mathrm{X}}(\alpha|\tilde{h}_{l|l-D}) > \varepsilon\right). \tag{3.78}$$

From the viewpoint of the receiver, the IBEP is obtained using $\hat{h}_{l|l}$, and is given by

$$F(\alpha|\hat{h}_{l|l}) = \frac{1}{2}\mathrm{erfc}\left(\frac{E_d|\hat{h}_{l|l}|^2\cos^2\alpha}{E_d 2V^2 + N_0}\right)^{1/2}. \tag{3.79}$$

Its average is given by

$$F(\alpha) = \int_0^\infty \frac{1}{2}\text{erfc}\left(\frac{E_d x \cos^2\alpha}{E_d 2V^2 + N_0}\right)^{1/2} p_{|\hat{h}_{l|l}|^2}(x)dx, \tag{3.80}$$

where

$$p_{|\hat{h}_{l|l}|^2}(x) = \frac{1}{2\lambda^2}\exp\left(-\frac{1}{2\lambda^2}x\right)u(x) \tag{3.81}$$

is the PDF of $|\hat{h}_{l|l}|^2$. The BEOP at the receiver is the probability

$$P_{\text{out}}(\alpha) \;=\; P\left(F(\alpha|\hat{h}_{l|l}) > \varepsilon\right). \tag{3.82}$$

Similar to that in the perfect CSI case, for a non-feedback system, the ABEP and the BEOP can be explicitly determined. They are given, respectively, by

$$F(\alpha) \;=\; \frac{1}{2}\left(1 - \sqrt{\frac{E_d 2\sigma^2\cos^2\alpha}{E_d 2V^2 + N_0 + E_d 2\sigma^2\cos^2\alpha}}\right), \tag{3.83}$$

and

$$P_{\text{out}}(\alpha) \;=\; 1 - \exp\left(-\frac{(E_d 2V^2 + N_0)C}{E_d 2\sigma^2\cos^2\alpha}\right), \tag{3.84}$$

where $C = \left(\text{erfc}^{-1}(2\varepsilon)\right)^2$ has been defined in (3.48).

In the following two sections, we explore different power control laws with imperfect CSI.

3.7 ABEP-based Power Control with Imperfect CSI

In the perfect CSI case, the ABEP-based power law is designed subject to a constraint on the average transmitted energy per symbol. In the imperfect CSI case, since pilot symbols are used, it is more reasonable to assume a constraint on the average energy per packet. Assuming the average packet energy is fixed at E_{pkt}, it is related to the effective average energy per data symbol $E_d^{\text{eff-ave}}$, as shown in (3.2). Therefore, a constraint on the E_{pkt} can also be represented as a constraint

on $E_d^{\text{eff-ave}}$. Moreover, besides minimizing the ABEP by adjusting the transmitted energy E_d, using the power allocation factor ξ, we can also decide the optimal power allocation between the pilot symbols and the data symbols.

With imperfect CSI, the ABEP at the transmitter has been shown in (3.80). The minimization problem is formulated as

$$\begin{aligned} \underset{E_d}{\text{minimize}} \quad F^{\text{X}}(\alpha) &= \int_0^\infty \frac{1}{2}\text{erfc}\left(\frac{E_d x\cos^2\alpha}{E_d 2V'^2 + N_0}\right)^{1/2} p_{|\tilde{h}_{l|l-D}|^2}(x)dx \\ \text{subject to} \quad E_d^{\text{eff-ave}} &= \int_0^\infty E_d p_{|\tilde{h}_{l|l-D}|^2}(x)dx. \end{aligned} \tag{3.85}$$

Using the method of Lagrange multipliers, and following the steps in Section 3.4, we find the equation that gives the optimal solution of E_d as

$$-\frac{1}{2\sqrt{\pi}}\exp\left(-\frac{E_d|\tilde{h}_{l|l-D}|^2\cos^2\alpha}{E_d 2V'^2 + N_0}\right)\frac{E_d^{-1/2}|\tilde{h}_{l|l-D}|\cos\alpha N_0}{(E_d 2V'^2 + N_0)^{3/2}} + \mu = 0, \tag{3.86}$$

where μ is the Lagrange multiplier. It is noted from (3.86) that an explicit expression of E_d is unobtainable. This expression of E_d is necessary, as we need to substitute it into (3.85) to obtain the value of μ subject to a given $E_d^{\text{eff-ave}}$. One way is to numerically solve for E_d for any given $|\tilde{h}_{l|l-D}|$ and a fixed μ, and solve for $E_d^{\text{eff-ave}}$ numerically from (3.85). However, this numerical calculation does not provide any useful expressions for the system performance. To make the performance analyzable and more tractable, we consider the following two approximate solutions for E_d.

3.7.1 Approximation 1

In this scenario, the transmitter views $\tilde{h}_{l|l-D}$ as if it were the true channel with no channel estimation errors. Therefore, the IBEP from the transmitter's view becomes

$$F^{\text{X}}(\alpha|\tilde{h}_{l|l-D}) = \frac{1}{2}\text{erfc}\left(\frac{E_d|\tilde{h}_{l|l-D}|^2\cos^2\alpha}{N_0}\right)^{1/2}. \tag{3.87}$$

The corresponding ABEP is obtained as

$$F^{\text{X}}(\alpha) = \int_0^\infty \frac{1}{2}\text{erfc}\left(\frac{E_d x\cos^2\alpha}{N_0}\right)^{1/2} p_{|\tilde{h}_{l|l-D}|^2}(x)dx. \tag{3.88}$$

The minimization problem is now

$$\begin{aligned} \underset{E_d}{\text{minimize}} \quad F^{\text{X}}(\alpha) &= \int_0^\infty \frac{1}{2}\text{erfc}\left(\frac{E_d x\cos^2\alpha}{N_0}\right)^{1/2} p_{|\tilde{h}_{l|l-D}|^2}(x)dx \\ \text{subject to} \quad E_d^{\text{eff-ave}} &= \int_0^\infty E_d p_{|\tilde{h}_{l|l-D}|^2}(x)dx. \end{aligned} \tag{3.89}$$

It describes the same minimization problem that has been solved in Section 3.4.1, except that the distribution of the channel changes. Following Section 3.4.1, the solution of E_d is given by

$$E_d = \frac{W\left(\frac{1}{8\pi\mu^2}\left(\frac{2|\tilde{h}_{l|l-D}|^2\cos^2\alpha}{N_0}\right)^2\right)}{\left(\frac{2|\tilde{h}_{l|l-D}|^2\cos^2\alpha}{N_0}\right)}, \tag{3.90}$$

where for a given $E_d^{\text{eff-ave}}$, μ is solved from

$$E_d^{\text{eff-ave}} = \int_0^\infty \frac{W\left(\frac{1}{8\pi\mu^2}\left(\frac{2x\cos^2\alpha}{N_0}\right)^2\right)}{\left(\frac{2x\cos^2\alpha}{N_0}\right)} \frac{1}{2\lambda'^2} e^{-\frac{1}{2\lambda'^2}x}dx. \tag{3.91}$$

Eq. (3.90) is an approximate solution for the minimization problem described in (3.85).

ABEP Analysis

Substituting (3.90) into (3.42), we obtain the IBEP at the receiver as

$$\begin{aligned} F(\alpha|\hat{h}_{l|l}) &= \frac{1}{2}\text{erfc}\left(\frac{E_d|\hat{h}_{l|l}|^2\cos^2\alpha}{E_d 2V^2 + N_0}\right)^{1/2} \\ &= \frac{1}{2}\text{erfc}\left(\frac{\frac{W\left(\frac{1}{8\pi\mu^2}\left(\frac{2|\tilde{h}_{l|l-D}|^2\cos^2\alpha}{N_0}\right)^2\right)}{\left(\frac{2|\tilde{h}_{l|l-D}|^2\cos^2\alpha}{N_0}\right)}|\hat{h}_{l|l}|^2\cos^2\alpha}{\frac{W\left(\frac{1}{8\pi\mu^2}\left(\frac{2|\tilde{h}_{l|l-D}|^2\cos^2\alpha}{N_0}\right)^2\right)}{\left(\frac{2|\tilde{h}_{l|l-D}|^2\cos^2\alpha}{N_0}\right)}2V^2 + N_0}\right)^{1/2}. \end{aligned} \tag{3.92}$$

It is noted that (3.92) contains both $\tilde{h}_{l|l-D}$ and $\hat{h}_{l|l}$. To compute the ABEP, we need to average (3.92) over $\tilde{h}_{l|l-D}$ and $\hat{h}_{l|l}$, respectively. In Section 3.2.3, we have shown that conditioned on $\tilde{h}_{l|l-D}$, $|\hat{h}_{l|l}|^2$ is conditionally noncentral chi-square

distributed, and the conditional PDF is given by (3.28). We first average (3.92) over $\hat{h}_{l|l}$ conditioned on $\tilde{h}_{l|l-D}$ being fixed. For notational simplicity, we let

$$a_1(|\tilde{h}_{l|l-D}|^2) = \frac{\frac{W\left(\frac{1}{8\pi\mu^2}\left(\frac{2|\tilde{h}_{l|l-D}|^2\cos^2\alpha}{N_0}\right)^2\right)}{\left(\frac{2|\tilde{h}_{l|l-D}|^2\cos^2\alpha}{N_0}\right)}\cos^2\alpha}{\frac{W\left(\frac{1}{8\pi\mu^2}\left(\frac{2|\tilde{h}_{l|l-D}|^2\cos^2\alpha}{N_0}\right)^2\right)}{\left(\frac{2|\tilde{h}_{l|l-D}|^2\cos^2\alpha}{N_0}\right)}2V^2 + N_0}. \tag{3.93}$$

Averaging (3.92) over the conditional PDF of $|\hat{h}_{l|l}|^2$ conditioned on $\tilde{h}_{l|l-D}$ gives

$$F(\alpha|\tilde{h}_{l|l-D}) = \int_0^\infty \frac{1}{2}\text{erfc}\left(a_1(|\tilde{h}_{l|l-D}|^2)x\right)^{1/2} p_{|\hat{h}_{l|l}|^2|\tilde{h}_{l|l-D}}(x|\tilde{h}_{l|l-D})dx. \tag{3.94}$$

Using [49, eq.(5.12)] and changing the variables accordingly, (3.94) can be computed as

$$\begin{aligned} F(\alpha|\tilde{h}_{l|l-D}) &= \frac{1}{\pi}\int_0^{\pi/2}\left(\frac{\sin^2\theta}{\sin^2\theta + 2\Omega^2 a_1(|\tilde{h}_{l|l-D}|^2)}\right)\times \\ &\quad \exp\left(-\frac{s^2 a_1(|\tilde{h}_{l|l-D}|^2)}{\sin^2\theta + 2\Omega^2 a_1(|\tilde{h}_{l|l-D}|^2)}\right)d\theta. \end{aligned} \tag{3.95}$$

In the above, recall from Section 3.2.3, $s = |\mathbb{E}[\hat{h}_{l|l}|\tilde{h}_{l|l-D}]|$ and $2\Omega^2 = \text{Var}[\hat{h}_{l|l}|\tilde{h}_{l|l-D}]$ are the conditional mean and variance of $\hat{h}_{l|l}$ conditioned on $\tilde{h}_{l|l-D}$, respectively. We assume that the channel estimation at the receiver is very accurate to generate a very small estimation error $\hat{e}_{l|l}$, such that $\hat{e}_{l|l}$ and $\tilde{h}_{l|l-D}$ can be assumed to be uncorrelated. Therefore, from (3.24) and (3.25), we have

$$s = |\tilde{h}_{l|l-D}|,\ 2\Omega^2 = 2V'^2 + 2V^2. \tag{3.96}$$

Substituting (3.96) into (3.95) and averaging (3.95) over the PDF of $|\tilde{h}_{l|l-D}|^2$, the ABEP at the receiver is explicitly obtained as

$$\begin{aligned} F(\alpha) &= \frac{1}{\pi}\int_0^\infty\int_0^{\pi/2}\left(\frac{\sin^2\theta}{\sin^2\theta + 2\Omega^2 a_1(x)}\right)\exp\left(-\frac{x a_1(x)}{\sin^2\theta + 2\Omega^2 a_1(x)}\right)d\theta \times \\ &\quad \frac{1}{2\lambda'^2}e^{-\frac{1}{2\lambda'^2}x}dx. \end{aligned} \tag{3.97}$$

For the special case where $2V'^2 = 0$ and $2V^2 = 0$, (3.97) reduces to (3.56).

BEOP Analysis

Substituting (3.92) into (3.82), and using the definition of $a_1(|\tilde{h}_{l|l-D}|^2)$ in (3.93), the BEOP at the receiver can be computed as

$$P_{\text{out}}(\alpha) = P\left(|\hat{h}_{l|l}|^2 < \frac{C}{a_1(|\tilde{h}_{l|l-D}|^2)}\right), \tag{3.98}$$

where $C = \left(\text{erfc}^{-1}(2\varepsilon)\right)^2$ has been defined in (3.48). Using the conditional CDF of $|\hat{h}_{l|l}|^2$ conditioned on $\tilde{h}_{l|l-D}$ which has been shown in (3.29), conditioned on $\tilde{h}_{l|l-D}$, (3.98) can be evaluated as

$$P_{\text{out}}(\alpha|\tilde{h}_{l|l-D}) = 1 - Q\left(\frac{s}{\Omega}, \frac{\sqrt{\frac{C}{a_1(|\tilde{h}_{l|l-D}|^2)}}}{\Omega}\right). \tag{3.99}$$

Based on the observations in (3.96), (3.99) is a function of $|\tilde{h}_{l|l-D}|^2$. Averaging (3.99) over the PDF of $|\tilde{h}_{l|l-D}|^2$, the BEOP at the receiver is explicitly obtained as

$$P_{\text{out}}(\alpha) = 1 - \int_0^\infty Q\left(\frac{\sqrt{x}}{\Omega}, \frac{\sqrt{\frac{C}{a_1(x)}}}{\Omega}\right) \frac{1}{2\lambda'^2} e^{-\frac{1}{2\lambda'^2}x} dx. \tag{3.100}$$

Optimal Power Allocation

We note from (3.91) that the Lagrange multiplier μ is some function of the power allocation factor ξ. Suppose this function is denoted by $\mu = Z(\xi)$. Substituting $Z(\xi)$ into (3.97) and (3.100), the ABEP and the BEOP can be represented as a function of ξ, respectively. By adjusting ξ, it is possible to optimize the ABEP or the BEOP. However, from (3.91), the explicit form of $Z(\xi)$ cannot be obtained, and therefore the optimal ξ is not theoretically analyzable. Nevertheless, using numerical calculations, we can find a suitable ξ for each given $E_d^{\text{eff-ave}}$. This will be further discussed later in Section 3.9.2.

3.7.2 Approximation 2

We note from (3.86) that the difficulty of solving for E_d lies in that E_d appears in the denominator in the form of $E_d 2V'^2 + N_0$. In this scenario, we assume that $2V'^2$,

which is the MMSE of the channel prediction process, is very small, such that for the term $E_d 2V'^2 + N_0$, N_0 dominates its value. Therefore, we replace the E_d in the denominator by its average $E_d^{\text{eff-ave}}$. Now, in (3.86), the E_d in the numerator is solvable and is given by

$$E_d = \frac{W\left(\frac{1}{8\pi\mu^2}\left(\frac{2N_0|\tilde{h}_{l|l-D}|^2\cos^2\alpha}{(E_d^{\text{eff-ave}}2V'^2+N_0)^2}\right)^2\right)}{\left(\frac{2|\tilde{h}_{l|l-D}|^2\cos^2\alpha}{E_d^{\text{eff-ave}}2V'^2+N_0}\right)}, \tag{3.101}$$

where for a given $E_d^{\text{eff-ave}}$, μ is solved from

$$E_d^{\text{eff-ave}} = \int_0^\infty \frac{W\left(\frac{1}{8\pi\mu^2}\left(\frac{2N_0x\cos^2\alpha}{(E_d^{\text{eff-ave}}2V'^2+N_0)^2}\right)^2\right)}{\left(\frac{2x\cos^2\alpha}{E_d^{\text{eff-ave}}2V'^2+N_0}\right)}\frac{1}{2\lambda'^2}e^{-\frac{1}{2\lambda'^2}x}dx. \tag{3.102}$$

Eq. (3.101) is another approximate solution for the minimization problem described in (3.85).

Following Section 3.7.1, the ABEP at the receiver is obtained as

$$\begin{aligned} F(\alpha) &= \frac{1}{\pi}\int_0^\infty\int_0^{\pi/2}\left(\frac{\sin^2\theta}{\sin^2\theta+2\Omega^2a_2(x)}\right)\exp\left(-\frac{xa_2(x)}{\sin^2\theta+2\Omega^2a_2(x)}\right)d\theta\times \\ &\quad \frac{1}{2\lambda'^2}e^{-\frac{1}{2\lambda'^2}x}dx, \end{aligned} \tag{3.103}$$

where $a_2(x)$ is defined as

$$a_2(x) = \frac{\frac{W\left(\frac{1}{8\pi\mu^2}\left(\frac{2N_0x\cos^2\alpha}{(E_d^{\text{eff-ave}}2V'^2+N_0)^2}\right)^2\right)}{\left(\frac{2x\cos^2\alpha}{E_d^{\text{eff-ave}}2V'^2+N_0}\right)}\cos^2\alpha}{\frac{W\left(\frac{1}{8\pi\mu^2}\left(\frac{2N_0x\cos^2\alpha}{(E_d^{\text{eff-ave}}2V'^2+N_0)^2}\right)^2\right)}{\left(\frac{2x\cos^2\alpha}{E_d^{\text{eff-ave}}2V'^2+N_0}\right)}2V^2+N_0}. \tag{3.104}$$

For the special case where $2V'^2 = 0$ and $2V^2 = 0$, (3.103) reduces to (3.56). The BEOP at the receiver is given by

$$P_{\text{out}}(\alpha) = 1 - \int_0^\infty Q\left(\frac{\sqrt{x}}{\Omega}, \frac{\sqrt{\frac{C}{a_2(x)}}}{\Omega}\right)\frac{1}{2\lambda'^2}e^{-\frac{1}{2\lambda'^2}x}dx. \tag{3.105}$$

Similar to that in Section 3.7.1, the optimal power allocation can be solved through numerical calculations.

3.8 BEOP-based Power Control with Imperfect CSI

Under imperfect CSI, the purpose of design is to choose a suitable transmitter energy per data symbol E_d, such that the BEOP at the receiver would not exceed some QoS-specified threshold δ. We emphasize the phrase *at the receiver*, since under imperfect CSI, the CSIT is different from the CSIR, and the power law can only utilize the CSIT. Suppose the transmitter adjusts E_d to let the IBEP at the transmitter fit the same IBEP threshold ε as that employed by the receiver, such that the BEOP at the transmitter is kept within δ. By doing so, the BEOP at the receiver may be much greater than δ. Indeed, this phenomenon has been shown by our simulations. The reason is that the CSIT and the CSIR are different, and the value of the BEOP is very sensitive to the chosen IBEP threshold ε. More specifically, suppose that the transmitter adjusts E_d according to the CSIT such that the IBEP at the transmitter is fixed at ε. Therefore, the minimum energy is consumed to ensure zero outage from the viewpoint of the transmitter. However, when a symbol is actually received at the receiver, the CSIR is used for detection. If the CSIR $|\hat{h}_{l|l}|$ is smaller than the CSIT $|\tilde{h}_{l|l-D}|$, the outage-free transmission from the viewpoint of the transmitter is not true from the viewpoint of the receiver, as the IBEP at the receiver exceeds ε. Based on these observations, it is suggested that the transmitter should have a more stringent requirement on the IBEP threshold, to tolerate the variation of the CSIR from the CSIT.

To solve the problem, we consider to design the power law with the aid of a multiplicative factor κ. At the receiver, a BEO event is defined as the event that the IBEP of the received bit exceeds the IBEP threshold ε. Now, at the transmitter, we define a new BEO event as the event that the transmitter predicted IBEP exceeds a new threshold, say, $\kappa\varepsilon$. By adjusting κ, we can achieve the desired δ at the receiver. In the following, we formulate the power law and analyze its performance. We use BEOPT and BEOPR to denote the BEOP at the transmitter and at the receiver,

respectively.

3.8.1 Formulation of the Power Law

In this subsection, we formulate the power law based on the above observations. From the viewpoint of the transmitter, the IBEP and the BEOP have been given by (3.75) and (3.78), respectively. Substituting (3.75) into (3.78), and noting that in (3.78), we replace ε with $\kappa\varepsilon$, the BEOPT is rewritten as

$$P_{\text{out}}(\alpha) \;=\; P\left(E_d\left(|\tilde{h}_{l|l-D}|^2\cos^2\alpha - 2V'^2C_\kappa\right) < N_0C_\kappa\right). \tag{3.106}$$

where C_κ is defined as $C_\kappa = \left(\text{erfc}^{-1}(2\kappa\varepsilon)\right)^2$. Following the idea in Section 3.5, we want to choose an E_d such that $E_d\left(|\tilde{h}_{l|l-D}|^2\cos^2\alpha - 2V'^2C_\kappa\right) = N_0C_\kappa$. However, it is noted that when $|\tilde{h}_{l|l-D}|^2\cos^2\alpha - 2V'^2C_\kappa \le 0$, i.e., $|\tilde{h}_{l|l-D}|^2 \le \frac{2V'^2C_\kappa}{\cos^2\alpha}$, there is no solution for E_d, as E_d must be greater than zero for a fixed rate system. Under imperfect CSI, this phenomenon is caused by the uncertainty of the channel due to channel prediction errors. To solve this problem, we set $E_d = E_{\text{pk}}$ when $|\tilde{h}_{l|l-D}|^2 \le \frac{2V'^2C_\kappa}{\cos^2\alpha}$ happens. Now, the power law under a peak energy constraint E_{pk} is given by

$$E_d = \begin{cases} E_{\text{pk}}, & |\tilde{h}_{l|l-D}|^2 < \frac{(N_0+E_{\text{pk}}2V'^2)C_\kappa}{E_{\text{pk}}\cos^2\alpha} \\ \frac{N_0C_\kappa}{|\tilde{h}_{l|l-D}|^2\cos^2\alpha - 2V'^2C_\kappa}, & |\tilde{h}_{l|l-D}|^2 \ge \frac{(N_0+E_{\text{pk}}2V'^2)C_\kappa}{E_{\text{pk}}\cos^2\alpha} \end{cases} \tag{3.107}$$

Note that the case where $|\tilde{h}_{l|l-D}|^2 \le \frac{2V'^2C_\kappa}{\cos^2\alpha}$ is included in the case where $|\tilde{h}_{l|l-D}|^2 < \frac{(N_0+E_{\text{pk}}2V'^2)C_\kappa}{E_{\text{pk}}\cos^2\alpha}$. By adjusting κ, we can control the value of E_d, such that the desired BEOPR is achieved.

The average energy of this power law is obtained by averaging (3.107) over the distribution of $\tilde{h}_{l|l-D}$. Following the calculation of (3.66), the result is given by

$$\begin{aligned} E_d^{\text{ave}} \;=\; & E_{\text{pk}}\left(1 - e^{-\frac{(N_0+E_{\text{pk}}2V'^2)C_\kappa}{E_{\text{pk}}2\lambda'^2\cos^2\alpha}}\right) + \\ & \frac{N_0C_\kappa}{2\lambda'^2\cos^2\alpha}e^{-\frac{2V'^2C_\kappa}{2\lambda'^2\cos^2\alpha}}\Gamma\left(0, \frac{N_0C_\kappa}{E_{\text{pk}}2\lambda'^2\cos^2\alpha}\right). \end{aligned} \tag{3.108}$$

Due to the use of pilots, the effective average transmitted energy per data symbol is

$$E_d^{\text{eff-ave}} = \frac{E_d^{\text{ave}}}{1+\xi}. \tag{3.109}$$

3.8.2 ABEP and BEOP Analysis

We first compute the ABEP at the receiver. Let $\varphi = \frac{E_d \cos^2\alpha}{E_d 2V^2 + N_0}$, where E_d is given in (3.107). Therefore, φ is a function of $\tilde{h}_{l|l-D}$. The IBEP at the receiver conditioned on $\tilde{h}_{l|l-D}$ is obtained as

$$F(\alpha|\tilde{h}_{l|l-D}) = \int_0^\infty \frac{1}{2}\mathrm{erfc}\left(\varphi x\right)^{1/2} p_{|\hat{h}_{l|l}|^2|\tilde{h}_{l|l-D}}(x|\tilde{h}_{l|l-D})dx. \tag{3.110}$$

where the conditional PDF $p_{|\hat{h}_{l|l}|^2|\tilde{h}_{l|l-D}}(x|\tilde{h}_{l|l-D})$ has been given in (3.28). Using [49, eq.(5.12)] and changing the variables accordingly, (3.110) can be computed as

$$F(\alpha|\tilde{h}_{l|l-D}) = \frac{1}{\pi}\int_0^{\pi/2}\left(\frac{\sin^2\theta}{\sin^2\theta + 2\Omega^2\varphi}\right)\exp\left(-\frac{|\tilde{h}_{l|l-D}|^2\varphi}{\sin^2\theta + 2\Omega^2\varphi}\right)d\theta. \tag{3.111}$$

Substituting (3.107) into φ, and then averaging (3.111) over the PDF of $|\tilde{h}_{l|l-D}|^2$, the ABEP at the receiver is finally obtained as

$$\begin{aligned} F(\alpha) = {} & \frac{1}{\pi}\int_0^{g_\kappa}\int_0^{\pi/2}\left(\frac{\sin^2\theta}{\sin^2\theta + 2\Omega^2\varphi_{\mathrm{pk}}}\right)\exp\left(-\frac{x\varphi_{\mathrm{pk}}}{\sin^2\theta + 2\Omega^2\varphi_{\mathrm{pk}}}\right)d\theta\frac{1}{2\lambda'^2}e^{-\frac{1}{2\lambda'^2}x}dx + \\ & \frac{1}{\pi}\int_{g_\kappa}^{\infty}\int_0^{\pi/2}\left(\frac{\sin^2\theta}{\sin^2\theta + 2\Omega^2\varphi_h}\right)\exp\left(-\frac{x\varphi_h}{\sin^2\theta + 2\Omega^2\varphi_h}\right)d\theta\frac{1}{2\lambda'^2}e^{-\frac{1}{2\lambda'^2}x}dx, \end{aligned} \tag{3.112}$$

where

$$\varphi_{\mathrm{pk}} = \frac{E_{\mathrm{pk}}\cos^2\alpha}{E_{\mathrm{pk}}2V^2 + N_0}, \tag{3.113}$$

$$\varphi_h = \frac{C_\kappa}{x + \frac{(2V^2 - 2V'^2)C_\kappa}{\cos^2\alpha}}, \tag{3.114}$$

and we have let

$$g_\kappa = \frac{(N_0 + E_{\mathrm{pk}}2V'^2)C_\kappa}{E_{\mathrm{pk}}\cos^2\alpha} \tag{3.115}$$

for notational simplicity.

Next, we compute the BEOP at the receiver. Substituting (3.107) into (3.79), the IBEP at the receiver is given by

$$F(\alpha|\hat{h}_{l|l}) = \begin{cases} \frac{1}{2}\mathrm{erfc}\left(\frac{E_{\mathrm{pk}}|\hat{h}_{l|l}|^2\cos^2\alpha}{E_{\mathrm{pk}}2V^2 + N_0}\right)^{1/2}, & |\tilde{h}_{l|l-D}|^2 < g_\kappa \\ \frac{1}{2}\mathrm{erfc}\left(\frac{C_\kappa|\hat{h}_{l|l}|^2}{|\tilde{h}_{l|l-D}|^2 + \frac{2V^2 - 2V'^2}{\cos^2\alpha}C_\kappa}\right)^{1/2}, & |\tilde{h}_{l|l-D}|^2 \geq g_\kappa \end{cases} \tag{3.116}$$

Substituting (3.116) into (3.82), the BEOPR is obtained as

$$P_{\text{out}}(\alpha) = \begin{cases} P\left(|\hat{h}_{l|l}|^2 < \frac{(E_{\text{pk}}2V^2+N_0)C}{E_{\text{pk}}\cos^2\alpha}\right), & |\tilde{h}_{l|l-D}|^2 < g_\kappa \\ P\left(|\hat{h}_{l|l}|^2 < \frac{C}{C_\kappa}\left(|\tilde{h}_{l|l-D}|^2 + \frac{2V^2-2V'^2}{\cos^2\alpha}C_\kappa\right)\right), & |\tilde{h}_{l|l-D}|^2 \geq g_\kappa \end{cases} \tag{3.117}$$

Using the PDF of $|\hat{h}_{l|l}|^2$ and the conditional CDF of $|\hat{h}_{l|l}|^2$ conditioned on $\tilde{h}_{l|l-D}$, which has been respectively given in (3.81) and (3.29), the BEOPR can be written as

$$P_{\text{out}}(\alpha) = \begin{cases} 1 - \exp\left(-\frac{(E_{\text{pk}}2V^2+N_0)C}{E_{\text{pk}}2\lambda^2\cos^2\alpha}\right), & |\tilde{h}_{l|l-D}|^2 < g_\kappa \\ 1 - Q\left(\frac{|\tilde{h}_{l|l-D}|}{\Omega}, \frac{\sqrt{\frac{C}{C_\kappa}\left(|\tilde{h}_{l|l-D}|^2 + \frac{(2V^2-2V'^2)C_\kappa}{\cos^2\alpha}\right)}}{\Omega}\right), & |\tilde{h}_{l|l-D}|^2 \geq g_\kappa \end{cases} \tag{3.118}$$

Averaging (3.118) over the PDF of $|\tilde{h}_{l|l-D}|^2$, the BEOPR is finally obtained as

$$\begin{aligned} P_{\text{out}}(\alpha) &= \left[1 - \exp\left(-\frac{C}{2\lambda^2\varphi_{\text{pk}}}\right)\right]\left[1 - \exp\left(-\frac{g_\kappa}{2\lambda'^2}\right)\right] + \\ &\int_{g_\kappa}^{\infty}\left[1 - Q\left(\frac{\sqrt{x}}{\Omega}, \frac{\sqrt{\frac{C}{\varphi_h(x)}}}{\Omega}\right)\right]\frac{1}{2\lambda'^2}e^{-\frac{1}{2\lambda'^2}x}dx, \end{aligned} \tag{3.119}$$

This BEOPR is also recognized as the best QoS-specified δ that can be provided by the system for a given peak energy E_{pk}. In other words, this BEOPR itself is the QoS-specified δ, and it indicates how much peak energy is required to ensure the BEOP being no more than δ.

3.9 Numerical Results

In Sections 3.4 and 3.5, and Sections 3.7 and 3.8, we analyzed different power control laws under perfect CSI and under imperfect CSI, respectively. In this section, we examine their performance through numerical results. We first show the performance under perfect CSI.

3.9.1 Performance under Perfect CSI

Without loss of generality, we assume that the transmission rate R, the symbol duration T, the variance of the channel fading coefficient $2\sigma^2$, and the variance of

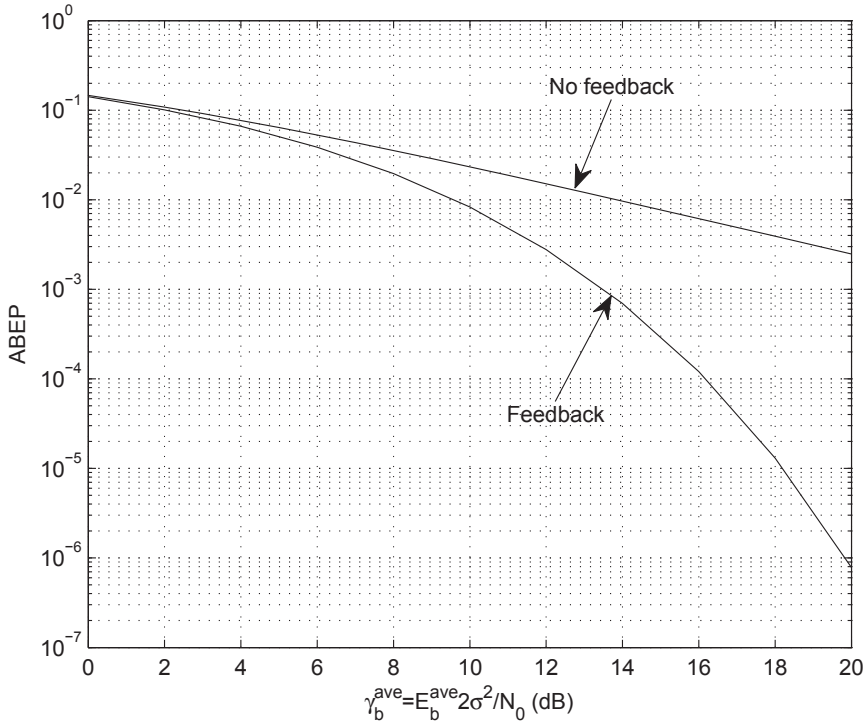

Figure 3.2: ABEP performance comparison of a feedback system employing the ABEP-based law and a non-feedback system, under perfect CSI.

the AWGN, N_0, are all normalized to 1. All the performance is shown with respect to the average SNR per bit γ_b^{ave}. It is defined as $\gamma_b^{\text{ave}} = E_b^{\text{ave}} 2\sigma^2/N_0$, where E_b^{ave} is the average energy per bit, and $E_b^{\text{ave}} = E_s^{\text{ave}}$ for BPSK modulation, and $E_b^{\text{ave}} = E_s^{\text{ave}}/2$ for QPSK modulation. It is noted that under perfect CSI, given the same E_b^{ave}, the ABEPs of the BPSK and QPSK modulations are identical, and the BEOPs of them are also identical. This property is the same as that in a non-feedback system.

In [6], Hayes has shown that for transmission with coherent BPSK over a Rayleigh fading multipath channel, the ABEP with feedback power control is significantly reduced compared with that without any feedback. Here, we review the ABEP performance of the ABEP-based power control law, and also examine its BEOP performance.

Fig. 3.2 compares the ABEP performance of a feedback system employing the

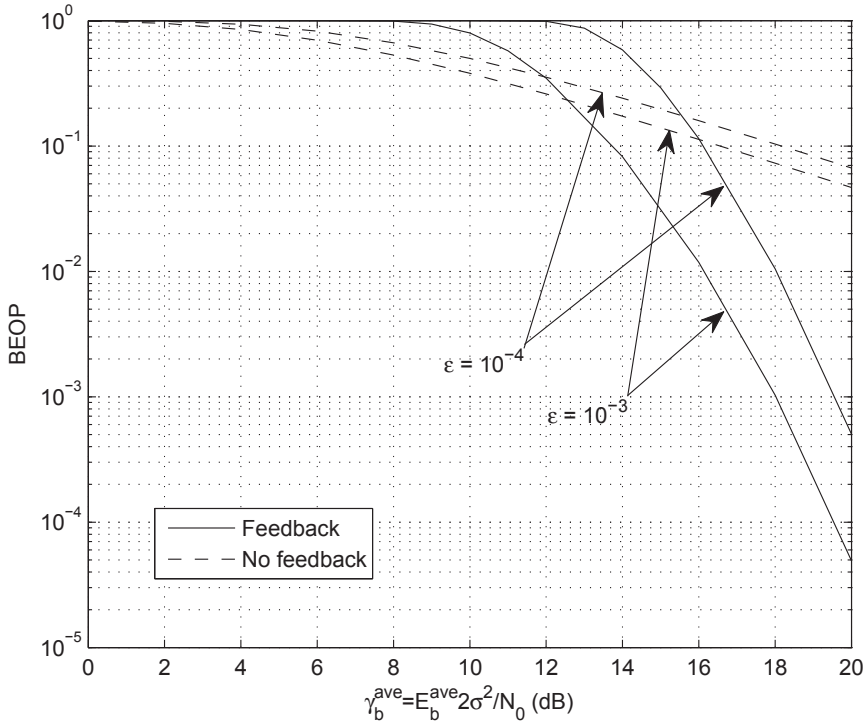

Figure 3.3: BEOP performance comparison of a feedback system employing the ABEP-based law and a non-feedback system, under perfect CSI.

ABEP-based law and a non-feedback system. Their ABEPs are given in (3.56) and (3.46), respectively. As can be seen, the ABEP of the feedback system employing the ABEP-based law is much smaller than that of the non-feedback system. At the probability level of 10^{-2}, the performance gain of the feedback system is about 5dB. As SNR goes higher, this gain further increases.

Fig. 3.3 compares the BEOP performance of a feedback system employing the ABEP-based law and a non-feedback system. To show the BEOP performance, we use an IBEP threshold of $\varepsilon = 10^{-3}$ or 10^{-4}. The choice of ε is based on the QoS requirement. For example, $\varepsilon = 10^{-4}$ denotes that when a received bit has IBEP greater than 10^{-4}, an outage happens (the QoS requirement is not met). Our choices of ε here are acceptable in common wireless communications applications. The BEOPs of the feedback system with the ABEP-based law and the non-feedback

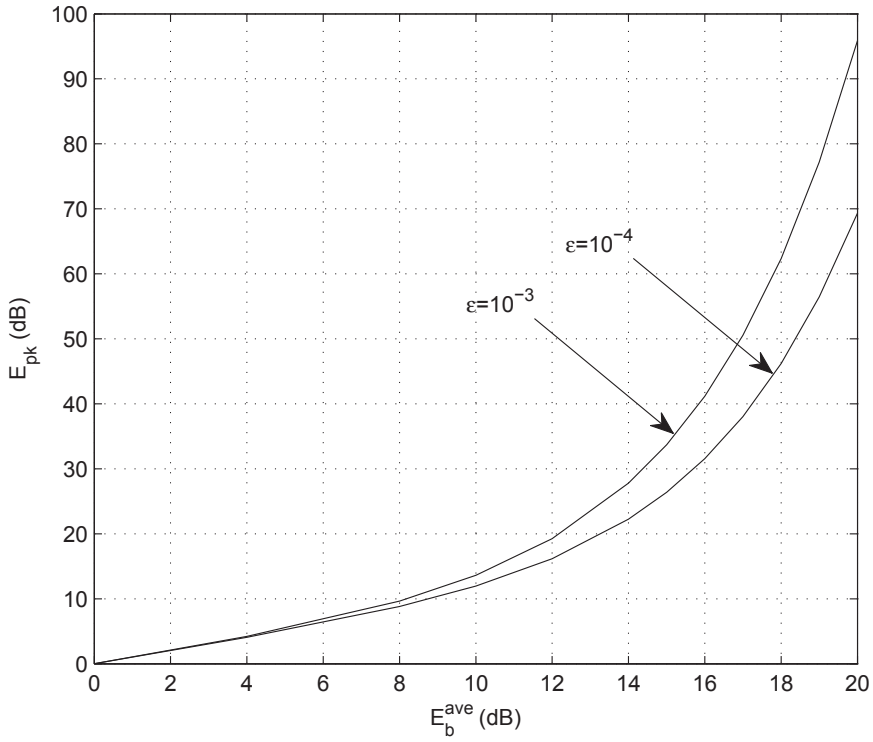

Figure 3.4: The relationship between $E_{\mathbf{pk}}$ and $E_b^{\mathbf{ave}}$ of the BEOP-based law with perfect CSI, for different ε.

system are given in (3.60) and (3.47), respectively. As can be seen, the BEOP of the non-feedback system decreases smoothly and very slowly as SNR increases. The BEOP of the ABEP-based law remains 1 when the SNR is below some threshold. For example, the threshold values are about 8dB and 12dB for the cases where $\varepsilon = 10^{-3}$ and $\varepsilon = 10^{-4}$, respectively. Clearly, as ε decreases, the threshold value increases. When SNR is below the SNR threshold, the IBEPs of the received bits of the ABEP-based law always exceed the corresponding IBEP threshold. The BEOP of the ABEP-based law only begins to drop significantly after the SNR increases beyond the threshold, and it can be much smaller than that of the non-feedback system at high SNR. Generally, at moderate or low SNR, the ABEP-based power control system does not provide any performance advantage over the non-feedback system in terms of BEOP.

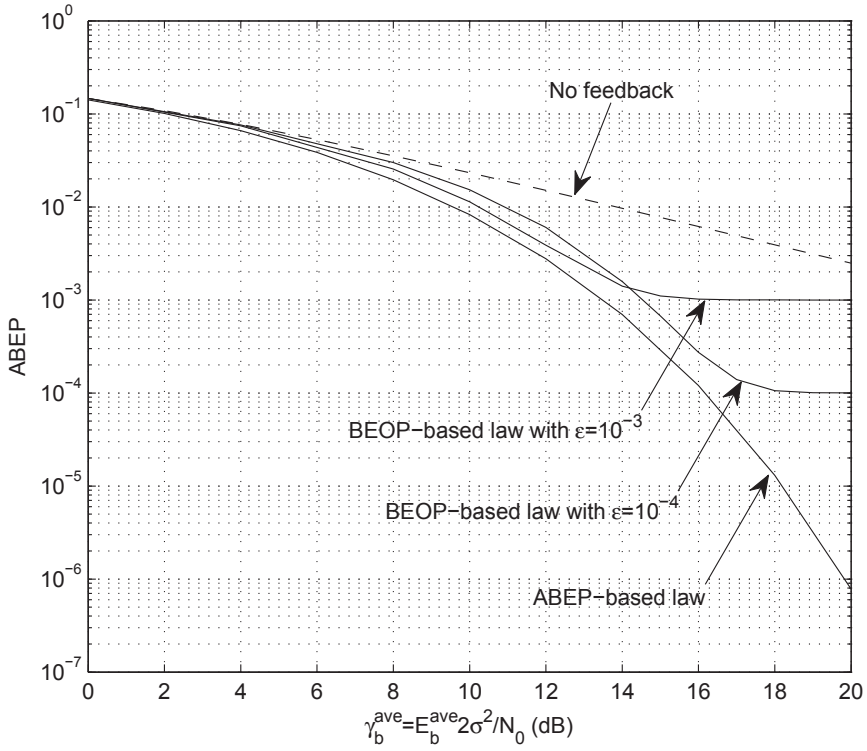

Figure 3.5: ABEP performance comparison of the ABEP-based power law and the BEOP-based power law, under perfect CSI.

Now, we focus on examining the performance of the new BEOP-based law. We first plot in Fig. 3.4, the relationship between $E_{\rm pk}$ and $E_b^{\rm ave}$, which has been shown in (3.67). In (3.67), the average energy is expressed in terms of $E_s^{\rm ave}$. It is noted that given the same $E_b^{\rm ave}$, the values of $E_{\rm pk}$ with BPSK and QPSK, respectively, are identical. Therefore, the curves in Fig. 3.4 represent both BPSK and QPSK. As can be seen in Fig. 3.4, for a given $E_{\rm pk}$, a smaller ε results in a larger bit energy on the average. Vice versa, for a given $E_b^{\rm ave}$, a smaller ε leads to a smaller $E_{\rm pk}$. We emphasize that this does not mean that when $E_b^{\rm ave}$ is fixed, a smaller $E_{\rm pk}$ is required for a smaller ε. Rather, it can be explained as follows. When $E_b^{\rm ave}$ and ε are fixed, $E_{\rm pk}$ is determined. From (3.65), this also indicates that the best (smallest) δ that the BEOP-based law can achieve is determined. As $E_b^{\rm ave}$ is fixed, when ε reduces, the best δ that can be achieved is reduced, and so does the required $E_{\rm pk}$.

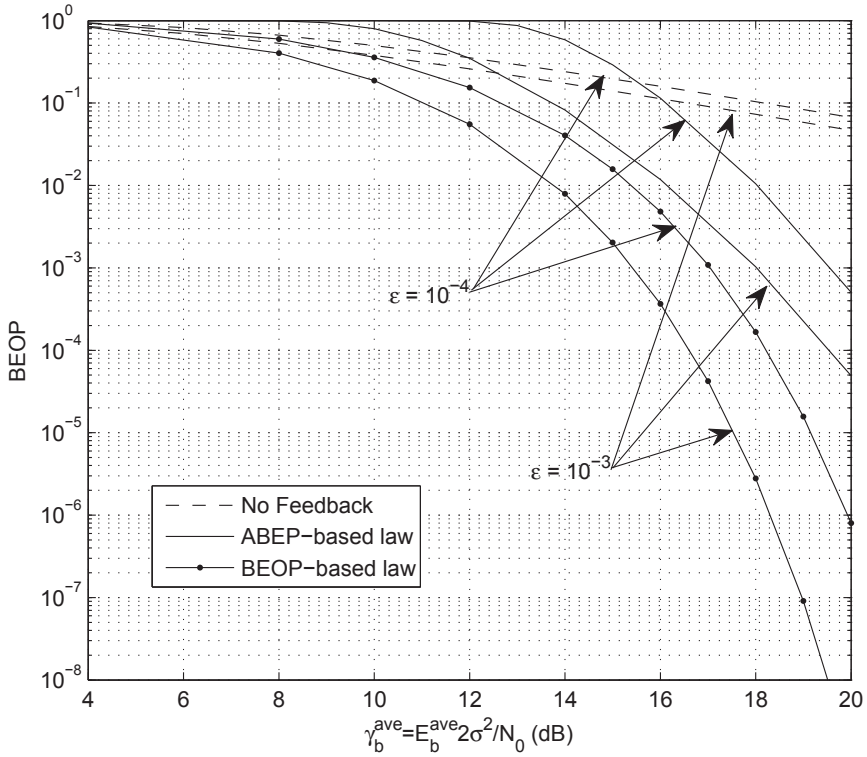

Figure 3.6: BEOP performance comparison of the ABEP-based power law and the BEOP-based power law, under perfect CSI.

Fig. 3.5 compares the ABEPs of the ABEP-based law and the BEOP-based law, which are given in (3.56) and (3.74), respectively. From (3.74), it is noted that the ABEP of the BEOP-based law depends on the value of ε. As can be seen from the firure, when ε is chosen smaller, the ABEP decreases slower but arrives at a smaller error floor. The value of the error floor is equal to ε, which can also be derived from (3.74) as $\gamma_{\rm pk}$ tends to infinity. Here, we emphasize that the ABEP performance of the BEOP-based law is determined by the chosen ε, which is a system-defined parameter depends on what level of QoS we want to achieve. For example, seen from Fig. 3.5, if the wanted QoS level is achieved with the chosen ε, when the ABEP arrives at the error floor, the further increasing on SNR becomes a waste of energy. It is also noted that not surprisingly, the ABEP-based law performs the best, as it is designed to minimize the ABEP. For the BEOP-based law, its

performance gain over the non-feedback system is significant for a properly chosen ε corresponding to a fixed γ_b^{ave}. In practice, if the ABEP performance is of concern, we can adjust ε to achieve the desired ABEP for the BEOP-based law. Or more advancingly, we can design a sliding ε based on the available average SNR to optimize the performance. By choosing a suitable ε according to the availability of γ_b^{ave}, the performance loss of the BEOP-based law compared with the ABEP-based law can be kept within 1dB. Fig. 3.6 compares the BEOP performance of the two laws for different IBEP threshold values. The BEOPs of the two laws are shown in (3.60) and (3.63), respectively. As can be seen, given the same average transmitted energy, the BEOP-based law performs significantly better than the ABEP-based law. For example, the performance gain is about 3dB at the probability level of 10^{-3}. This performance gain is further increased as SNR increases. We point out that for the BEOP-based law, its BEOP is also recognized as the value of the QoS-specified threshold δ, which has been discussed in Section 3.5.

From Figs. 3.5 and 3.6, we conclude that compared with the ABEP-based law, the BEOP-based law sacrifices a little in the ABEP performance, but leads to a remarkable gain in the BEOP performance.

3.9.2 Performance under Imperfect CSI

Following that in the perfect CSI case, without loss of generality, we assume that the transmission rate R, the symbol duration T, the variance of the channel fading coefficient $2\sigma^2$ and the variance of the AWGN, N_0, are all normalized to 1. As has been mentioned, in a practical system, the number of pilots that can be added to a data packet is determined by the maximal BEF. Here, as the effect of the imperfect CSI can also be reflected by adjusting the power allocation factor ξ, we simply assume a fixed packet length of $N = 500$ that fits the blockwise static channel assumption. We further assume that a packet consists of $N_d = 490$ data symbols prefixed by $N_p = 10$ pilots symbols. The issue of the maximal BEF will be more carefully discussed in Section 5.5. For the Rayleigh fading, we assume that the

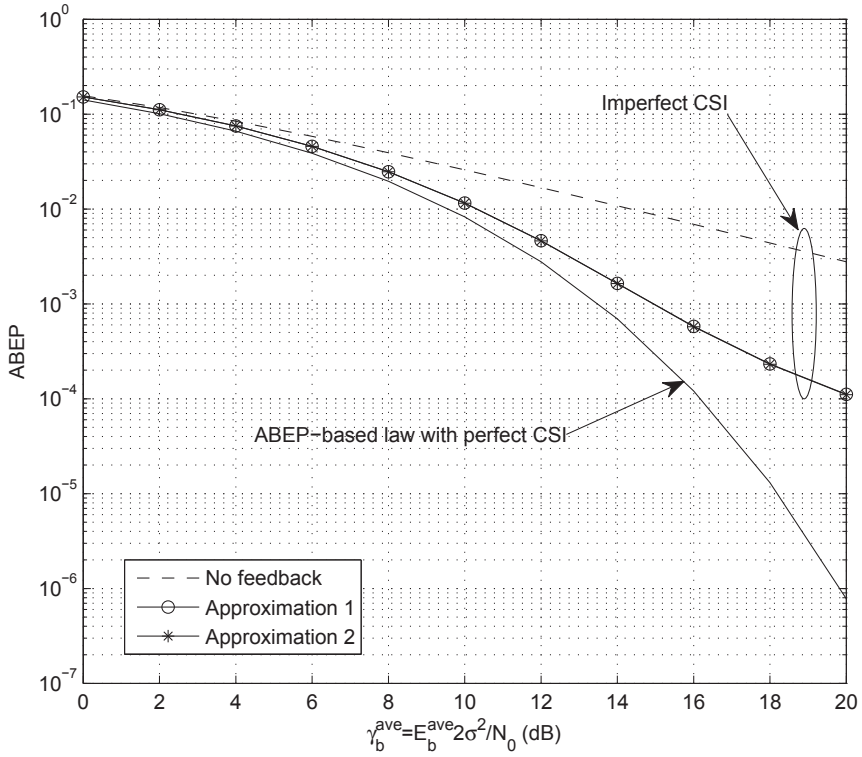

Figure 3.7: ABEP performance of the ABEP-based power law under imperfect CSI, with BPSK modulation, for a fixed $\xi = 0.1$.

value of the normalized Doppler fade rate is $f_D T = 0.002$. The MMSE of the channel estimation/prediction is generated from the simplified model introduced in the last part of Section 3.2.3, and for channel prediction, we assume that the delay factor $D = 2$.

All performance is evaluated with respect to the average SNR per bit, which has been defined as $\gamma_b^{\text{ave}} = E_b^{\text{ave}} 2\sigma^2/N_0$. Due to the use of pilots, the effective average energy per bit is given by $E_b^{\text{eff-ave}} = E_b^{\text{ave}}/(1+\xi)$, and $E_d^{\text{eff-ave}} = E_b^{\text{eff-ave}}$ for BPSK modulation, and $E_d^{\text{eff-ave}} = 2E_b^{\text{eff-ave}}$ for QPSK modulation. It is noted that the performance of QPSK modulation is quite close to that of BPSK modulation, and therefore, we only present the curves for BPSK. The slightly different performance is caused by the channel estimation errors.

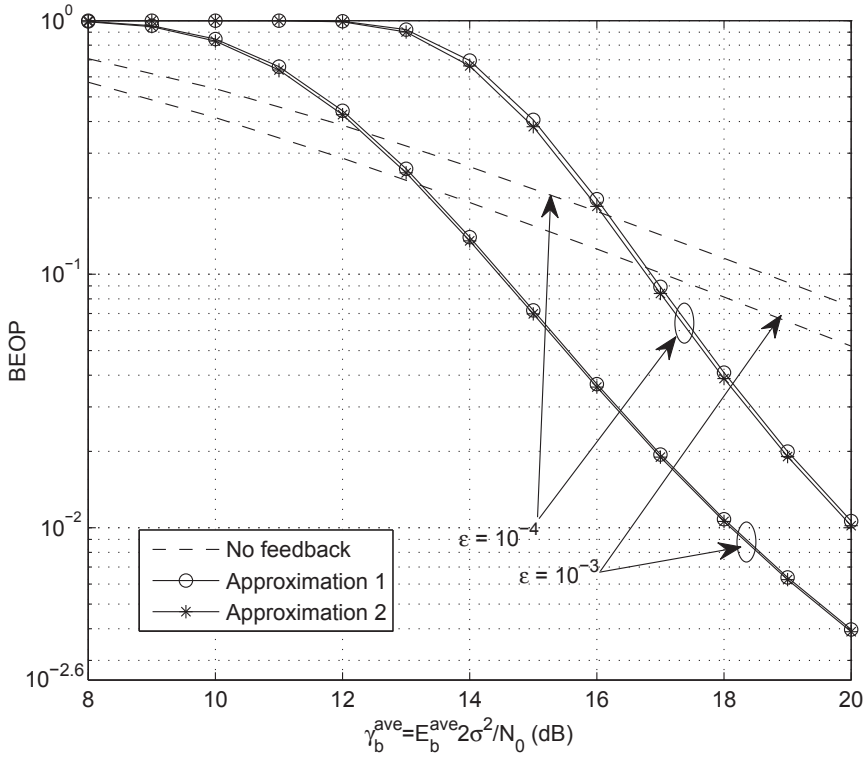

Figure 3.8: BEOP performance of the ABEP-based power law under imperfect CSI, with BPSK modulation, for a fixed $\xi = 0.1$; comparisons are made to a non-feedback system.

We first examine the performance of the ABEP-based law. Fig. 3.7 shows the ABEPs of the ABEP-based law with Approximation 1 and Approximation 2, respectively, for a fixed $\xi = 0.1$. Their ABEP expressions are shown in (3.97) and (3.103), respectively. The ABEPs of the ABEP-based law under the perfect CSI scenario and a non-feedback system are also included for comparison. As can be seen, under imperfect CSI, Approximation 1 and Approximation 2 perform nearly the same, and both of them perform increasingly better than the non-feedback system as SNR increases. It is also found that the performance gain of the feedback system over the non-feedback system under imperfect CSI is much less than that under perfect CSI, where the latter has been shown in Fig. 3.2. Comparing the feedback system under imperfect CSI with that under perfect CSI, the performance loss is

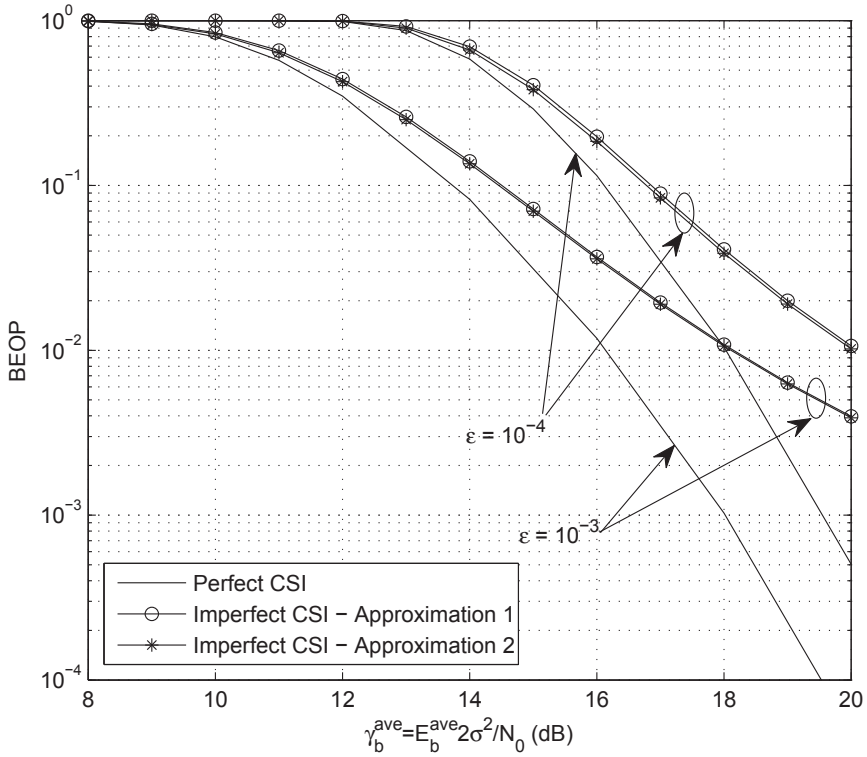

Figure 3.9: BEOP performance of the ABEP-based power law under imperfect CSI, with BPSK modulation, for a fixed $\xi = 0.1$; comparisons are made to the perfect CSI scenario.

significant. For example, at the probability level of 10^{-4}, the loss is approximately 4dB. This loss further increases as SNR increases.

In Fig. 3.8, we show the BEOP performance of the ABEP-based law under imperfect CSI with BPSK modulation, for a fixed $\xi = 0.1$. The BEOP expressions for Approximation 1 and Approximation 2 of the ABEP-based law are shown in (3.100) and (3.105), respectively. As can be seen, Approximation 2 performs slightly better than Approximation 1 in terms of BEOP. Similar to the findings from Fig. 3.3, the BEOP of the ABEP-based law only begins to drop after the SNR increases beyond some threshold. Again, we conclude that at moderate or low SNR, the ABEP-based power control system does not provide any performance advantage over the non-feedback system in terms of BEOP.

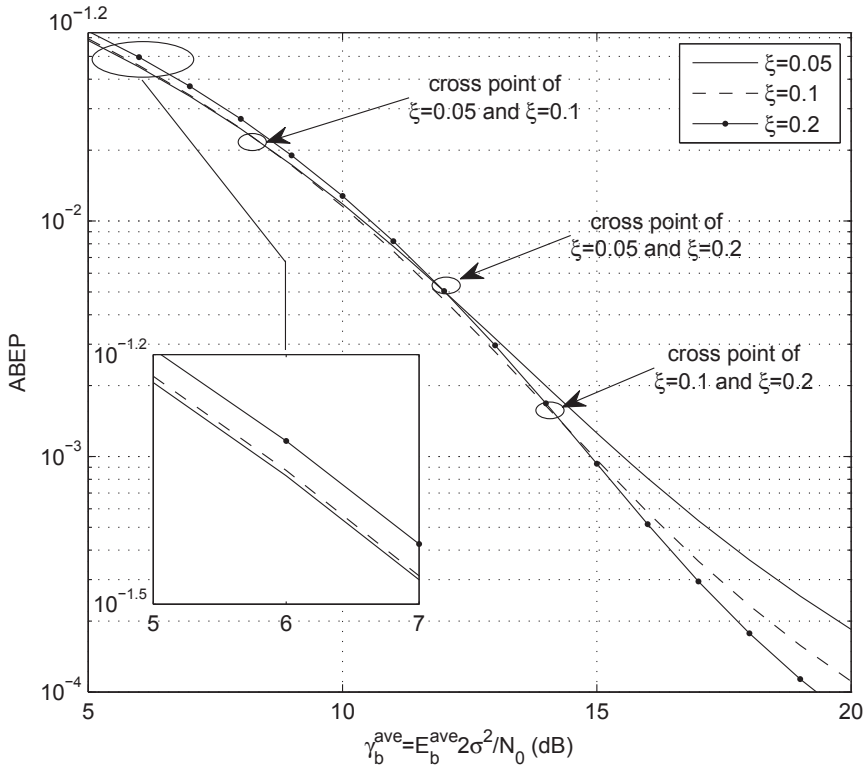

Figure 3.10: ABEP performance of the ABEP-based power law using Approximation 1, for different ξ.

In Fig. 3.9, we show the BEOP performance of the ABEP-based law with imperfect CSI and with perfect CSI, respectively. The latter has been shown in Fig. 3.3. As can be seen, as SNR increases, the performance loss due to the imperfect CSI increases. At the probability level of 10^{-2}, the loss is about 2dB for both $\varepsilon = 10^{-3}$ and $\varepsilon = 10^{-4}$ cases. From the trend of the curves, it can be deduced that at high SNR, the performance loss due to the imperfect CSI can be very large.

As has been mentioned at the end of Section 3.7.1, the power allocation factor ξ is related to the $E_d^{\text{eff-ave}}$, and has an effect on the performance. Here, we consider the effect of ξ on the ABEP performance of the ABEP-based law using Approximation 1, with BPSK modulation. For the cases of QPSK or Approximation 2, the problem can be analyzed in the same way. Fig. 3.10 shows the ABEP performance of Approximation 1 with ξ being set to 0.05, 0.1 and 0.2, respectively. As can be seen,

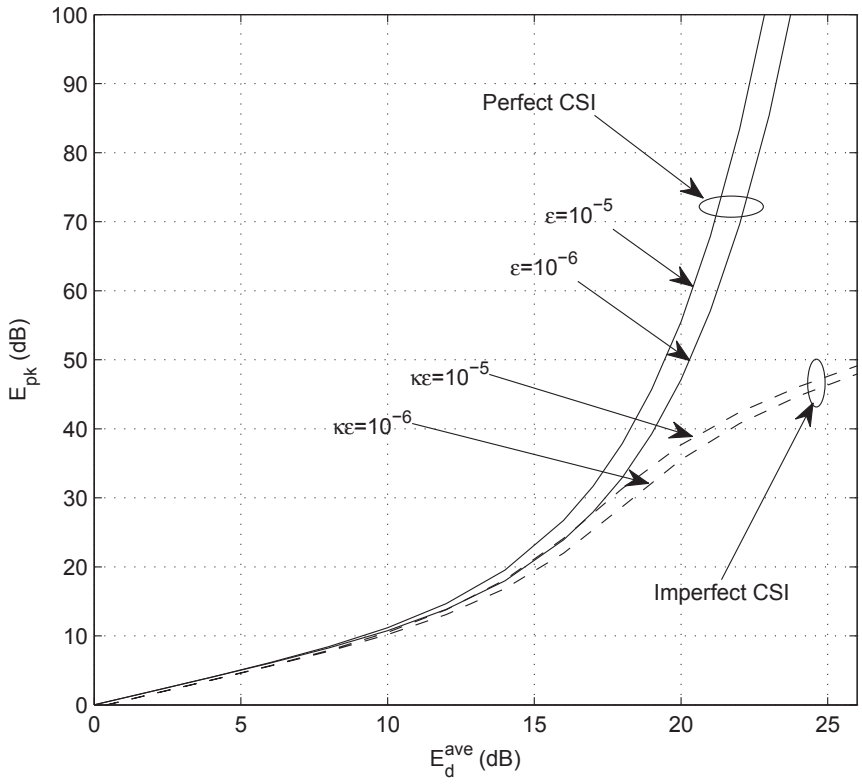

Figure 3.11: The relationship between $E_{\mathbf{pk}}$ and $E_d^{\mathbf{ave}}$ of the BEOP-based law with imperfect CSI, for different $\kappa\varepsilon$.

as SNR (or $E_d^{\text{eff-ave}}$) increases, the value of ξ that results in the best performance increases. This means that as the total amount of available transmitter energy, $E_d^{\text{eff-ave}}$ increases, more energy should be used for channel estimation to improve the ABEP performance. Although the optimal value of ξ is not analytically obtainable, we can find it through extensive search for any given $E_d^{\text{eff-ave}}$. For example, when $\gamma_b^{\text{ave}} = 15\text{dB}$ (or $E_d^{\text{eff-ave}} = 14.37\text{dB}$), the optimal value of ξ is found to be approximately 0.157.

Now, we evaluate the performance of the BEOP-based law under imperfect CSI. Again, we note that the performance of BPSK and QPSK modulations are quite close, and therefore, we only show the result for BPSK. We skip the discussion of the optimal power allocation between pilot symbols and data symbols here, and use

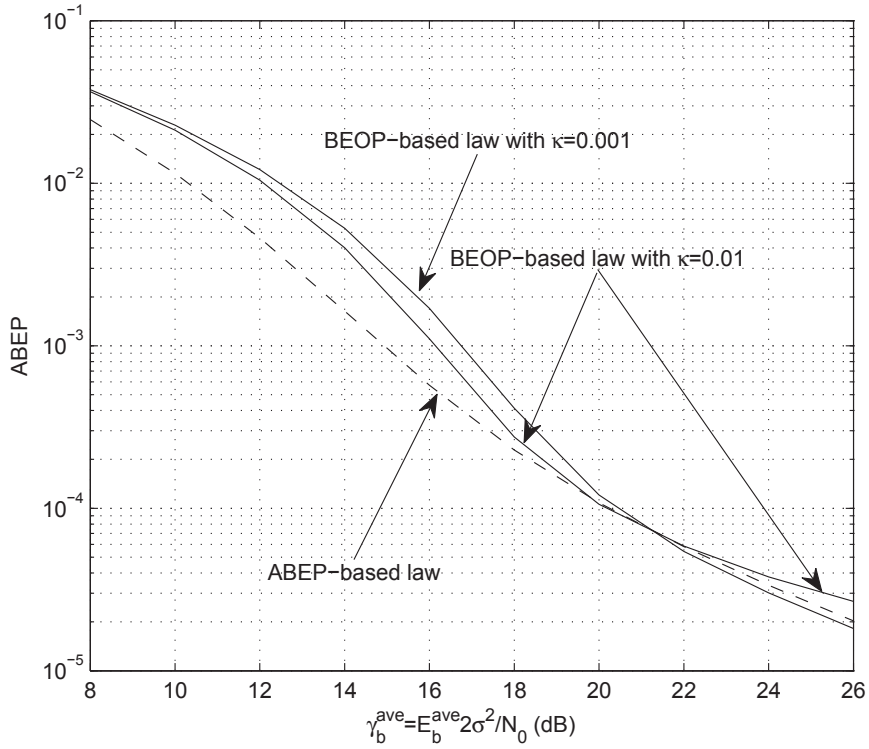

Figure 3.12: ABEP performance of the BEOP-based law versus the ABEP-based law using Approximation 1, with BPSK modulation, under imperfect CSI, for $\xi = 0.1$ and $\varepsilon = 10^{-3}$.

a fixed $\xi = 0.1$ for all cases. Nevertheless, we mention that from (3.109), the power allocation factor ξ is related to the effective average transmitted energy per data symbol $E_d^{\text{eff-ave}}$, and thereby, it has an effect on the performance. In Fig. 3.10, we have shown the effect of ξ on the ABEP performance of the ABEP-based law, and also discussed how to choose the optimal ξ. Following a similar way, we can decide the optimal ξ for the BEOP-based law. Here, we are more concerned about the multiplicative factor κ, since it has a significant effect on the performance.

We show in Fig. 3.11 the relationship between E_{pk} and E_d^{ave}, which is given in (3.108). The curves for the perfect CSI case are also included for comparison. As can be seen, when the average energy is small, the values of E_{pk} for the perfect CSI case and for the imperfect CSI case, respectively, are quite close. Therefore, it is

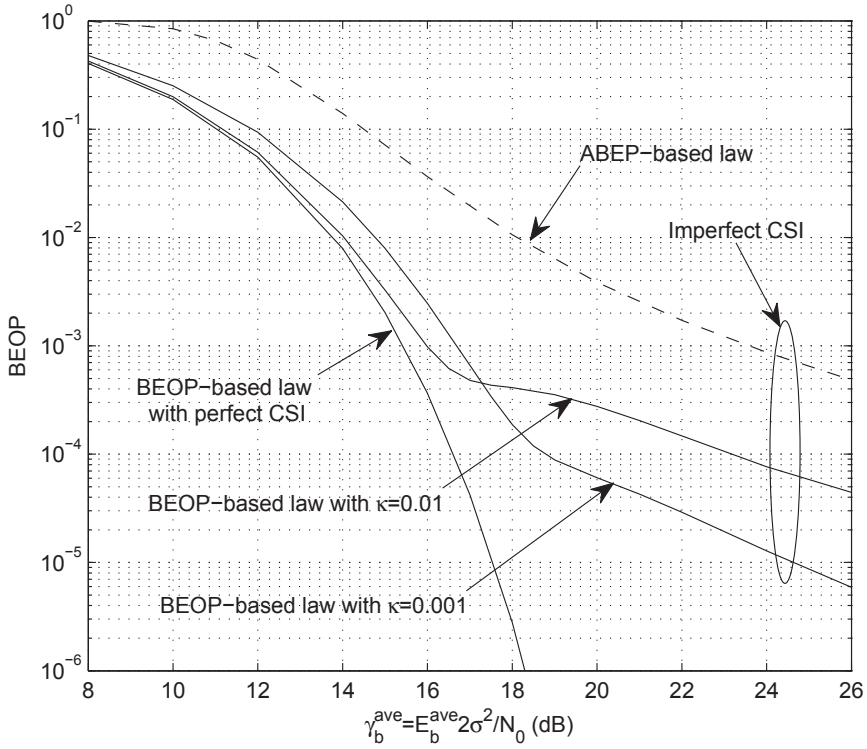

Figure 3.13: BEOP performance of the BEOP-based law versus the ABEP-based law using Approximation 1, with BPSK modulation, under imperfect CSI, for $\xi = 0.1$ and $\varepsilon = 10^{-3}$.

expected that in the low SNR regime, the BEOPs that the BEOP-based law can achieve under perfect CSI and under imperfect CSI, respectively, would be close. As SNR increases, the value of $E_{\rm pk}$ for the perfect CSI case sharply increases. In contrast, the value of $E_{\rm pk}$ for the imperfect CSI case tends to increase slower, which implies that the achievable BEOP will be larger.

Fig. 3.12 shows the ABEP performance of the BEOP-based law under imperfect CSI. The ABEP expression is explicitly given in (3.112). Comparisons are made to the ABEP-based law using Approximation 1. For the BEOP-based law, the IBEP threshold ε is fixed at 10^{-3}, and the multiplicative factor κ is set to 0.01 and 0.001, respectively. As can be seen, by carefully choosing κ, the BEOP-based law can perform comparably to, or even better than the ABEP-based law. The better

performance is due to the fact that Approximation 1 is not optimal for ABEP minimization under imperfect CSI. It is also noted that for the BEOP-based law, a larger κ leads to a faster drop in the ABEP, but this would also result in a larger ABEP as SNR further increases. The ABEP at the receiver of the BEOP-based law would finally converge to an error floor, whose value is $\kappa\varepsilon$. This can be numerically examined from (3.112).

Fig. 3.13 shows the BEOP performance of the BEOP-based law under imperfect CSI. The expression of the BEOP is given in (3.119). Again, the multiplicative factor κ is set to 0.01 and 0.001, respectively. The curves for the BEOP-based law with perfect CSI and the ABEP-based law with imperfect CSI are included for comparison. For both laws, the IBEP threshold ε is chosen to be 10^{-3}. As can be seen, the performance loss of the BEOP-based law due to the channel estimation errors is small at low SNR. When SNR increases beyond some threshold, there is a sharp reduction in the BEOP drop rate, and the performance loss becomes significant. Under imperfect CSI, compared with the ABEP-based law, the BEOP-based law performs much better even after SNR increases beyond the above-mentioned threshold. For example, at the probability level of 10^{-3}, the gains are approximately 7dB and 8dB for the BEOP-based law with $\kappa = 0.001$ and $\kappa = 0.01$, respectively. The above findings enhance our conclusion drawn from the comparison between the BEOP-based law and the ABEP-based law under perfect CSI, i.e., the BEOP-based law sacrifices a little in the ABEP performance, but leads to a remarkable gain in the BEOP performance. Finally, we mention that a sliding κ can be designed based on the available average SNR. From Fig. 3.13, it is seen that as SNR increases, the κ needs to be decreased to ensure the desired performance, i.e., to achieve the QoS-specified δ.

3.10 Conclusions

In this chapter, we proposed to use the BEOP as a new performance measure in the design of a feedback system. The BEOP is recognized as a more meaningful

performance measure than the traditional measure ABEP, in high data-rate wireless communications. The BEOP-based power control law adjusts the transmitted power according to the variations of the channel such that the BEOP is kept within some QoS-specified threshold. We built up a practical system model with channel estimation, based on which, we developed both the ABEP-based and the BEOP-based power control laws for the imperfect CSI scenario. For both laws under perfect CSI and under imperfect CSI, respectively, we derived explicit ABEP and BEOP results. These results show that for each power law, the performance loss due to the channel estimation errors is considerable. However, it achieves a significant gain over a non-feedback system. Under either perfect CSI or imperfect CSI, the BEOP-based law shows a remarkable gain over the ABEP-based law in terms of BEOP, and sacrifices only a little in the ABEP performance. The BEOP-based power control law provides an attractive solution for instantaneous QoS assurance for communications over fading channels.

Chapter 4

Receiver Design of DF Relay Communication Systems

We consider receiver design of a general DF multiple relay system under the Rayleigh environment. The optimum (ML) detector for a DF multiple relay system with an arbitrary M-QAM is derived. The only reference on the ML detector for a coherent DF relay system is [20], which considers a single relay case with BPSK modulation under perfect CSI. Our derived detector generalizes both perfect and imperfect CSI scenarios. It is important to note that our receiver result clearly shows that for optimum detection at the destination, the instantaneous decoding error probability at the relay is required. In many previous works, this instantaneous probability has been replaced by its average. The loss of the instantaneous information of the source-relay link for detection at the destination causes the loss of diversity, and therefore, should be avoided in the design of high-performance receivers. Due to the complexity of the ML detector with higher order modulations, we confine our further study to the ML detector with BPSK. We propose the WSD and the CWSD to approximate the ML detector. These two approximate detectors improve the traditional MRC and the PL detector, respectively.

4.1 Introduction

In wireless communications, transmitting signals through multiple relays is a way to obtain the space diversity and is effective in mitigating signal fading [12]. Various relaying protocols have been proposed to achieve the benefits from relay cooperation, e.g., AF, DF and SR [11]. As the SR protocol can employ either AF or DF relays, to distinguish, when talking about the AF or the DF protocol solely, it refers to relaying without selection. Among those protocols, the DF protocol is considered as the most practical relaying strategy. It can be directly employed by most of the current wireless networks with the existing terminals. In comparison, the AF protocol requires additional, expensive analog processing at the relays, and the SR protocol is usually accompanied by interaction from a high layer. It has been shown that relay transmission incorporating error control codes can significantly improve the overall performance. However, in analysis, to isolate the diversity gain achieved through relaying from the coding gain, an uncoded data stream is widely used. For the above reasons, our study focuses on uncoded DF relay systems.

A common misunderstanding to the DF protocol is that systems employing the DF relaying protocol without relay selection do not achieve full diversity. The cause for this misunderstanding is that all the existing works attempting to analyze the ML detector for a DF relay system, fall into the analysis of a suboptimum detector which utilizes the statistical information of the source-relay link for detection at the destination. For example, [25] proposes and analyzes a general detector with either coherent or noncoherent BFSK for a DF multiple relay system. The authors of [25] called their detector the ML detector. However, it should be noted that the detector proposed by [25] is not truly optimum, as it uses the ABEP at the relay. In fact, the optimum detector at the destination for a DF relay system utilizes the instantaneous instead of the statistical information of the source-relay link. In [20], this point has been shown for a DF single relay system with coherent binary transmission. The instantaneous information of interest is simply summarized as the IBEP at the relay. Unfortunately, the importance of using the IBEP at the relay for optimum detection

at the destination is not emphasized in [20].

To avoid to study the complex optimum (ML) detector, some works have proposed suboptimum detectors [21–24] to approximate the ML detector. Referring to Table 2.1, for a coherent, uncoded DF relay system, the ML detector has only been derived in [20] for a single relay case with BPSK. The ML detector for a multiple relay system with general M-QAM remains unsolved.

Driven by the need of the ML detector in the most general form, from which we can fairly assess the performance of the DF relaying protocol (without relay selection), in this chapter, we study the fundamental issue of ML receiver design for a general, uncoded DF multiple relay system. We explicitly derive the ML detector with an arbitrary M-QAM. The derived detector has taken into consideration of the effect of imperfect CSI at all the relays and at the destination. In addition, all the links between each pair of communication nodes are assumed to be independent, non-identically, distributed (i.n.d.). Our receiver result clearly shows that for optimum (ML) detection at the destination, the instantaneous information of the source-relay link is required. To illustrate, for BPSK, the instantaneous information is summarized as the IBEP at the relay for decoding the source message. Due to the complexity of the ML detector for higher order modulations, we confine ourself to study the ML detector with BPSK. In this case, the contribution of the relay to the ML detector is summarized as a nonlinear function. For ease of implementation and analysis, we provide a batch of suboptimum detectors to approximate the ML detector. In particular, we reconsider the traditional MRC and the classic PL detector [25], and fit them into the DF relay system. We also propose the WSD and the CWSD that marginally improve the MRC and the PL detector, respectively. To summarize and compare these detectors, we create an insightful, geometrical view of them.

The remainder of this chapter is organized as follows. Section 4.2 introduces the system model. In Section 4.3, we explicitly derive the ML detector structure. In Section 4.4, we specialize the detector to the one with BPSK for simplicity. Section

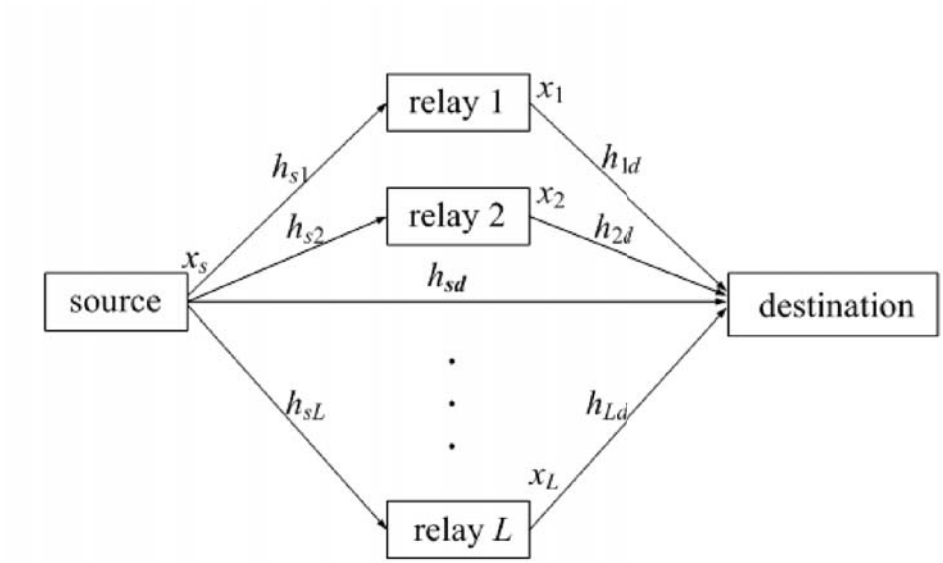

Figure 4.1: A multiple relay system with L parallel relays.

4.5 introduces a batch of suboptimum detectors that approximate the ML detector. Finally, we conclude with Section 4.6.

4.2 System Model

We consider an uncoded DF multiple relay system as illustrated in Fig. 4.1. This model is of great academic interest and also has its applications in practice. For example, in a sensor network, the node that detects an event, known as source, would sponsor a transmission to the sink, known as destination. Other intermediate nodes that overhear the source information may serve as relays to help forward the source information. In our study, all the nodes are assumed to operate in half-duplex mode and each node is equipped with a single transmit and receive antenna. The communication between the source and the destination is established in two phases. In the first phase, the source broadcasts to the destination as well as the L parallel relays. Upon receiving the source message, the relays decode and forward it to the destination in the second phase. We assume that all the links between each pair of

nodes are independent and quasi-static, and each introduces frequency-nonselective Rayleigh fading in addition to AWGN. In the second phase of transmission, we assume L orthogonal channels available. The message is transmitted in packets and symbol-by-symbol detection is performed at each receiving node. In addition, the channel is assumed to be block-faded, such that it remains constant over the duration of a packet. Without loss of generality, the data symbols and the pilot symbols are transmitted with equal energy, and N_d data symbols are prefixed with N_p pilot symbols to form a packet of length N, i.e., $N = N_p + N_d$. In practice, the number of pilot symbols that can be added to a data packet is determined by the maximal allowable BEF ζ defined as $\zeta = (N_p + N_d)/N_d$.

4.2.1 Channel Model

Let $x_s(k)$ denote the symbol sent by the source at time point k, and each symbol is transmitted with energy E_s. Thus, the corresponding received signals at the r-th relay and at the destination in the k-th symbol interval $kT \leq t \leq (k+1)T$ are

$$y_{sr}(k) = E_s^{1/2} h_{sr}(k) x_s(k) + n_{sr}(k), \tag{4.1}$$

$$y_{sd}(k) = E_s^{1/2} h_{sd}(k) x_s(k) + n_{sd}(k), \tag{4.2}$$

where the subscripts s, d represent the source and the destination, respectively, and $r = 1, 2, ..., L$, represents the r-th relay. In the DF protocol, each relay r generates an estimate $x_r(k)$ of $x_s(k)$, and transmits $x_r(k)$ to the destination with energy E_r. The received signal at the destination from the r-th relay is

$$y_{rd}(k) = E_r^{1/2} h_{rd}(k) x_r(k) + n_{rd}(k). \tag{4.3}$$

Here, $h_{ij}(k)$, $ij \in \{sd, sr, rd\}_{r=1}^{L}$ denotes the fading coefficient of the $i-j$ link during the k-th bit interval, and is a complex Gaussian random variable with mean zero and variance $2\sigma_{ij}^2$. The fading coefficient remains constant over the duration of a packet, i.e. $h_{ij}(k) = h_{ij}, k \in 1, 2, ..., N$. The channel AWGN is modeled by the sequence $\{n_{ij}(k)\}_k$. Each sequence $\{n_{ij}(k)\}_k$ consists of samples of a white, complex,

Gaussian random process with mean zero and variance N_{ij}. We assume that the channel fading processes in different transmission links are mutually independent, i.e., $\forall i \neq m$ or $j \neq n$, we have $\mathbb{E}[h_{ij}(k)h^*_{mn}(k)] = 0$. In addition, all the AWGN sequences are mutually independent and are independent of all the channel fading processes. The instantaneous received SNR at the j-th node over the $i-j$ link is defined as $\gamma_{ij}(k) = E_i|h_{ij}(k)|^2/N_{ij}$, and the average received SNR is defined as $\gamma_{ij}^{\text{ave}} = E_i 2\sigma_{ij}^2/N_{ij}$. Since σ_{ij}^2 and N_{ij} are only related to the $i-j$ link, all the links between each pair of nodes are i.n.d..

4.2.2 Channel Estimation

Channel estimation is required at the destination and at all the L relays to obtain estimates of the CSIs for coherent detection. Without loss of generality, we assume that all pilot symbols have the same value of 1. When node j receives a packet from node i, the N_p pilot symbols in that packet are feeded into a Wiener filter to generate the MMSE estimate of $h_{ij}(k), k \in N_p+1, N_p+2, ..., N$. We denote the MMSE estimate by $\hat{h}_{ij}(k)$, and it can be represented as [70, eq.(2.1)]

$$\hat{h}_{ij}(k) = \sum_{l=1}^{N_p} w_{ij}(l) y_{ij}(l), \tag{4.4}$$

where $w_{ij}(l) = 2\sigma_{ij}^2 E_i^{1/2}(N_p E_i 2\sigma_{ij}^2 + N_{ij})^{-1}$ denotes the l-th filter coefficient and is the same for all l. The corresponding MMSE of the estimation process is given by [70, eq.(2.49)]

$$2V_{ij}^2 = \frac{2\sigma_{ij}^2}{1 + \frac{N_p E_i 2\sigma_{ij}^2}{N_{ij}}}. \tag{4.5}$$

The $\hat{h}_{ij}(k)$ is a complex Gaussian random variable with mean zero and variance $2\lambda_{ij}^2 = 2\sigma_{ij}^2 - 2V_{ij}^2$. Now, the instantaneous and average received SNRs at the j-th node over the $i-j$ link due to the imperfect CSI are given, respectively, as

$$\hat{\gamma}_{ij}(k) = \frac{E_i|\hat{h}_{ij}(k)|^2}{E_i 2V_{ij}^2 + N_{ij}}. \tag{4.6}$$

and

$$\hat{\gamma}_{ij}^{\text{ave}} = \frac{E_i 2\lambda_{ij}^2}{E_i 2V_{ij}^2 + N_{ij}}. \tag{4.7}$$

4.3 ML Detector at the Destination for A DF Relay System with Imperfect CSI

In the DF protocol, each relay decodes the source message and generates a copy of that message as an output to the destination. The destination receiver makes an ML decision on $x_s(k)$ based on the received signals from the source and from all the relays. Here, we do not consider the transmission delay and the delay due to the channel estimation process, as they will not affect the main results. We assume that for general M-QAM, all the symbol points in the signal constellation $\mathcal{X} = \{S_m\}_{m=1}^{|\mathcal{X}|}$ are with equal likelihood. Therefore, the maximum a posteriori probability (MAP) detector is equivalent to the ML detector. In the following, we consider the optimum detection at the relay and at the destination, respectively.

4.3.1 Detection at the r-th Relay

A relay makes optimum (ML) detection of the received signal from the source. Specifically, for the r-th relay, it calculates the likelihood of the received signal for each possible value S_m in $\mathcal{X}$, and declares that $x_r(k) = S_n$ if the likelihood function $p(y_{sr}(k)|\hat{h}_{sr}(k), x_s(k) = S_n) = \max\limits_{S_m \in \mathcal{X}} p(y_{sr}(k)|\hat{h}_{sr}(k), x_s(k) = S_m)$. Conditioned on $\hat{h}_{sr}(k)$ and $x_s(k) = S_m$, $y_{sr}(k)$ is a complex Gaussian random variable with mean $E_s^{1/2} S_m \hat{h}_{sr}(k)$ and variance $E_s|S_m|^2 2V_{sr}^2 + N_{sr}$. Therefore, the conditional PDF of $y_{sr}(k)$ is given by

$$p(y_{sr}(k)|\hat{h}_{sr}(k), x_s(k) = S_m) = \frac{1}{\pi(E_s|S_m|^2 2V_{sr}^2 + N_{sr})} \times \exp\left(-\frac{|y_{sr}(k) - E_s^{1/2} S_m \hat{h}_{sr}(k)|^2}{E_s|S_m|^2 2V_{sr}^2 + N_{sr}}\right). \quad (4.8)$$

Taking natural logarithm of the right hand side of (4.8), and ignoring those terms that are independent of S_m, it is clear that the maximization of (4.8) is equivalent to the minimization of $(E_s|S_m|^2 2V_{sr}^2 + N_{sr})^{-1}|y_{sr}(k) - E_s^{1/2} S_m \hat{h}_{sr}(k)|^2 - \ln(E_s|S_m|^2 2V_{sr}^2 +$

$N_{sr})^{-1}$. For notational simplicity, we let

$$\eta_{ij}^{m} = (E_i|S_m|^2 2V_{ij}^2 + N_{ij})^{-1} \tag{4.9}$$

and

$$\beta_{ij}^{m}(k) = |y_{ij}(k) - E_i^{1/2} S_m \hat{h}_{ij}(k)|^2, \tag{4.10}$$

where $i \in \{s, r\}_{r=1}^{L}$ denotes a transmitting node, $j \in \{r, d\}_{r=1}^{L}$ denotes a receiving node, and the superscript m denotes that the term depends on the symbol point S_m. Now, the ML decision rule at the r-th relay for detecting $x_s(k)$ declares that $x_r(k) = S_n$ if $\eta_{sr}^{n}\beta_{sr}^{n}(k) - \ln\eta_{sr}^{n} = \min\limits_{S_m \in \mathcal{X}} \left(\eta_{sr}^{m}\beta_{sr}^{m}(k) - \ln\eta_{sr}^{m}\right)$.

4.3.2 Detection at the Destination

The received signals at the destination in the k-th symbol interval consist of a group of signals $\{y_{rd}(k)\}_{r=1}^{L}$ from the L relays and a signal $y_{sd}(k)$ from the source. We express the received signals as a 1-by-(L+1) vector $\mathbf{y} = \begin{bmatrix} y_{sd}(k) & y_{1d}(k) & \ldots & y_{Ld}(k) \end{bmatrix}$. The destination receiver makes an ML decision on $x_s(k)$ based on $\mathbf{y}$. Conditioned on $\hat{h}_{ij}(k)$ and $x_s(k) = S_m$ being sent by the source, the conditional PDF of $\mathbf{y}$ is

$$\begin{aligned} & p(\mathbf{y}|\ \hat{h}_{ij}(k), ij \in \{sd, sr, rd\}_{r=1}^{L}, x_s(k) = S_m) \\ = \ & p(y_{sd}(k) \mid \hat{h}_{ij}(k), ij \in \{sd, sr, rd\}_{r=1}^{L}, x_s(k) = S_m) \times \\ & \prod_{r=1}^{L} p(y_{rd}(k) \mid \hat{h}_{ij}(k), ij \in \{sd, sr, rd\}_{r=1}^{L}, x_s(k) = S_m), \end{aligned} \tag{4.11}$$

where the equality is due to the mutual independence of all the $i - j$ links. Since $y_{sd}(k)$ is independent of $\hat{h}_{sr}(k)$ and $\hat{h}_{rd}(k)$, we have

$$\begin{aligned} & p(y_{sd}(k) \mid \hat{h}_{ij}(k), ij \in \{sd, sr, rd\}_{r=1}^{L}, x_s(k) = S_m) \\ = \ & p(y_{sd}(k)|\ \hat{h}_{sd}(k), x_s(k) = S_m). \end{aligned} \tag{4.12}$$

Moreover, since $y_{rd}(k)$ is independent of $\hat{h}_{sd}(k)$, we have

$$\begin{aligned} & p(y_{rd}(k) \mid \hat{h}_{ij}(k), ij \in \{sd, sr, rd\}, x_s(k) = S_m) \\ = \; & p(y_{rd}(k) \mid \hat{h}_{ij}(k), ij \in \{sr, rd\}, x_s(k) = S_m) \\ = \; & \sum_{S_n \in \mathcal{X}} p(y_{rd}(k) \mid \hat{h}_{ij}(k), ij \in \{sr, rd\}, x_r(k) = S_n, x_s(k) = S_m) \times \\ & p(x_r(k) = S_n \mid \hat{h}_{ij}(k), ij \in \{sr, rd\}, x_s(k) = S_m). \end{aligned} \tag{4.13}$$

In (4.13), we note that conditioned on $\hat{h}_{rd}(k)$ and $x_r(k)$, $y_{rd}(k)$ is independent of $\hat{h}_{sr}(k)$ and $x_s(k)$. In addition, $x_r(k)$ is independent of $\hat{h}_{rd}(k)$. Therefore, (4.13) can be rewritten as

$$\begin{aligned} & p(y_{rd}(k) \mid \hat{h}_{ij}(k), ij \in \{sd, sr, rd\}, x_s(k) = S_j) \\ = \; & \sum_{S_n \in \mathcal{X}} p(y_{rd}(k) \mid \hat{h}_{rd}(k), x_r(k) = S_n) p(x_r(k) = S_n \mid \hat{h}_{sr}(k), x_s(k) = S_m). \end{aligned} \tag{4.14}$$

Substituting (4.12) and (4.14) into (4.11), we have

$$\begin{aligned} & p(\mathbf{y} \mid \hat{h}_{ij}(k), ij \in \{sd, sr, rd\}_{r=1}^{L}, x_s(k) = S_m) \\ = \; & p(y_{sd}(k) \mid \hat{h}_{sd}(k), x_s(k) = S_m) \times \\ & \prod_{r=1}^{L} \sum_{S_n \in \mathcal{X}} p(y_{rd}(k) \mid \hat{h}_{rd}(k), x_r(k) = S_n) p(x_r(k) = S_n \mid \hat{h}_{sr}(k), x_s(k) = S_m). \end{aligned} \tag{4.15}$$

In the above, we note that conditioned on $\hat{h}_{sd}(k)$ and $x_s(k) = S_m$, $y_{sd}(k)$ is a complex Gaussian random variable with mean $E_s^{1/2} S_m \hat{h}_{sd}(k)$ and variance $E_s |S_m|^2 2V_{sd}^2 + N_{sd}$. Similarly, conditioned on $\hat{h}_{rd}(k)$ and $x_r(k) = S_m$, $y_{rd}(k)$ is a complex Gaussian random variable with mean $E_r^{1/2} S_m \hat{h}_{rd}(k)$ and variance $E_r |S_m|^2 2V_{rd}^2 + N_{rd}$. Therefore, we have

$$p(y_{sd}(k) \mid \hat{h}_{sd}(k), x_s(k) = S_m) = \frac{\eta_{sd}^m}{\pi} \exp\big(- \eta_{sd}^m \beta_{sd}^m(k) \big), \tag{4.16}$$

and

$$p(y_{rd}(k) \mid \hat{h}_{rd}(k), x_r(k) = S_m) = \frac{\eta_{rd}^m}{\pi} \exp\big(- \eta_{rd}^m \beta_{rd}^m(k) \big), \tag{4.17}$$

where η_{ij}^m and $\beta_{ij}^m(k)$ are defined in (4.9) and (4.10), respectively. We also note that $p(x_r(k) = S_n \mid \hat{h}_{sr}(k), x_s(k) = S_m)$ denotes the instantaneous probability of $x_s(k) = S_m$ being sent by the source and $x_r(k) = S_n$ being received by the relay, i.e., when $m = n$, it denotes the instantaneous probability of a correct decision on the received symbol at the relay; when $m \neq n$, it denotes the instantaneous symbol error probability (ISEP) at the relay. We denote the probability $p(x_r(k) = S_n \mid \hat{h}_{sr}(k), x_s(k) = S_m)$ by $P_{sr}^{m\to n}(k)$ for short. Now, substituting (4.16) and (4.17) into (4.15), taking the natural logarithm of the right hand side of (4.15) and ignoring those terms that are independent of S_m and S_n, the ML decision rule at the destination which maximizes the conditional PDF $p(\mathbf{y}|\ \hat{h}_{ij}(k), ij \in \{sd, sr, rd\}_{r=1}^{L}, x_s(k) = S_m)$, is obtained as

$$\hat{x}(k) = \max_{S_m \in \mathcal{X}} \left\{ -\eta_{sd}^m \beta_{sd}^m(k) + \sum_{r=1}^{L} \ln \left[\sum_{S_n \in \mathcal{X}} P_{sr}^{m\to n}(k) \exp(-\eta_{rd}^n \beta_{rd}^n(k)) \right] \right\}. \tag{4.18}$$

The (optimum) ML detector for a DF relay system with an available $s-d$ link has firstly been shown in [20] for a single relay case with BPSK. Our result (4.18) generalizes the ML detector structure for a DF multiple relay system with an arbitrary M-QAM. Moreover, it takes into account i.n.d. $s-d$, $s-r$ and $r-d$ links, and generalizes both perfect and imperfect CSI scenarios. This receiver result clearly shows that for optimum detection at the destination, the knowledge of the instantaneous quality of the $s-r$ links, which is summarized as the ISEPs at the relays, is required. We also note that when the $s-d$ link is not available, the ML detector is given by

$$\hat{x}(k) = \max_{S_m \in \mathcal{X}} \left\{ \sum_{r=1}^{L} \ln \left[\sum_{S_n \in \mathcal{X}} P_{sr}^{m\to n}(k) \exp(-\eta_{rd}^n \beta_{rd}^n(k)) \right] \right\}. \tag{4.19}$$

Comparing (4.19) with (4.18), the term $-\eta_{sd}^m \beta_{sd}^m(k)$ which represents the contribution of the $s-d$ link, is gone.

To analyze the ML detector, we need to specify the modulation scheme. In the following, we specialize the ML detector to the one with BPSK for simplicity.

4.4 ML detector with BPSK

With BPSK modulation, the signal constellation $\mathcal{X}$ only consists of $\{+1, -1\}$. Without loss of generality, let $S_0 = -1$ and $S_1 = +1$. The ML decision rule at the r-th relay becomes [93]

$$\Re\big[y_{sr}(k)\hat{h}^*_{sr}(k)S_0\big] \underset{S_1}{\overset{S_0}{\gtrless}} \Re\big[y_{sr}(k)\hat{h}^*_{sr}(k)S_1\big], \tag{4.20}$$

and the corresponding detection error probability, i.e., the IBEP, is given by

$$\varepsilon_{sr}(k) = \frac{1}{2}\mathrm{erfc}\left(\hat{\gamma}_{sr}(k)\right)^{1/2}. \tag{4.21}$$

We note that $\varepsilon_r(k)$ is determined by the instantaneous received SNR $\hat{\gamma}_{sr}(k)$ defined in (4.6), and it summarizes the quality of the $s-r$ link. Averaging $\varepsilon_{sr}(k)$ over the distribution of $\hat{h}_{sr}(k)$ (or $\hat{\gamma}_{sr}(k)$), the ABEP at the r-th relay is given by [93]

$$\varepsilon^{\mathrm{ave}}_{sr} = \frac{1}{2}\left[1 - \left(\frac{\gamma^{\mathrm{ave}}_{sr}}{1+\gamma^{\mathrm{ave}}_{sr}}\right)^{1/2}\right], \tag{4.22}$$

where $\gamma^{\mathrm{ave}}_{sr}$ is defined in (4.7). It is noted that this ABEP is obtainable at the destination in advance, given the channel statistics of the $s-r$ link, the source transmitting energy E_s and the number of pilots per packet N_p.

Now, we show the ML detector at the destination with BPSK. Substituting $S_0 = -1$ and $S_1 = +1$ into the argument on the right hand side of (4.18), respectively, and by comparing the differences between the two terms obtained above, the ML decision rule at the destination can be expressed, through a signum function, as

$$\hat{x}(k) = \mathrm{sgn}\left(t_s(k) + \sum_{r=1}^{L} f_r(t_r(k))\right). \tag{4.23}$$

Here, $f_r(t_r(k))$ is a nonlinear function related to the r-th relay, and is given by

$$f_r(t_r(k)) = \ln\frac{(1-\varepsilon_{sr}(k))\exp(t_r(k)) + \varepsilon_{sr}(k)}{(1-\varepsilon_{sr}(k)) + \varepsilon_{sr}(k)\exp(t_r(k))}, \tag{4.24}$$

where

$$t_s(k) = 4E_s^{1/2}\eta_{sd}\Re\big[y_{sd}(k)\hat{h}^*_{sd}(k)\big], \tag{4.25}$$

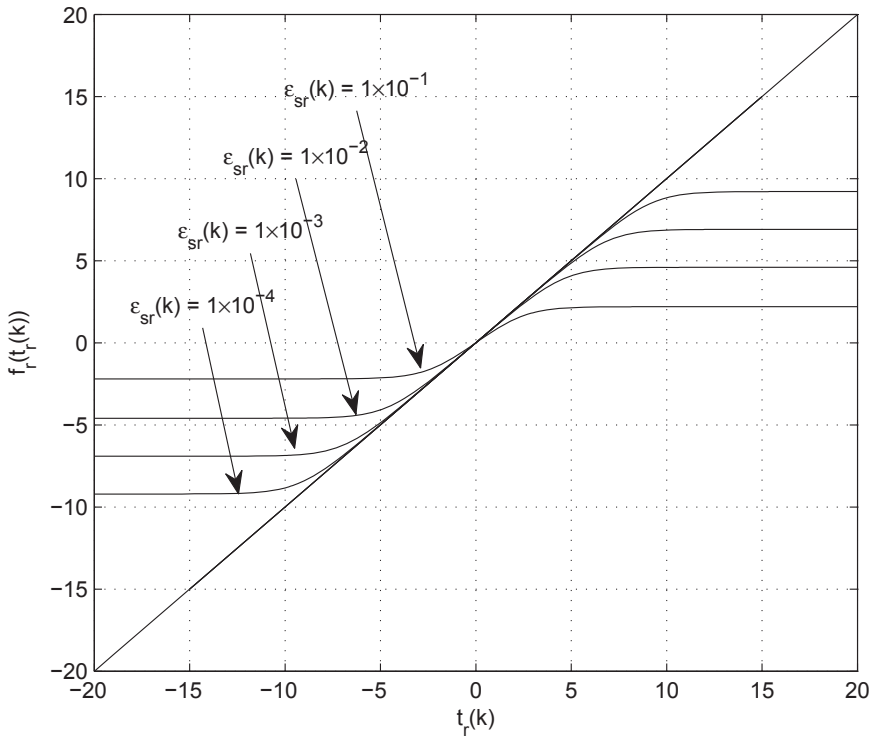

Figure 4.2: Plot of the nonlinear function $f_r(t_r(k))$.

$$t_r(k) = 4E_r^{1/2}\eta_{rd}\Re\big[y_{rd}(k)\hat{h}_{rd}^*(k)\big]. \tag{4.26}$$

This decision rule declares that S_1 is transmitted if the sum of the terms in the signum function is greater than zero. Otherwise, S_0 is transmitted. It is also worth noting that with BPSK, the term η_{ij}^m defined in (4.9) can be written as $\eta_{ij} = (E_i 2V_{ij}^2 + N_{ij})^{-1}$, since $|S_m|^2 = 1$, i.e., η_{ij} is independent of the symbol point S_m. Therefore, in (4.25) and (4.26), we have written η_{ij}^m as η_{ij} for simplicity.

The nonlinear function $f_r(t_r(k))$, as illustrated in Fig. 4.2, has a sigmoidal behavior, and it represents the contribution of the $s-r-d$ link to the ML detection at the destination. This function along with its sigmoidal behavior are firstly reported in [20] for a DF single relay system. For a DF multiple relay system, we note from (4.23) that each $s-r-d$ link independently contributes an $f_r(t_r(k))$ to the destination detector. Here, we emphasize that the ML detector uses $\varepsilon_{sr}(k)$, which is

the IBEP at the relay for decoding the source message. As has been mentioned in Section 4.1, in the literature, all the existing works attempting to analyze the ML detector, actually analyze the suboptimum detector which uses the ABEP at the relay. The use of the ABEP, of course, simplifies the detector for both analysis and implementation. However, it is noted that the penalty of using the ABEP is a loss in the achievable diversity order, which is quite undesirable for the receiver design of a multiple relay communication system.

Another fact that prevents the popularity of the ML detector is that it has been commonly assumed that the estimated channel fading gain of the $s-r$ link is required at the destination for coherent detection. However, (4.23) clearly shows that only the IBEP at the relay is involved, and it summarizes the CSI on the $s-r$ link. Compared with the transmission of the CSI, which consists of a real part and an imaginary part both ranging from $-\infty$ to ∞, one can expect to transmit $\varepsilon_{sr}(k)$ using much fewer bits, since it is a small, real number between 0 and 0.5. We illustrate the carry of the IBEP information from the relay to the destination in the following. In a practical DF relay system, when a relay decodes a source packet, it also computes the IBEP, and attaches this IBEP as an overhead to that source packet. Therefore, the new packet consists of three part of information, namely, the IBEP at the relay, the pilot bits and the relay-decoded data bits. Then, the new packet is forwarded to the destination for further use. For a heuristic study, we introduce a simple 8-bit-overhead scheme for carrying the IBEP information. More specifically, we represent $\varepsilon_{sr}(k)$ in the scientific form, and quantize its base and exponent separately, with each occupying 4 bits. This 8-bit information is attached to the decoded source packet as an overhead. We will verify the efficiency of this 8-bit-overhead scheme using simulations in the next chapter. We emphasize that our effort on retaining the IBEP information for detection at the destination is driven by the fact that the destination detector using the IBEP at the relay offers a substantial gain over the one using the ABEP at the relay. This will be demonstrated in the next chapter.

In the following, we consider approximations to the ML detector.

4.5 Approximations to the ML Detector with BPSK

To simplify the implementation of the ML detector, suboptimum detectors are widely considered. In Table 1.1, we have summarized and termed a few suboptimum detectors. In this section, we introduce them in detail. Generally, we can categorize those approximations to the ML detector into two groups. One group retains the use of the IBEP at the relay. The other one replaces the IBEP at the relay by the ABEP at the relay. In all the following parts of this chapter, we omit the time index k in the corresponding terms for notational simplicity, since it would not cause any ambiguity in interpretation.

4.5.1 The Traditional MRC

Although not suitable, the traditional MRC can be used as a suboptimum detector for DF relay systems for its simplicity. Actually, in the case where the $s-r$ link is much more reliable than the corresponding $r-d$ link, the MRC offers a good approximation to the ML detector. From our derivation of the ML detector, it is readily seen that the decision rule of the MRC is given by

$$\hat{x} = \operatorname{sgn}\left(t_s + \sum_{r=1}^{L} t_r\right). \tag{4.27}$$

Eq. (4.27) can also be derived from (4.23) by letting $f_r(t_r) = t_r$, i.e., by setting ε_{sr} to zero. As can be seen, the MRC simply assumes that the relay makes no decision errors, and it combines all the received signals in the traditional way of diversity receptions. It is also worth noting that from a geometrical point of view, in the MRC, the nonlinear function $f_r(t_r)$ in the ML detector is approximated by a straight line whose slope is equal to 1. This is clearly shown in Fig. 4.3.

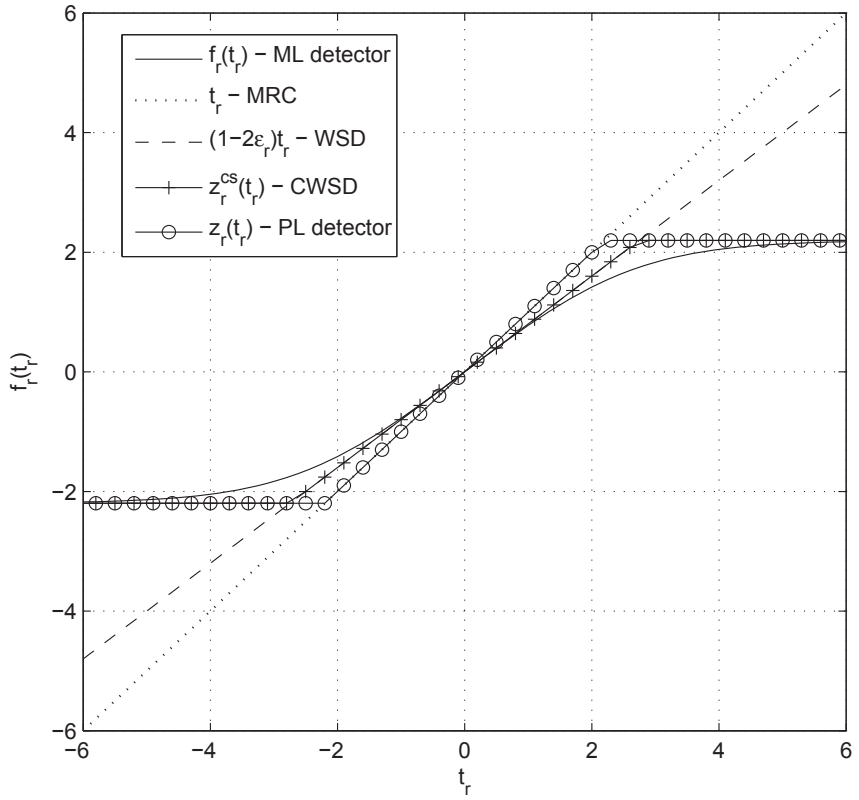

Figure 4.3: Geometrical representations of approximations to the nonlinear function $f_r(t_r)$.

4.5.2 The WSD

As can be seen from Fig. 4.3, an intuitive improvement on the MRC is to include the IBEP at the relay, where the nonlinear function $f_r(t_r)$ is approximated by a straight line whose slope is equal to the slope of $f_r(t_r)$ at $t_r = 0$. To show the improvement in more detail, we differentiate (4.24) with respect to t_r, which gives

$$\frac{d}{dt_r} f_r(t_r) = \frac{(1 - 2\varepsilon_{sr})}{(1 - 2\varepsilon_{sr} + 2\varepsilon_{sr}^2)e^{t_r} + \varepsilon_{sr}(1 - \varepsilon_{sr})(1 + e^{2t_r})}. \tag{4.28}$$

Evaluating (4.28) at $t_r = 0$ gives

$$\frac{d}{dt_r} f_r(t_r)|_{t_r=0} = 1 - 2\varepsilon_{sr}. \tag{4.29}$$

Therefore, the term $1-2\varepsilon_{sr}$ is the slope of $f_r(t_r)$ at $t_r = 0$. From Fig. 4.3, it is clear that a better approximation to $f_r(t_r)$ than that in the traditional MRC is given by

$$f_r(t_r) \approx (1 - 2\varepsilon_{sr})t_r. \tag{4.30}$$

Using the above approximation, we arrive at the destination detector. We term it as the WSD, since compared with the ML detector, the contribution of each $s - r - d$ link is reduced from $f_r(t_r)$ to a weighed term weighting by the slope of $f_r(t_r)$ at $t_r = 0$. The WSD is expressed as

$$\hat{x}(k) = \mathrm{sgn}\Big(t_s + \sum_{r=1}^{L}(1 - 2\varepsilon_{sr})t_r\Big). \tag{4.31}$$

Although simple, the WSD captures part of the effect of the decoding errors at the relay.

4.5.3 The CWSD

As has been noted in [20] and also been shown in Fig. 4.2, the nonlinear function $f_r(t_r)$ essentially "clips" its input to the values $\pm\ln(1-\varepsilon_{sr})/\varepsilon_{sr}$. Therefore, compared with the WSD, a more accurate approximation to $f_r(t_r)$ is achieved by clipping the WSD with $\pm\ln(1-\varepsilon_{sr})/\varepsilon_{sr}$. This results in the CWSD as given by

$$\hat{x}(k) = \mathrm{sgn}\Big(t_s + \sum_{r=1}^{L} z_r^{cs}(t_r)\Big), \tag{4.32}$$

where the function $z_r^{cs}(t_r)$ is given by

$$z_r^{cs}(t_r) = \begin{cases} -\ln\tau_r, & t_r < -\frac{\ln\tau_r}{1-2\varepsilon_{sr}} \\ (1-2\varepsilon_{sr})t_r, & -\frac{\ln\tau_r}{1-2\varepsilon_{sr}} \le t_r < \frac{\ln\tau_r}{1-2\varepsilon_{sr}} \\ \ln\tau_r, & t_r \ge \frac{\ln\tau_r}{1-2\varepsilon_{sr}} \end{cases}, \tag{4.33}$$

and τ_r is defined as

$$\tau_r = \frac{1-\varepsilon_{sr}}{\varepsilon_{sr}}. \tag{4.34}$$

Fig. 4.3 clearly shows how $z_r^{cs}(t_r)$ approximates $f_r(t_r)$.

4.5.4 The PL Detector

In [25], a popular approximation to the nonlinear function $f_r(t_r)$ has been proposed, and is termed as the PL approximation. It approximates $f_r(t_r)$ by a PL function $z_r(t_r)$ defined as

$$z_r(t_r) = \begin{cases} -\ln \tau_r, & t_r < -\ln \tau_r \\ t_r, & -\ln \tau_r \leq t_r < \ln \tau_r, \\ \ln \tau_r, & t_r \geq \ln \tau_r \end{cases} \tag{4.35}$$

Here, we emphasize that we retain the use of the IBEP at the relay in the PL function. This distinguishes (4.35) from the classic PL approximation [25]. In [25], the PL function is defined using the ABEP at the relay, which results in an averaged detector. As has been discussed in Section 1.2.2, the main drawback of averaged detectors is a loss of diversity. The ML detector with the PL approximation, or simply, the PL detector, is denoted by

$$\hat{x} = \text{sgn}\left(t_s + \sum_{r=1}^{L} z_r(t_r) \right). \tag{4.36}$$

It is readily seen that $z_r(t_r)$ can be derived from (4.33) by setting the slope $1 - 2\varepsilon_{sr}$ to 1, i.e., the PL detector can be viewed as the CWSD with a fixed slope of 1. From Fig. 4.3, it is noted that the PL detector can also be viewed as a clipped MRC.

As shown in Fig. 4.3, the geometrical view of these approximations to the nonlinear function $f_r(t_r)$ provides us with an insightful view of the relationship among those suboptimum detectors. It is clear that as the SNR of the $s - r$ link increases, ε_{sr} decreases, and this results in that the slope $1 - 2\varepsilon_{sr}$ tends to 1. Consequently, the WSD tends to the traditional MRC, and the CWSD tends to the PL detector.

4.6 Conclusions

In this chapter, we derived the ML detector at the destination for a general, uncoded DF multiple relay system with an arbitrary M-QAM. The detector generalizes

both perfect and imperfect CSI scenarios. The imperfect CSI case which takes into account of the channel estimation errors at all receiving nodes, has not been considered elsewhere. Our derived ML detector can be specialized to [20]'s result easily. It is important to note that our receiver result clearly shows that for optimum detection at the destination, the ISEP at the relay is required. Specializing to BPSK, we introduced several approximations to the ML detector. The performance of these detectors will be examined in the next chapter.

Chapter 5

Performance Analysis of A DF Relay System with BPSK

We provide performance analysis for a DF relay system. For a single relay case, we derive a closed-form ABEP for the MRC and closed-form conditional BEPs conditioned on the IBEP at the relay, for the WSD, the CWSD, and the PL detector, respectively. It is noted that in these conditional BEP results, replacing the IBEP at the relay with its average, it gives the ABEPs of the A-WSD, the A-CWSD and the A-PL detector, respectively. The conditional BEP of the PL detector provides the most tractability. Therefore, we further obtain a closed-form, approximate ABEP for the PL detector. We emphasize that this obtained ABEP, although being an approximation, is for the PL detector which utilizes the IBEP at the relay. This distinguishes our work from those which analyze the A-PL detector using the ABEP at the relay. The exact ABEP of the ML detector is not obtainable. Nevertheless, the performance of the ML detector can be well approximated by the PL detector. Considering a multiple relay system with an arbitrary number of relays, the exact ABEP performance at the destination cannot be obtained in general. For that reason, we derive closed-form Chernoff upper bounds on the ABEPs of the A-PL and the PL detectors, respectively. Simulations are used to validate of our analysis. It is shown that the detectors retaining using the IBEP at the relay offer a substantial

gain over the averaged detectors which only use the ABEP at the relay. Our Chernoff bound results prove that for a DF relay system, the destination detector using the IBEP at the relay achieves full diversity.

5.1 Introduction

The performance analysis of a general, uncoded DF relay communication system is a long-standing, open problem. To the best of our knowledge, no closed-form ABEP result for the ML detector (4.23) has been obtained, even for a single relay case. The two main difficulties on the analysis lie in the nonlinearity of the $f_r(t_r)$ function and the averaging of the obtained conditional BEP at the destination over the statistics of the $s-r$ link. As has been shown in Section 4.5, to circumvent the first difficulty, the PL detector or the CWSD can be used instead. To circumvent the second difficulty, as we have mentioned in Section 4.4, another commonly made approximation is to replace the IBEP at the relay with its average. By doing so, the averaging of the conditional BEP at the destination over the statistics of the $s-r$ link is obviated.

Generally, the approximation based on the replacement of the IBEP with the ABEP should be avoided to maintain full diversity of the destination receiver. Unfortunately, this has been an overlooked issue in the literature. As has been noted, in the attempt to analyze the ML detector, all the previous works [25,26,52,54,55,57] have made the approximation to replace the IBEP at the relay with the ABEP. More specifically, they all examined the performance of the A-PL detector. It is noted that [26] aims to solve the exact ABEP of the A-ML detector. However, due to the use of an approximation in arriving at a closed-form result, the obtained final result for the A-ML detector amounts to that for the A-PL detector. Thus, we term this approximation used in [26] as the equivalent-PL approximation for clarity. Another limitation of those above-mentioned works is that their exact performance analysis is mainly restricted to a single relay or a two-relay case. Reference [23] has noted the importance of using the instantaneous information of the $s-r$ link

for detection at the destination, and it considers a multiple relay system. However, in [23], the ABEP at the destination is only analyzed from the diversity point of view, where extremely high SNR is assumed. Motivated by these facts, we analyze the performance of a DF relay system where the IBEP at the relay is used for detection at the destination. We provide exact, closed-form results for both a single relay case and a multiple relay case. Moreover, our analysis takes into account of the effect of channel estimation errors, which has not been considered elsewhere. To specialize the obtained results to the perfect CSI scenario, we simply set the variances of the estimation errors defined in (4.5) to zeros. We confine ourselves to the analysis with BPSK, as the ML detector for higher order modulations is fairly complex.

In our analysis, we first consider a single relay system. We derive closed-form conditional BEPs conditioned on the IBEP at the relay, for the WSD, the CWSD, and the PL detector, respectively. It is noted that in those derived conditional BEP results, replacing the IBEP at the relay with its average, it gives the ABEPs of the A-WSD, the A-CWSD and the A-PL detector, respectively. The conditional BEP of the PL detector provides the most tractability. Therefore, we further obtain a closed-form, approximate ABEP for the PL detector. We emphasize that this obtained ABEP, although being an approximation, is for the PL detector which uses the IBEP at the relay. To analyze the performance of the ML detector, we first derive the conditional BEP at the destination conditioned on the IBEP at the relay. This conditional BEP result contains integrals. Again, it is noted that in the derived conditional BEP, replacing the IBEP at the relay with its average, it gives the ABEP of the A-ML detector. To arrive at a closed-form conditional BEP for the ML detector for further analysis, we apply an approximation which is similar to the equivalent-PL approximation [26]. The use of this approximation results in that the obtained closed-form, approximate, conditional BEP of the ML detector amounts to the conditional BEP of the PL detector. Therefore, the obtained ABEP result for the PL detector applies to the ML detector as approximate ABEP result. Considering a multiple relay system with an arbitrary number of relays, the exact

ABEP result for the ML detector cannot be obtained in general. For that reason, we derive closed-form Chernoff upper bounds on the ABEPs of the A-PL and the PL detectors, respectively. The Chernoff bounds become tighter as the number of relays increases. Our derived results are verified through simulations. It is shown that the detectors retaining using the IBEP at the relay offer a substantial gain over the averaged detectors which only use the ABEP at the relay. Our Chernoff bound results prove that for a DF relay system, the detector using the IBEP at the relay achieves full diversity.

The rest of this chapter is organized as follows. In section 5.2, we first decide the statistics of the decision metrics at the destination. Section 5.3 and Section 5.4 provide theoretical analysis for a single relay system and a multiple relay system, respectively. Numerical and simulation results are presented in Section 5.5. Section 5.6 concludes this chapter.

5.2 Statistics of Destination Decision Metrics

To analyze the ABEP at the destination, we first study the statistics of the destination decision metrics for the ML detector, namely, t_s, t_r and $f_r(t_r)$. In addition, we show the statistics of $z_r^{cs}(t_r)$ and $z_r(t_r)$, which are the decision metrics for the CWSD and the PL detector, respectively.

The t_s and t_r are given by (4.25) and (4.26), respectively. It is noted that conditioned on $\hat{h}_{sd}$ and x_s, t_s is conditionally Gaussian distributed with mean $4x_s E_s \eta_{sd} |\hat{h}_{sd}|^2$ and variance $8E_s\eta_{sd}|\hat{h}_{sd}|^2$. From the definitions of $\hat{\gamma}_{sd}$ in (4.6) and η_{sd} in (4.9), we note that $\hat{\gamma}_{sd} = E_s\eta_{sd}|\hat{h}_{sd}|^2$. Therefore, t_s is conditionally Gaussian distributed with mean $4x_s\hat{\gamma}_{sd}$ and variance $8\hat{\gamma}_{sd}$. Similarly, it is easy to obtain that conditioned on $\hat{h}_{rd}$ (or say, $\hat{\gamma}_{rd}$) and x_r, t_r is conditionally Gaussian distributed with mean $4x_r\hat{\gamma}_{rd}$ and variance $8\hat{\gamma}_{rd}$. We mention that $\hat{\gamma}_{ij}$ is the instantaneous received SNR at the j-th node over the $i-j$ link due to the imperfect CSI. It is easy to see

that $\hat{\gamma}_{ij}$ is exponentially distributed with the parameter

$$\theta_{ij} = 1/\hat{\gamma}_{ij}^{\text{ave}}, \tag{5.1}$$

where $\hat{\gamma}_{ij}^{\text{ave}}$ is defined in (4.7). Therefore, the PDF of $\hat{\gamma}_{ij}$ is given by

$$p_{\hat{\gamma}_{ij}}(x) = \theta_{ij} \exp\left(-\theta_{ij} x\right) u(x). \tag{5.2}$$

Now, it is straightforward to obtain that conditioned on $\hat{\gamma}_{sd}$ and x_s, the conditional CDF of t_s is given by

$$\begin{aligned} F_{t_s|\hat{\gamma}_{sd},x_s}(X) &= P(t_s < X|\hat{\gamma}_{sd}, x_s) \\ &= Q\left(\frac{4x_s\hat{\gamma}_{sd} - X}{2\sqrt{2}\sqrt{\hat{\gamma}_{sd}}}\right). \end{aligned} \tag{5.3}$$

Similarly, conditioned on $\hat{\gamma}_{rd}$ and x_r, the conditional CDF of t_r is given by

$$\begin{aligned} F_{t_r|\hat{\gamma}_{rd},x_r}(X) &= P(t_r < X|\hat{\gamma}_{rd}, x_r) \\ &= Q\left(\frac{4x_r\hat{\gamma}_{rd} - X}{2\sqrt{2}\sqrt{\hat{\gamma}_{rd}}}\right). \end{aligned} \tag{5.4}$$

Following the procedure proposed by [26], we present Theorems 5.2.1 and 5.2.2 as below, which can be readily shown to be the same as [26, Theorem 3.1] and [26, Theorem 3.2], respectively.

Theorem 5.2.1. The conditional CDF of t_i conditioned on x_i, $i \in \{s, r\}$, is given by

$$F_{t_i|x_i}(X) = \begin{cases} 1 - \frac{g_i}{v_i(-1,x_i)} \exp\left(-v_i(-1, x_i)X\right), & X \geq 0 \\ \frac{g_i}{v_i(1,x_i)} \exp(v_i(1, x_i)X), & X < 0. \end{cases} \tag{5.5}$$

where

$$g_i = \frac{\theta_{id}}{4\sqrt{1+\theta_{id}}}, \tag{5.6}$$

and

$$v_i(a, x_i) = \frac{ax_i + \sqrt{1+\theta_{id}}}{2}, a = \pm 1. \tag{5.7}$$

Proof: We note from (5.3) that the expression is conditioned on the $\hat{\gamma}_{sd}$. To compute the unconditional result, we uncondition $F_{t_s|\hat{\gamma}_{sd},x_s}(X)$ with respect to $\hat{\gamma}_{sd}$ to have

$$F_{t_s|x_s}(X) = \int_0^\infty Q\left(\frac{4x_s x - X}{2\sqrt{2}\sqrt{x}}\right)\theta_{sd}\exp\left(-\theta_{sd}x\right)dx. \tag{5.8}$$

To calculate the above integral, we use the following formula [94] (or [26, eq.(10)])

$$\int_0^\infty Q(\frac{ax+b}{\sqrt{x}})e^{-cx}dx = \frac{\exp\big(-b(a+\sqrt{a^2+2c})\big)}{\sqrt{a^2+2c}(a+\sqrt{a^2+2c})}, \tag{5.9}$$

where $a, b > 0, c > 0$ are constant. Using (5.9) and changing the variables accordingly, (5.8) can be evaluated as

$$F_{t_s|x_s}(X) = \begin{cases} 1 - \frac{\theta_{sd}}{4\sqrt{1+\theta_{sd}}}\frac{2}{-x_s+\sqrt{1+\theta_{sd}}}\exp\left(-\frac{-x_s+\sqrt{1+\theta_{sd}}}{2}X\right), & X \geq 0 \\ \frac{\theta_{sd}}{4\sqrt{1+\theta_{sd}}}\frac{2}{x_s+\sqrt{1+\theta_{sd}}}\exp\left(\frac{x_s+\sqrt{1+\theta_{sd}}}{2}X\right), & X < 0. \end{cases} \tag{5.10}$$

For notational simplicity, we define

$$\begin{aligned} g_s &= \frac{\theta_{sd}}{4\sqrt{1+\theta_{sd}}}, \\ v_s(a, x_s) &= \frac{ax_s + \sqrt{1+\theta_{sd}}}{2}, a = \pm 1. \end{aligned} \tag{5.11}$$

Therefore, we have

$$F_{t_s|x_s}(X) = \begin{cases} 1 - \frac{g_s}{v_s(-1,x_s)}\exp\left(-v_s(-1,x_s)X\right), & X \geq 0 \\ \frac{g_s}{v_s(1,x_s)}\exp(v_s(1,x_s)X), & X < 0. \end{cases} \tag{5.12}$$

The conditional CDF of t_r conditioned on x_r can be obtained in the same way. Generalizing the above observations, we get Theorem 5.2.1.

□

Corollary. The conditional PDF of t_i conditioned on x_i, $i \in \{s, r\}$, is given by

$$p_{t_i|x_i}(X) = \begin{cases} g_i\exp(-v_i(-1,x_i)X), & X \geq 0 \\ g_i\exp(v_i(1,x_i)X), & X < 0. \end{cases} \tag{5.13}$$

Proof: We note that $F_{t_i|x_i}(X)$ is continuous at $X = 0$. Therefore, differentiating (5.5) with respect to X gives (5.13).

□

Theorem 5.2.2. The conditional CDF of $f_r(t_r)$ conditioned on x_r and ε_{sr}, is given by

$$F_{f_r(t_r)|x_r,\varepsilon_{sr}}(X) = \begin{cases} 0, & X < -\ln\tau_r \\ \frac{g_r}{v_r(1,x_r)} s_r(X)^{v_r(1,x_r)}, & -\ln\tau_r \le X < 0 \\ 1 - \frac{g_r}{v_r(-1,x_r)} s_r(X)^{-v_r(-1,x_r)}, & 0 \le X < \ln\tau_r \\ 1, & X \ge \ln\tau_r \end{cases} \tag{5.14}$$

where $s_r(X)$ is defined as

$$s_r(X) = \frac{(1-\varepsilon_{sr})\exp(X) - \varepsilon_{sr}}{(1-\varepsilon_{sr}) - \varepsilon_{sr}\exp(X)}, X \in [-\ln\tau_r, \ln\tau_r), \tag{5.15}$$

and τ_r has been defined in (4.34).

Proof: The conditional CDF of $f_r(t_r)$ conditioned on x_r and ε_{sr} can be written as

$$F_{f_r(t_r)|x_r,\varepsilon_{sr}}(X) = P(f_r(t_r) < X|x_r, \varepsilon_{sr}). \tag{5.16}$$

We note that $f_r(t_r)$ is a monotonically increasing function and is clipped by $-\ln\tau_r$ and $\ln\tau_r$ [25]. Therefore, for $X < -\ln\tau_r$, $P(f_r(t_r) < X|x_r, \varepsilon_{sr}) = 0$, and for $X \ge \ln\tau_r$, $P(f_r(t_r) < X|x_r, \varepsilon_{sr}) = 1$. For $-\ln\tau_r \le X < \ln\tau_r$, we can write

$$\begin{aligned} F_{f_r(t_r)|x_r,\varepsilon_{sr}}(X) &= P(f_r(t_r) < X|x_r, \varepsilon_{sr}) \\ &= P(t_r < \ln s_r(X)|x_r, \varepsilon_{sr}) \end{aligned} \tag{5.17}$$

where $s_r(X)$ is defined in (5.15) and $Y = \ln s_r(X)$ can be viewed as the inverse function of $X = f_r(Y)$. It is noted that the function $\ln s_r(X)$ only takes value on $[-\ln\tau_r, \ln\tau_r)$ and for $X \ge 0$, $\ln s_r(X) \ge 0$; for $X < 0$, $\ln s_r(X) < 0$. Based on these observations, using Theorem 5.2.1, (5.17) can be computed as

$$F_{f_r(t_r)|x_r,\varepsilon_{sr}}(X) = \begin{cases} 1 - \frac{g_r}{v_r(-1,x_r)} s_r(X)^{-v_r(-1,x_r)}, & 0 \le X < \ln\tau_r \\ \frac{g_r}{v_r(1,x_r)} s_r(X)^{v_r(1,x_r)}, & -\ln\tau_r \le X < 0. \end{cases} \tag{5.18}$$

Therefore, Theorem 5.2.2 is proved.

□

Using Theorem 5.2.1, it is easy to obtain the CDF of $z_r^{cs}(t_r)$ and $z_r(t_r)$, which are the decision metrics for the CWSD and the PL detector, respectively. We omit the proof as it is straightforward. The results are summarized in the following two theorems. Here, we note that τ_r is defined in (4.34).

Theorem 5.2.3. The conditional CDF of $z_r^{cs}(t_r)$ conditioned on x_r and ε_{sr}, is given by

$$F_{z_r^{cs}(t_r)|x_r,\varepsilon_{sr}}(X) = \begin{cases} 0, & X < -\ln\tau_r \\ \frac{g_r}{v_r(1,x_r)} \exp\left(v_r(1,x_r)\frac{X}{1-2\varepsilon_{sr}}\right), & -\ln\tau_r \le X < 0 \\ 1 - \frac{g_r}{v_r(-1,x_r)} \exp\left(-v_r(-1,x_r)\frac{x}{1-2\varepsilon_{sr}}\right), & 0 \le X < \ln\tau_r \\ 1, & X \ge \ln\tau_r \end{cases} \tag{5.19}$$

□

Theorem 5.2.4. The conditional CDF of $z_r(t_r)$ conditioned on x_r and ε_{sr}, is given by

$$F_{z_r(t_r)|x_r,\varepsilon_{sr}}(X) = \begin{cases} 0, & X < -\ln\tau_r \\ \frac{g_r}{v_r(1,x_r)} \exp(v_r(1,x_r)), & -\ln\tau_r \le X < 0 \\ 1 - \frac{g_r}{v_r(-1,x_r)} \exp(-v_r(-1,x_r)), & 0 \le X < \ln\tau_r \\ 1, & X \ge \ln\tau_r \end{cases} \tag{5.20}$$

□

Here, we also derive the conditional PDF of $z_r(t_r)$, which will be used in the analysis of a multiple relay system. It is shown in the following theorem.

Theorem 5.2.5. The conditional PDF of $z_r(t_r)$ conditioned on x_r and ε_{sr}, is given by

$$p_{z_r(t_r)|x_r,\varepsilon_{sr}}(X) = \begin{cases} \frac{g_r}{v_r(1,x_r)} \tau_r^{-v_r(1,x_r)} \dot{\delta}(X + \ln\tau_r), & X = -\ln\tau_r \\ \frac{g_r}{v_r(-1,x_r)} \tau_r^{-v_r(-1,x_r)} \dot{\delta}(X - \ln\tau_r), & X = \ln\tau_r \\ g_r \exp(v_r(1,x_r)X), & -\ln\tau_r < X < 0 \\ g_r \exp(-v_r(-1,x_r)X), & 0 \le X < \ln\tau_r \\ 0, & \text{elsewhere} \end{cases} \tag{5.21}$$

where $\dot{\delta}(\cdot)$ denotes the Dirac delta function.

Proof: We note from Theorem 5.2.4 that $F_{z_r(t_r)|x_r,\varepsilon_{sr}}(X)$ is continuous at $X = 0$ and is discontinuous at $X = \pm \ln \tau_r$. It is easy to calculate

$$\begin{aligned} P(z_r(t_r) = -\ln \tau_r | x_r, \varepsilon_{sr}) &= F_{z_r(t_r)|x_r,\varepsilon_{sr}}(-\ln \tau_r) - 0 \\ &= \frac{g_r}{v_r(1, x_r)} \tau_r^{-v_r(1,x_r)}, \end{aligned} \tag{5.22}$$

and

$$\begin{aligned} P(z_r(t_r) = \ln \tau_r | x_r, \varepsilon_{sr}) &= 1 - F_{z_r(t_r)|x_r,\varepsilon_{sr}}(\ln \tau_r) \\ &= \frac{g_r}{v_r(-1, x_r)} \tau_r^{-v_r(-1,x_r)}. \end{aligned} \tag{5.23}$$

Therefore, differentiating $F_{z_r(t_r)|x_r,\varepsilon_{sr}}(X)$ with respect to X generates the PDF shown in (5.21), where the two Dirac delta functions, respectively, result from the differentiation of $F_{z_r(t_r)|x_r,\varepsilon_{sr}}(X)$ at the two discontinuous points, i.e., $X = \pm \ln \tau_r$.

□

In the next section, we analyze the performance for a single relay system.

5.3 BEP Performance of A Single Relay System

In this section, we consider a single relay case, and analyze the performance of the traditional MRC, the WSD, the CWSD, the PL detector, and the ML detector, respectively. We assume that the single relay is denoted by r. To maintain simplicity and clarity of the results, we propose the following two lemmas first.

Lemma 5.3.1. Representing the ABEP of the $i - d$ link by $\varepsilon_{id}^{\text{ave}}$, where $i \in \{s, r\}$, we have

$$\varepsilon_{id}^{\text{ave}} = \frac{g_i}{v_i(1,1)} \text{ and } 1 - \varepsilon_{id}^{\text{ave}} = \frac{g_i}{v_i(-1,1)}. \tag{5.24}$$

Proof: The ABEP of the $i - d$ link is given by

$$\varepsilon_{id}^{\text{ave}} = \frac{1}{2}\left[1 - \left(\frac{\gamma_{id}^{\text{ave}}}{1 + \gamma_{id}^{\text{ave}}}\right)^{1/2}\right]. \tag{5.25}$$

Noting that $\gamma_{id}^{\text{ave}} = 1/\theta_{id}$ and using the definitions of g_i and $v_i(a, x_i)$ in (5.6) and (5.7), respectively, after some manipulation, Lemma 5.3.1 is easy to be shown. It is also worth noting that $v_i(1,1) = v_i(-1,-1)$ and $v_i(-1,1) = v_i(1,-1)$.

□

Lemma 5.3.2. We define

$$\Phi = \frac{\sqrt{1+\theta_{rd}} + \sqrt{1+\theta_{sd}}}{2}, \tag{5.26}$$

and therefore

$$\begin{aligned} v_r(-1,1) + v_s(1,1) &= \Phi, \\ v_r(1,1) + v_s(-1,1) &= \Phi, \\ v_r(-1,-1) + v_s(1,1) &= \Phi + 1, \\ v_r(1,-1) + v_s(-1,1) &= \Phi - 1. \end{aligned} \tag{5.27}$$

Proof: the proof is straightforward using the definition of $v_i(a, x_i)$ in (5.7).

□

Now, we show the exact BEP analysis for different detectors.

5.3.1 BEP Analysis for the Traditional MRC

Theorem 5.3.1. The closed-form ABEP of the traditional MRC for a single relay system is given by

$$P_e^{\text{MRC}}(e) = \varepsilon_{sd}^{\text{ave}} + (1-\varepsilon_{sr}^{\text{ave}})(-1+2\varepsilon_{rd}^{\text{ave}})\frac{g_s}{\Phi} - \varepsilon_{sr}^{\text{ave}}\varepsilon_{rd}^{\text{ave}}\frac{g_s}{\Phi+1} + \varepsilon_{sr}^{\text{ave}}(1-\varepsilon_{rd}^{\text{ave}})\frac{g_s}{\Phi-1}. \tag{5.28}$$

Proof: The decision rule of the traditional MRC for a single relay system is given by

$$\hat{x} = \text{sgn}\left(t_s + t_r\right). \tag{5.29}$$

From (5.29), the ABEP of the MRC is expressed as

$$P_e^{\mathrm{MRC}}(e) \;=\; P\left(t_s + t_r < 0 | x_s = 1\right) \tag{5.30}$$

Using Theorem 5.2.1 and its corollary, the evaluation of this probability is straightforward. The result is shown as Theorem 5.3.1.

□

5.3.2 BEP Analysis for the WSD

Theorem 5.3.2. The conditional BEP of the WSD for a single relay system conditioned on ε_{sr}, is given by

$$\begin{aligned} & P_e^{wsd}(e|\varepsilon_{sr}) \\ = \;& \varepsilon_{sd}^{\mathrm{ave}} - (1-\varepsilon_{sr})(1-\varepsilon_{rd}^{\mathrm{ave}})\frac{(1-2\varepsilon_{sr})g_s}{\Phi - 2\varepsilon_{sr}v_s(1,1)} + (1-\varepsilon_{sr})\varepsilon_{rd}^{\mathrm{ave}}\frac{(1-2\varepsilon_{sr})g_s}{\Phi - 2\varepsilon_{sr}v_s(-1,1)} - \\ & \varepsilon_{sr}\varepsilon_{rd}^{\mathrm{ave}}\frac{(1-2\varepsilon_{sr})g_s}{\Phi + 1 - 2\varepsilon_{sr}v_s(1,1)} + \varepsilon_{sr}(1-\varepsilon_{rd}^{\mathrm{ave}})\frac{(1-2\varepsilon_{sr})g_s}{\Phi - 1 - 2\varepsilon_{sr}v_s(-1,1)}. \end{aligned} \tag{5.31}$$

□

The proof of Theorem 5.3.2 is quite similar to the proof of Theorem 5.3.1. Therefore, we do not repeat it.

We mention that in (5.31), if we replace ε_{sr} with its average, ε_{sr}^{ave}, it gives the closed-form ABEP of the A-WSD. The term *averaged* means that the corresponding detector uses the ABEP at the relay for detection at the destination. Averaging (5.31) over the statistics of the $s-r$ link (or say, the PDF of $\hat{\gamma}_{sr}$) gives the ABEP of the WSD. We note from (5.31) that the only term related to $\hat{\gamma}_{sr}$ is ε_{sr}. However, it is also noted that ε_{sr} consists of an erfc function of $\hat{\gamma}_{sr}$ as shown in (4.21). In addition, in (5.31), ε_{sr} appears in the numerators and the denominators with different weights. Therefore, it would be very difficult to perform the averaging of (5.31) over the PDF of $\hat{\gamma}_{sr}$. Nevertheless, we can use numerical calculations to obtain a precise result.

5.3.3 BEP Analysis for the CWSD

Theorem 5.3.3. The conditional BEP of the CWSD for a single relay system conditioned on ε_{sr}, is given by

$$\begin{aligned}
& P_e^{cwsd}(e|\varepsilon_{sr}) \\
= \; & \varepsilon_{sd}^{\text{ave}} - (1-\varepsilon_{sr})(1-\varepsilon_{rd}^{\text{ave}})\frac{(1-2\varepsilon_{sr})g_s}{\Phi - 2\varepsilon_{sr}v_s(1,1)}\left(1-\tau_r^{-\frac{\Phi-2\varepsilon_{sr}v_s(1,1)}{1-2\varepsilon_{sr}}}\right) \\
& +(1-\varepsilon_{sr})\varepsilon_{rd}^{\text{ave}}\frac{(1-2\varepsilon_{sr})g_s}{\Phi - 2\varepsilon_{sr}v_s(-1,1)}\left(1-\tau_r^{-\frac{\Phi-2\varepsilon_{sr}v_s(-1,1)}{1-2\varepsilon_{sr}}}\right) \\
& -\varepsilon_{sr}\varepsilon_{rd}^{\text{ave}}\frac{(1-2\varepsilon_{sr})g_s}{\Phi + 1 - 2\varepsilon_{sr}v_s(1,1)}\left(1-\tau_r^{-\frac{\Phi+1-2\varepsilon_{sr}v_s(1,1)}{1-2\varepsilon_{sr}}}\right) \\
& +\varepsilon_{sr}(1-\varepsilon_{rd}^{\text{ave}})\frac{(1-2\varepsilon_{sr})g_s}{\Phi - 1 - 2\varepsilon_{sr}v_s(-1,1)}\left(1-\tau_r^{-\frac{\Phi-1-2\varepsilon_{sr}v_s(-1,1)}{1-2\varepsilon_{sr}}}\right). \qquad (5.32)
\end{aligned}$$

Proof: Conditioned on the instantaneous CSIs of all links, the conditional BEP of the CWSD is given by

$$\begin{aligned}
& P_e^{cwsd}\left(e|\hat{h}_{ij}, ij \in \{sd, sr, rd\}\right) \\
= \; & P\left(t_s + z_r^{cs}(t_r) < 0 | \hat{h}_{ij}, ij \in \{sd, sr, rd\}, x_s = 1\right) \\
= \; & P\left(t_s + z_r^{cs}(t_r) < 0 | \hat{h}_{sd}, \hat{h}_{rd}, x_s = 1, x_r = 1\right) P(x_r = 1 | \hat{h}_{sr}, x_s = 1) + \\
& P\left(t_s + z_r^{cs}(t_r) < 0 | \hat{h}_{sd}, \hat{h}_{rd}, x_s = 1, x_r = -1\right) P(x_r = -1 | \hat{h}_{sr}, x_s = 1),
\end{aligned} \qquad (5.33)$$

where we note that $P(x_r = -1|\hat{h}_{sr}, x_s = 1)$ represents the IBEP at the relay, i.e., ε_{sr}. To evaluate (5.33), we fix t_s first, and evaluate (5.33) using Theorem 5.2.3, and then we average the obtained conditional probability result over the PDF of t_s. After some manipulation, we get the result shown in Theorem 5.3.3.

□

We mention that in (5.32), if we replace ε_{sr} with its average, ε_{sr}^{ave}, it gives the closed-form ABEP of the A-CWSD. It is noted that the averaging of (5.32) over the statistics of the the $s-r$ link is even harder than that in evaluating the WSD, since τ_r is also a function of ε_{sr}. Anyway, numerical calculations can be used to compute

the ABEP of the CWSD. To obtain an analytical, closed-form ABEP result for the CWSD, a simpler conditional BEP result rather than (5.32) is desired. In the next subsection, we evaluate the BEP performance of the PL detector. As we will see, the PL detector provides better tractability than the WSD or the CWSD, and a closed-form, approximate ABEP result for the PL detector is analytically obtained.

5.3.4 BEP Analysis for the PL Detector

Theorem 5.3.4. The conditional BEP of the PL detector for a single relay system conditioned on ε_{sr}, is given by

$$\begin{aligned} & P_e^{\mathrm{PL}}(e|\varepsilon_{sr}) \\ = \; & \varepsilon_{sd}^{\mathrm{ave}} + (1-\varepsilon_{sr})(-1+2\varepsilon_{rd}^{\mathrm{ave}})\frac{g_s}{\Phi}(1-\tau_r^{-\Phi}) - \\ & \varepsilon_{sr}\varepsilon_{rd}^{\mathrm{ave}}\frac{g_s}{\Phi+1}(1-\tau_r^{-(\Phi+1)}) + \varepsilon_{sr}(1-\varepsilon_{rd}^{\mathrm{ave}})\frac{g_s}{\Phi-1}(1-\tau_r^{-(\Phi-1)}). \end{aligned} \tag{5.34}$$

□

The proof of Theorem 5.3.4 is quite similar to the proof of Theorem 5.3.3, and it is noted that in this proof here, the conditional CDF result of $z_r(t_r)$ in Theorem 5.2.4 is used.

We mention that in (5.34), if we replace ε_{sr} with its average, $\varepsilon_{sr}^{\mathrm{ave}}$, it gives the ABEP of the A-PL detector. A similar closed-form ABEP result for the A-PL detector has been reported in [26] and [52] for the perfect CSI scenario. Our result here generalizes both perfect and imperfect CSI scenarios. We emphasize that the A-PL detector does not provide full diversity as it uses $\varepsilon_{sr}^{\mathrm{ave}}$ instead of ε_{sr}. We are more concerned about the performance of the PL detector using ε_{sr}.

From (5.34), it is seen that the conditional BEP expression is very neat, and is possible for the uncondioning with respect to the statistics of the $s-r$ link. Again, we note that τ_r defined in (4.34) is a function of ε_{sr}, and ε_{sr} defined in (4.21) is a function of $\hat{\gamma}_{sr}$. Usually, to obtain the ABEP, the conditional BEP shown in (5.34) is required to be averaged over the PDF of $\hat{\gamma}_{sr}$ given by (5.2). As can be seen, this averaging is not straightforward, as ε_{sr} is an erfc function of $\hat{\gamma}_{sr}$. Therefore, we

propose the following two ways to approximate the calculation, and arrive at two different, simple, approximate ABEP expressions for the PL detector. We simply refer to the two cases as PL-App1 and PL-App2, respectively.

PL-App1

In this case, ε_{sr} is treated as a random variable, and (5.34) is averaged with respect to the PDF of ε_{sr}. We first introduce the following lemma.

Lemma 5.3.3. The PDF of ε_{sr} is approximated by

$$p_{\varepsilon_{sr}}(x) \approx \begin{cases} 2^{\theta_{sr}}\theta_{sr}x^{\theta_{sr}-1}, & 0 < x < 1/2 \\ 0, & \text{otherwise} \end{cases} \tag{5.35}$$

Proof: The ε_{sr} is given by (4.21). Denoting the CDF of ε_{sr} by $F_{\varepsilon_{sr}}(x)$, it is clear that when $x \leq 0$, $F_{\varepsilon_{sr}}(x) = 0$, and when $x \geq 1/2$, $F_{\varepsilon_{sr}}(x) = 1$. When $0 < x < 1/2$, we approximate ε_{sr} using the exponential bound on the erfc function, i.e.,

$$\varepsilon_{sr} \approx \frac{1}{2}\exp(-\hat{\gamma}_{sr}). \tag{5.36}$$

Using (5.36), $F_{\varepsilon_{sr}}(x), x \in (0, 1/2)$ is approximated as

$$\begin{aligned} F_{\varepsilon_{sr}}(x) &= P\left(\varepsilon_{sr} < x\right) \\ &\approx P\left(\hat{\gamma}_{sr} > \ln\frac{1}{2}\right). \end{aligned} \tag{5.37}$$

Using the PDF of $\hat{\gamma}_{sr}$ given by (5.2), (5.37) can be easily evaluated. Concluding the above results, an approximate CDF of ε_{sr} can be represented as

$$F_{\varepsilon_{sr}}(x) \approx \begin{cases} 0, & x \leq 0 \\ (2x)^{\theta_{sr}}, & 0 < x < 1/2 \\ 1, & x \geq 1/2 \end{cases} \tag{5.38}$$

We note that $F_{\varepsilon_{sr}}(x)$ is continuous at both $x = 0$ and $x = 1/2$. Now, the PDF of ε_{sr} is obtained by differentiating (5.38) with respect to x, which leads to Lemma 5.3.3.

□

Using Lemma 5.3.3, averaging (5.34) over the approximate PDF of ε_{sr},we obtain the following theorem.

Theorem 5.3.5. The approximate ABEP of the PL detector for a single relay system in the case of PL-App1 is given by

$$\begin{aligned} & P_e^{\text{PL-App1}}(e) \\ = \; & \varepsilon_{sd}^{\text{ave}} + (-1 + 2\varepsilon_{rd}^{\text{ave}}) \frac{g_s}{\Phi} 2^{\theta_{sr}} \theta_{sr} \int_0^{1/2} (1-x) \Big[1 - \big(\frac{x}{1-x} \big)^{\Phi} \Big] x^{\theta_{sr}-1} dx \\ & - \varepsilon_{rd}^{\text{ave}} \frac{g_s}{\Phi+1} 2^{\theta_{sr}} \theta_{sr} \int_0^{1/2} \Big[1 - \big(\frac{x}{1-x} \big)^{\Phi+1} \Big] x^{\theta_{sr}} dx \\ & + (1 - \varepsilon_{rd}^{\text{ave}}) \frac{g_s}{\Phi-1} 2^{\theta_{sr}} \theta_{sr} \int_0^{1/2} \Big[1 - \big(\frac{x}{1-x} \big)^{\Phi-1} \Big] x^{\theta_{sr}} dx. \end{aligned} \tag{5.39}$$

□

As can be seen, the above result is in a form of sum of single integrals with finite limits, which can be easily evaluated. We emphasize that (5.39) shows the approximate ABEP of the PL detector which uses the IBEP at the relay for detection.

PL-App2

Here, the calculation is based on the following lemma.

Lemma 5.3.4. For moderate and high SNR of the $s-r$ link, the τ_r defined in (4.34) can be approximated as $\tau_r \approx \exp(\hat{\gamma}_{sr})$.

Proof: From the definition of τ_r, we write

$$\ln \tau_r \;=\; \ln \left(\frac{1}{\varepsilon_{sr}} - 1 \right). \tag{5.40}$$

For moderate and high SNR, it is reasonable to approximate $\ln \tau_r$ by $\ln (1/\varepsilon_{sr})$, since for small ε_{sr}, $1/\varepsilon_{sr} \gg 1$. Furthermore, from the expression of ε_{sr} given by (4.21) and using the exponential bound on the erfc function, it is easy to show that $\ln (1/\varepsilon_{sr}) \geq \hat{\gamma}_{sr} + \ln 2$. When $\hat{\gamma}_{sr}$ is large, the constant $\ln 2$ can be dropped. Therefore, $\ln \tau_r$ can be simply approximated as $\ln \tau_r \approx \hat{\gamma}_{sr}$, i.e., Lemma 5.3.4 is proved.

□

Using Lemma 5.3.4, we obtain the following theorem.

Theorem 5.3.6. The approximate ABEP of the PL detector for a single relay system in the case of PL-App2 is given by

$$\begin{aligned} & P_e^{\text{PL-App2}}(e) \\ = \; & \varepsilon_{sd}^{\text{ave}} + (-1 + 2\varepsilon_{rd}^{\text{ave}})\frac{g_s}{\Phi}\left(1 - \frac{\theta_{sr}}{2(1+\theta_{sr})} - \frac{\theta_{sr}}{\Phi+\theta_{sr}} + \frac{\theta_{sr}}{2(1+\Phi+\theta_{sr})}\right) - \\ & \varepsilon_{rd}^{\text{ave}}\frac{g_s}{2(\Phi+1)}\left(\frac{\theta_{sr}}{1+\theta_{sr}} + \frac{\theta_{sr}}{2+\Phi+\theta_{sr}}\right) + (1-\varepsilon_{rd}^{\text{ave}})\frac{g_s}{2(\Phi-1)}\left(\frac{\theta_{sr}}{1+\theta_{sr}} - \frac{\theta_{sr}}{\Phi+\theta_{sr}}\right) \end{aligned} \tag{5.41}$$

Proof: In (5.34), we first replace τ_r with $\exp(\hat{\gamma}_{sr})$, and substitute ε_{sr} by its exponentially bounded value, i.e., $1/2\exp(-\hat{\gamma}_{sr})$. Then, averaging the obtained expression over the PDF of $\hat{\gamma}_{sr}$, we arrive at (5.41).

□

As can be seen, (5.41) is a closed-form expression, and again, we emphasize that (5.41) approximates the ABEP of the PL detector which retains using the IBEP at the relay.

Theorems 5.3.5 and 5.3.6 show the ABEP result for the PL detector, not the A-PL detector, since the destination BEP result has been averaged over the statistics of the $s - r$ link. This work has not been done in the previous works.

Next, we analyze the performance of the ML detector.

5.3.5 BEP Analysis for the ML Detector

Theorem 5.3.7. The conditional BEP of the ML detector for a single relay system conditioned on ε_{sr}, is given by

$$\begin{aligned} P_e^{\mathrm{ML}}(e|\varepsilon_{sr}) &= (1-\varepsilon_{sr})\Bigg(\frac{g_s}{v_s(1,1)}+\int_0^{-\ln\tau_r}\frac{g_r}{v_r(-1,1)}s_r(-x)^{-v_r(-1,1)}g_s e^{xv_s(1,1)}dx \\ &\quad +\int_0^{\ln\tau_r}\frac{g_r}{v_r(1,1)}s_r(-x)^{v_r(1,1)}g_s e^{-xv_s(-1,1)}dx\Bigg) \\ &\quad +\varepsilon_{sr}\Bigg(\frac{g_s}{v_s(1,1)}+\int_0^{-\ln\tau_r}\frac{g_r}{v_r(-1,-1)}s_r(-x)^{-v_r(-1,-1)}g_s e^{xv_s(1,1)}dx \\ &\quad +\int_0^{\ln\tau_r}\frac{g_r}{v_r(1,-1)}s_r(-x)^{v_r(1,-1)}g_s e^{-xv_s(-1,1)}dx\Bigg). \end{aligned} \tag{5.42}$$

□

The proof of Theorem 5.3.7 is similar to the proof of Theorem 5.3.3, and it is noted that in this proof here, the conditional CDF result of $f_r(t_r)$ in Theorem 5.2.2 is used.

We mention that in (5.42), if we replace ε_{sr} with its average, $\varepsilon_{sr}^{\mathrm{ave}}$, it gives the ABEP of the A-ML detector, and this ABEP result is in a single integral form. In (5.42), if we further uncondition the probability with respect to ε_{sr}, or say, $\hat{\gamma}_{sr}$, it gives the ABEP of the ML detector. However, as can be seen, since ε_{sr} is an erfc function of $\hat{\gamma}_{sr}$, and it appears in the limit of the integrals in terms of $\ln\tau_r$ and also in the nonlinear function $s_r(x)$, it would be very difficult to carry out the unconditioning. Therefore, approximations are needed to simplify the calculation. We note that the integrals in (5.42) can be eliminated through the following lemma.

Lemma 5.3.5. For $-\ln\tau_r \le X \le 0$, the function $s_r(X)$ can be approximated as

$$s_r(X) \approx \exp(X). \tag{5.43}$$

Proof: For the $s_r(X)$ defined in (5.15), we first note that for $-\ln\tau_r \le X \le 0$, $s_r(X) \ge 0$. In (5.15), we take out a common factor, $\exp(X)$ to get

$$s_r(X) = \frac{(1-\varepsilon_{sr})-\varepsilon_{sr}\exp(-X)}{(1-\varepsilon_{sr})-\varepsilon_{sr}\exp(X)}\exp(X). \tag{5.44}$$

It is noted that for $-\ln \tau_r \leq X \leq 0$, $(1-\varepsilon_{sr})-\varepsilon_{sr}\exp(X) \geq (1-\varepsilon_{sr})-\varepsilon_{sr}\exp(-X) \geq 0$, and $(1-\varepsilon_{sr})-\varepsilon_{sr}\exp(X)$ is always greater than zero. Therefore, we have

$$s_r(X) \quad \leq \quad \exp(X), -\ln \tau_r \leq X \leq 0. \tag{5.45}$$

This exp bound on $s_r(X)$ is increasingly tighter as X tends to zero, and the equality holds when $X = 0$. The largest amount of difference between $s_r(X)$ and $\exp(X)$ appears at $x = -\ln \tau_r$, and is given by $\varepsilon_{sr}/(1-\varepsilon_{sr})$, which is a very small number when ε_{sr} is small. Therefore, for $-\ln \tau_r \leq X \leq 0$, $\exp(X)$ offers a good approximation to $s_r(X)$, i.e., Lemma 5.3.5 is proved.

□

Using Lemma 5.3.5, (5.42) can be easily simplified. It is interesting to note that this simplified result is identical to (5.34), which is the conditional BEP of the PL detector. In other words, the use of the approximation in (5.43) results in a closed-form, approximate, conditional BEP of the ML detector, and it amounts to the conditional BEP of the PL detector shown in (5.34). Therefore, those approximate ABEP results in (5.39) and (5.41) also applies to the ML detector. The equivalence of the two conditional BEP results also indicates that the approximation in (5.43) made to the ML detector is equivalent to the PL approximation. We recall that [26] uses the equivalent-PL approximation to approximate the ABEP of the A-ML detector. Actually, it is noted that Lemma 5.3.5 is quite similar to the equivalent-PL approximation. In [26], the equivalent-PL approximation is used without a rigorous proof.

5.4 BEP Performance of A Multiple Relay System

As can been seen from Section 5.3, the performance analysis of the ML detector in a single relay system can be rather involved without appropriate approximations. The PL approximation offers a way to analytically track the performance of the ML

detector. In this section, we analyze the ABEP of the PL detector in a multiple relay system, i.e., $L \geq 1$. It is noted that the complexity of analysis increases exponentially in the number of relays. Therefore, it is very difficult to obtain an exact ABEP result in general. For that reason, we develop a closed-form Chernoff upper bound on the ABEP of a general DF multiple relay system with an arbitrary number of relays. The main results of this section are summarized in the following two theorems.

Theorem 5.4.1. The Chernoff bound on the conditional BEP of the PL detector conditioned on $\varepsilon_{sr}, r = 1, 2, ..., L$, is given by

$$\begin{aligned} & P_e^{\mathrm{PL}}(e|\varepsilon_{sr}, r = 1, 2, ..., L) \\ \leq\ & \frac{\theta_{sd}}{1+\theta_{sd}} \prod_{r=1}^{L} \left\{ (1-\varepsilon_{sr}) \left(\frac{\theta_{rd}}{1+\theta_{rd}} + \frac{1}{1+\theta_{rd}} \tau_r^{-\frac{\sqrt{1+\theta_{rd}}}{2}} \right) + \right. \\ & \varepsilon_{sr} \left[\left(1 - \varepsilon_{rd}^{\mathrm{ave}} - \frac{\theta_{rd}}{2\sqrt{1+\theta_{rd}}(-2+\sqrt{1+\theta_{rd}})} \right) \tau_r^{1-\frac{\sqrt{1+\theta_{rd}}}{2}} + \right. \\ & \left. \left. \left(\varepsilon_{rd}^{\mathrm{ave}} - \frac{\theta_{rd}}{2\sqrt{1+\theta_{rd}}(2+\sqrt{1+\theta_{rd}})} \right) \tau_r^{-\left(1+\frac{\sqrt{1+\theta_{rd}}}{2}\right)} + \frac{\theta_{rd}}{-3+\theta_{rd}} \right] \right\}. \end{aligned} \tag{5.46}$$

Theorem 5.4.2. The Chernoff bound on the ABEP of the PL detector is given by

$$\begin{aligned} P_e^{\mathrm{PL}}(e) \ \leq\ & \frac{\theta_{sd}}{1+\theta_{sd}} \prod_{r=1}^{L} \left[\frac{\theta_{rd}}{1+\theta_{rd}} - \frac{\theta_{sr}\theta_{rd}}{2(1+\theta_{sr})(1+\theta_{rd})} + \frac{\theta_{sr}}{(1+\theta_{rd})(\frac{\sqrt{1+\theta_{rd}}}{2}+\theta_{sr})} - \right. \\ & \frac{\theta_{sr}}{2(1+\theta_{rd})(1+\frac{\sqrt{1+\theta_{rd}}}{2}+\theta_{sr})} + \frac{\theta_{sr}\theta_{rd}}{2(1+\theta_{sr})(-3+\theta_{rd})} + \\ & \frac{\theta_{sr}}{\sqrt{1+\theta_{rd}}+2\theta_{sr}} \left(1 - \varepsilon_{rd}^{\mathrm{ave}} - \frac{\theta_{rd}}{2\sqrt{1+\theta_{rd}}(-2+\sqrt{1+\theta_{rd}})} \right) + \\ & \left. \frac{\theta_{sr}}{4+\sqrt{1+\theta_{rd}}+2\theta_{sr}} \left(\varepsilon_{rd}^{\mathrm{ave}} - \frac{\theta_{rd}}{2\sqrt{1+\theta_{rd}}(2+\sqrt{1+\theta_{rd}})} \right) \right]. \end{aligned} \tag{5.47}$$

Proof: The conditional BEP of the PL detector (shown in (4.36)) conditioned on

the instantaneous CSIs of all links, is denoted by

$$\begin{aligned} & P_e^{\mathrm{PL}}(e|\hat{h}_{ij}, ij \in \{sd, sr, rd\}_{r=1}^{L}) \\ = \; & P\left(t_s + \sum_{r=1}^{L} z_r(t_r) < 0 | \hat{h}_{ij}, ij \in \{sd, sr, rd\}_{r=1}^{L}, x_s = 1\right). \end{aligned} \tag{5.48}$$

Applying the Chernoff bound [12, Section 2.1.5], (5.48) can be upper bounded by

$$\begin{aligned} & P_e^{\mathrm{PL}}(e|\hat{h}_{ij}, ij \in \{sd, sr, rd\}_{r=1}^{L}) \\ \leq \; & \mathbb{E}\left[\exp\left(\delta t_s + \delta \sum_{r=1}^{L} z_r(t_r)\right) | \hat{h}_{ij}, ij \in \{sd, sr, rd\}_{r=1}^{L}, x_s = 1\right] \\ = \; & \mathbb{E}\left[\exp(\delta t_s)|\hat{h}_{sd}, x_s = 1\right] \prod_{r=1}^{L} \Bigg\{ (1-\varepsilon_{sr}) \mathbb{E}\left[\exp(\delta z_r(t_r))|\hat{h}_{sr}, \hat{h}_{rd}, x_r = 1\right] + \\ & \varepsilon_{sr} \mathbb{E}\left[\exp(\delta z_r(t_r))|\hat{h}_{sr}, \hat{h}_{rd}, x_r = -1\right] \Bigg\}, \end{aligned} \tag{5.49}$$

where the equality is due to the mutual independence of all $i-j$ links, and $\delta \leq 0$ is the parameter to be optimized. Unconditioning (5.49) with respect to $\hat{h}_{sd}$ and $\hat{h}_{rd}$, we obtain that the conditional BEP conditioned on ε_r only, is upper bounded by

$$\begin{aligned} & P_e^{\mathrm{PL}}(e|\varepsilon_{sr}, r = 1, 2, ..., L) \\ \leq \; & \mathbb{E}\left[\exp(\delta t_s)|x_s = 1\right] \prod_{r=1}^{L} \Bigg\{ (1-\varepsilon_{sr}) \mathbb{E}\left[\exp(\delta z_r(t_r))|\varepsilon_{sr}, x_r = 1\right] + \\ & \varepsilon_{sr} \mathbb{E}\left[\exp(\delta z_r(t_r))|\varepsilon_{sr}, x_r = -1\right] \Bigg\}. \end{aligned} \tag{5.50}$$

Using Corollary of Theorem 5.2.1, the term $\mathbb{E}\left[\exp(\delta t_s)|x_s = 1\right]$ can be evaluated as

$$\begin{aligned} \mathbb{E}\left[\exp(\delta t_s)|x_s = 1\right] &= \int_{-\infty}^{\infty} \exp(\delta x) p_{ts|x_s=1}(x) dx \\ &= \frac{g_s}{\delta + v_s(1,1)} + \frac{g_s}{-\delta + v_s(-1,1)}, \end{aligned} \tag{5.51}$$

where g_s and $v_s(\pm 1, x_s)$ are defined in (5.6) and (5.7), respectively. The tightest Chernoff bound is obtained by selecting δ that minimizes the right hand side of (5.50). However, it is difficult to find this δ as (5.50) is fairly complex. Therefore, we select a δ that only minimizes the term $\mathbb{E}\left[\exp(\delta t_s)|x_s = 1\right]$, and use it elsewhere.

Differentiating (5.51) with respect to δ, and equating it to zero, we obtain $\delta = -1/2$. Substituting $\delta = -1/2$ into (5.51) and using the expressions of g_s and $v_s(\pm 1, 1)$, we can manipulate (5.51) into the following simple expression,

$$\mathbb{E}\left[\exp(\delta t_s)|x_s = 1\right] = \frac{\theta_{sd}}{1+\theta_{sd}}, \tag{5.52}$$

where θ_{sd} is defined in (5.1). Using Theorem 5.2.5, the term $\mathbb{E}\left[\exp(\delta z_r(t_r))|\varepsilon_{sr}, x_r\right]$ can be evaluated as

$$\begin{aligned}
&\mathbb{E}\left[\exp(\delta z_r(t_r))|\varepsilon_{sr}, x_r\right] \\
= \;& \frac{g_r}{v_r(1,x_r)}\tau_r^{-v_r(1,x_r)}\int_{-\infty}^{\infty}\exp(\delta x)\dot{\delta}(x+\ln\tau_r)dx + \\
& \frac{g_r}{v_r(-1,x_r)}\tau_r^{-v_r(-1,x_r)}\int_{-\infty}^{\infty}\exp(\delta x)\dot{\delta}(x-\ln\tau_r)dx + \\
& \int_{-\ln\tau_r}^{0}\exp(\delta x)g_r\exp(v_r(1,x_r)x)dx + \int_{0}^{\ln\tau_r}\exp(\delta x)g_r\exp(-v_r(-1,x_r)x)dx.
\end{aligned} \tag{5.53}$$

In (5.53), using the expressions of g_r and $v_r(\pm 1, x_r)$, and noting that $\delta = -1/2$, $\mathbb{E}\left[\exp(\delta z_r(t_r))|\varepsilon_{sr}, x_r = 1\right]$ and $\mathbb{E}\left[\exp(\delta z_r(t_r))|\varepsilon_{sr}, x_r = -1\right]$ can be obtained, respectively, in neat form as

$$\mathbb{E}\left[\exp(\delta z_r(t_r))|\varepsilon_{sr}, x_r = 1\right] = \frac{\theta_{rd}}{1+\theta_{rd}} + \frac{1}{1+\theta_{rd}}\tau_r^{-\frac{\sqrt{1+\theta_{rd}}}{2}}, \tag{5.54}$$

and

$$\begin{aligned}
&\mathbb{E}\left[\exp(\delta z_r(t_r))|\varepsilon_{sr}, x_r = -1\right] \\
= \;& \left(1 - \varepsilon_{rd}^{\text{ave}} - \frac{\theta_{rd}}{2\sqrt{1+\theta_{rd}}(-2+\sqrt{1+\theta_{rd}})}\right)\tau_r^{1-\frac{\sqrt{1+\theta_{rd}}}{2}} + \\
& \left(\varepsilon_{rd}^{\text{ave}} - \frac{\theta_{rd}}{2\sqrt{1+\theta_{rd}}(2+\sqrt{1+\theta_{rd}})}\right)\tau_r^{-\left(1+\frac{\sqrt{1+\theta_{rd}}}{2}\right)} + \frac{\theta_{rd}}{-3+\theta_{rd}},
\end{aligned} \tag{5.55}$$

where θ_{rd} and $\varepsilon_{rd}^{\text{ave}}$ are defined in (5.1) and (5.25), respectively. Substituting (5.52), (5.54) and (5.55) into (5.50), we get (5.46), i.e., Theorem 5.4.1 is proved. Using Lemma 5.3.4 and replacing ε_{sr} with its exponentially bounded value, i.e., $1/2\exp(-\hat{\gamma}_{sr})$, it is possible to average (5.46) over the PDF of $\hat{\gamma}_{sr}$. This calculation is straightforward from former experience. The result is given in Theorem 5.4.2.

□

It is noted that the Chernoff bounds obtained in Theorems 5.4.1 and 5.4.2 are partially optimized, as the parameter δ is only optimized with respect to the term $\mathbb{E}\left[\exp(\delta t_s)|x_s = 1\right]$. Eq. (5.46) shows the Chernoff bound on the conditional BEP of the PL detector conditioned on ε_{sr}. We mention that in (5.46), if we replace ε_{sr} with its average, $\varepsilon_{sr}^{\text{ave}}$, it gives the Chernoff bound on the ABEP of the A-PL detector. For the Chernoff bound shown in (5.47), we emphasize that it results from the destination detector who retains the use of the IBEP at the relay for detection. These Chernoff bound results here apply to a general DF relay system with an arbitrary number of relays.

5.5 Numerical and Simulation Results

In this section, we present numerical and simulation results for the ABEP performance of a DF relay system with different destination detectors. The variances of the fading gains of different links are assigned using the path-loss model $2\sigma_{ij}^2 \propto d_{ij}^{-u}$, where d_{ij} is the distance from node i to node j, and u is usually a constant within the range $3 \leq u \leq 5$. Here, we choose $u = 4$. Without loss of generality, the quantities $2\sigma_{sd}^2$ and d_{sd} are normalized to 1. The variance of the AWGN of each link is also normalized to 1, i.e., $N_{ij} = 1, ij \in \{sd, sr, rd\}_{r=1}^{L}$. For fair comparisons, the total transmitted energy per bit (for BPSK, 1 bit is equivalent to 1 symbol) is fixed at $E_b = E_s + \Sigma_{r=1}^{L} E_r$, and for simplicity, the source and each of the relays are assumed to have the same transmitted energy, i.e. $E_s = E_r, r \in \{1, 2, ..., L\}$.

In a practical communication system, since the bandwidth is limited, the number of pilot bits that can be added to a data packet is determined by the maximal allowable BEF ζ defined as $\zeta = (N_p + N_d)/N_d$, where N_p and N_d denote the number of pilot bits per packet and the number of data bits per packet, respectively. The ζ is always fixed. To illustrate, we consider the following example. Assume that the carrier frequency is 1900MHz and the vehicle moves at 20m/s. The coherence

time of the channel is thus 1.4ms [1]. We assume that the fading channel remains constant over the duration of 1ms, which allows the transmission of one packet. Therefore, the blockwise static channel assumption is valid for the duration of one packet. Assuming the total available bandwidth is 500kHz, the symbol duration is thus 1/500ms. Therefore, the number of bits affordable per packet is 500. We assume that the maximum allowable BEF is 1.021. It is easy to see that a packet contains at least 490 data bits, and at most 10 overhead bits can be used for pilot transmission. Following the above illustration, in our simulations, we use a packet of the packet length $N = 500$ bits, and it consists of $N_d = 490$ data bits prefixed by $N_p = 10$ pilot bits. Since pilots are used, the effective transmitted energy per data bit is given by $E_b^{\text{eff}} = (N_d/N)E_b$. Under block fading, all bits in a packet undergo the same fading. In all the following figures, the SNR is defined as $10\log(E_b/N_{sd})$, and each simulated error probability point is drawn when at least 100 errors are detected.

5.5.1 Performance of A Single Relay System

In this subsection, we consider a single relay system and examine the performance of those detectors discussed in Section 5.3. Unless otherwise specified, the relay is assumed to be located at the midpoint between the source and the destination, i.e. $d_{sr}/d_{sd} = d_{rd}/d_{sd} = 0.5$.

Fig. 5.1 compares the performance of different detectors. As can be seen, the A-WSD which uses the ABEP at the relay, performs almost the same as the MRC. However, it is noted that when the IBEP at the relay is used, the WSD performs slightly better than the MRC. The MRC does not need the IBEP at the relay, and simply assumes that the relay has decoded correctly. We also note that the A-CWSD performs almost the same as the A-PL detector, and the CWSD performs almost the same as the PL detector. It is important to note that the use of the IBEP at the relay offers an increasing gain over the use of the ABEP at the relay as SNR increases, for detection at the destination. For example, at the probability level of

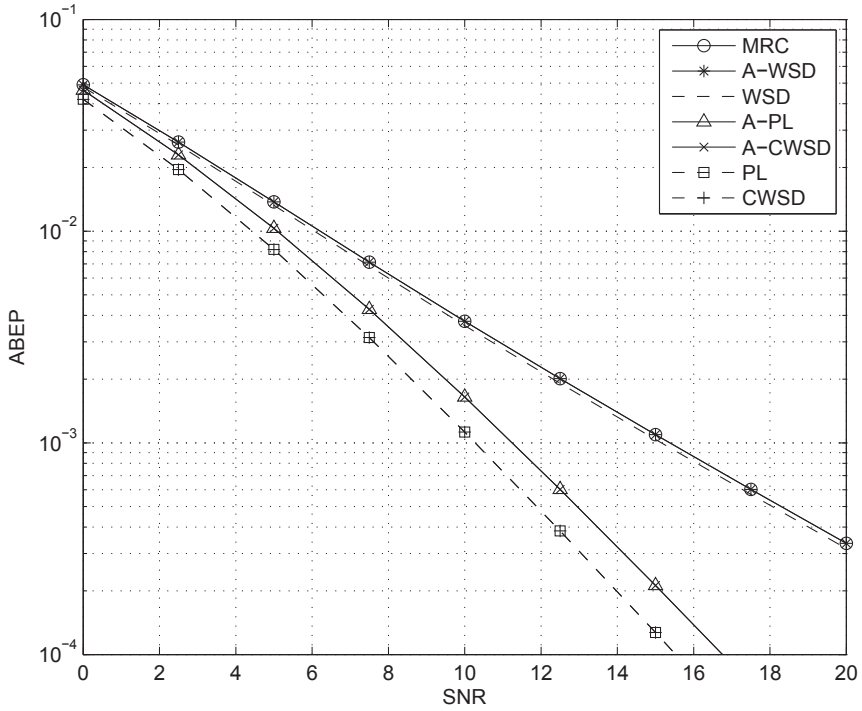

Figure 5.1: ABEP performance of the MRC, the A-WSD, the WSD, the A-PL detector, the A-CWSD, the PL detector and the CWSD in a single relay system.

10^{-3}, the performance gain of the CWSD or the PL detector over the A-CWSD or the A-PL detector is about 0.5dB, and it increases to about 1dB at the probability level of 10^{-4}. Here, we mention that the ABEP curves for the MRC and the A-WSD are, respectively, draw from (5.28) and (5.31), and the ABEP curve for the WSD is draw from numerically averaging (5.31) over the PDF of $\hat{\gamma}_{sr}$. We also mention that the ABEP curves for the A-CWSD and the A-PL detector are, respectively, draw from (5.32) and (5.34), and the ABEP curves for the CWSD and the PL detector are, respectively, draw from numerically averaging (5.32) and (5.34) over the PDF of $\hat{\gamma}_{sr}$. Since the MRC and the PL detector are, respectively, simpler than the WSD and the CWSD, and at the same time, provide nearly the same performance as the latter two, in the following, we only use the MRC and the PL detector for further

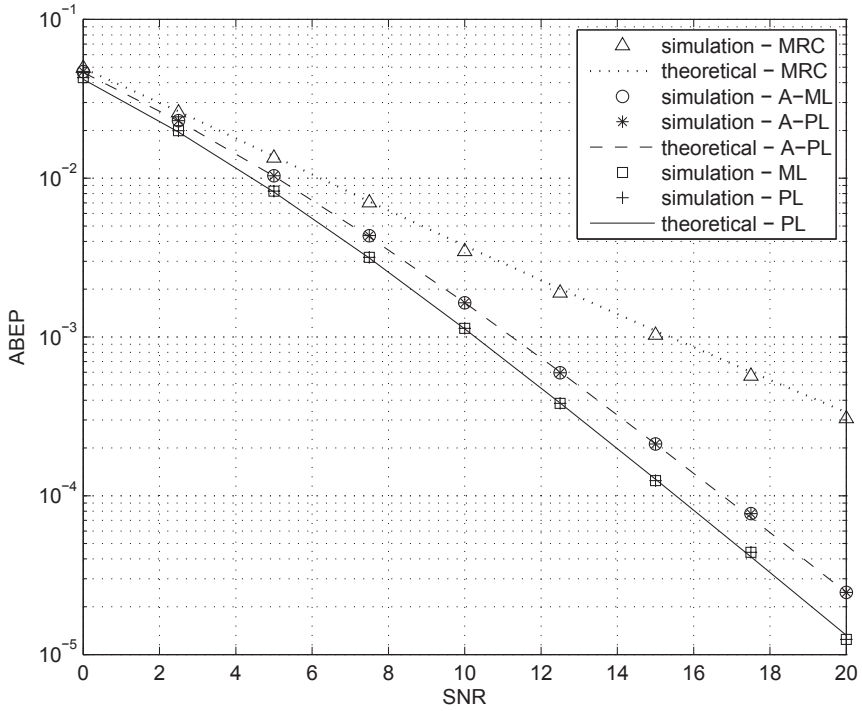

Figure 5.2: ABEP performance of the MRC, the A-PL, the A-ML, the PL and the ML detectors in a single relay system.

comparisons.

Fig. 5.2 compares the ABEP performance of the MRC, the A-PL, the A-ML, the PL and the ML detectors. Simulations are used to validate our theoretical results. It is seen that the theoretical curves well match the simulated points. Here, we do not show the theoretical curve for the A-ML or the ML detector, since no simple ABEP results are obtained for them. As shown in Fig. 5.2, the A-PL detector and the PL detector closely approximate the A-ML detector and the ML detector, respectively. This demonstrates that the PL approximation made to the nonlinear function $f_r(t_r)$ is well-suited, and so is the clipped slope-approximation. Besides the above observations, we emphasize that as can be seen in Fig. 5.1 and Fig. 5.2, from an error probability perspective, the A-CWSD, the A-PL and the A-ML detectors suffer a loss in the diversity (the diversity is represented by the slope of the ABEP

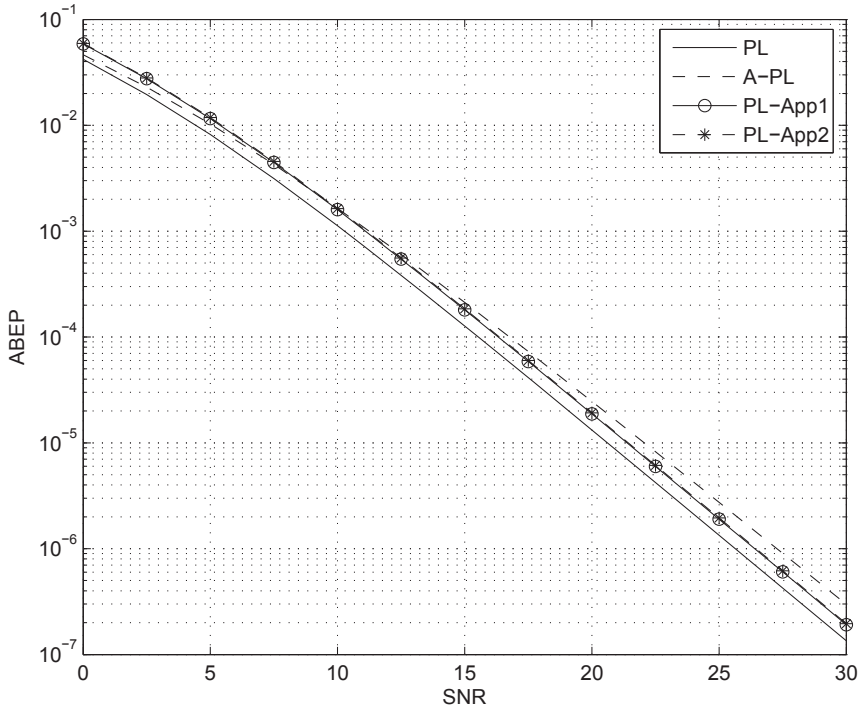

Figure 5.3: Theoretical, approximate ABEP of the PL detector in a single relay system.

curve), compared with the CWSD, the PL and the ML detectors. This loss is caused by the use of the ABEP at the relay in the averaged detectors. The traditional MRC, of course, shows a much poorer performance than the other detectors in Fig. 5.3, as it does not make use of the decoding errors at the relay.

Fig. 5.3 examines the two theoretical, approximate ABEP results for the PL detector, which are shown in (5.39) and (5.41), respectively. As can be seen, the two approximations perform quite close to each other. Therefore, we suggest the use of the second one shown in (5.41), since it is in simple, closed form. We mention that the exact ABEP of the PL detector without any approximations is obtained from the numerical calculation of some double integrals. For analytical purpose, the closed-form expression shown in (5.41) is more useful. We note from Fig. 5.3 that the two approximations provide the same diversity order as the PL detector does,

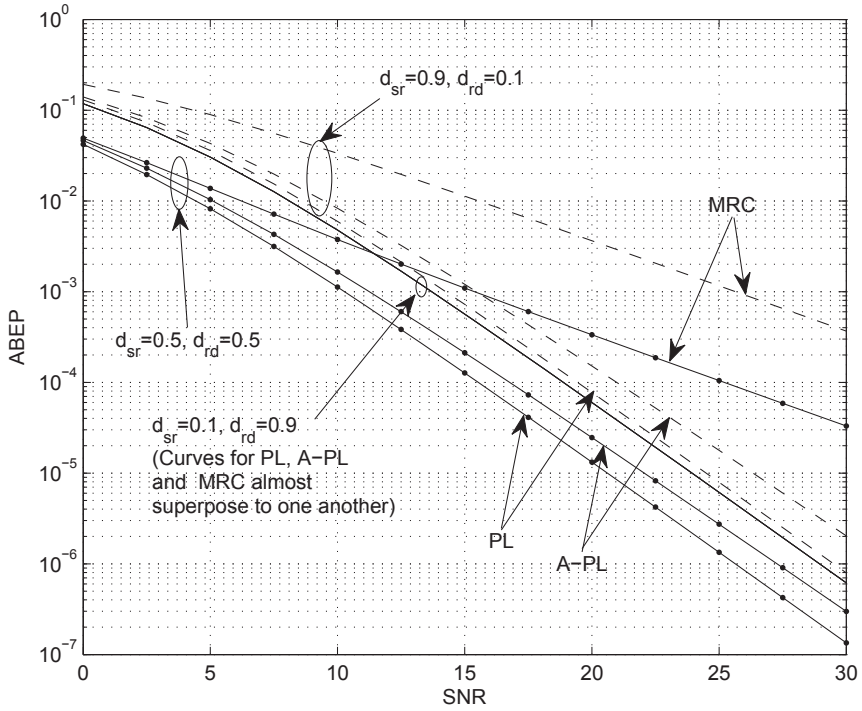

Figure 5.4: Effect of the location of the relay on the ABEP performance of different destination detectors in a single relay system.

although there is always an about 0.8dB loss in the performance gain. Later, we will show that this diversity order is 2, i.e., full diversity is achieved. In contrast, the ABEP curve for the A-PL detector drifts away as SNR increases, i.e., compared with the PL detector, the A-PL detector loses diversity.

In Fig. 5.4, we show the effect of the location of the relay on the ABEP performance of different destination receivers. We assume that the source, the relay and the destination are collinear, i.e., $d_{sd} = d_{sr} + d_{rd}$. First, it is noted that when the relay is very close to the source, e.g., $d_{sr}/d_{sd} = 0.1$, the ABEP curves for the MRC, the A-PL and the PL detectors nearly superpose to one another, i.e., these destination detectors make little difference in detection. For the MRC, since it assumes no detection errors at the relay, its performance becomes better when the relay gets closer to the source. This is shown in Fig. 5.4 that as SNR increases,

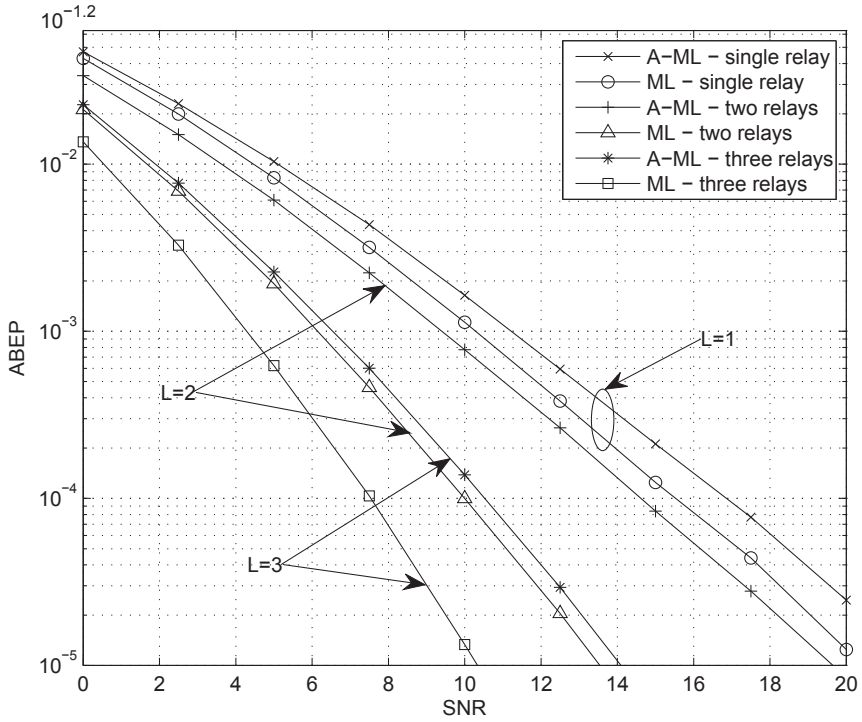

Figure 5.5: ABEP performance of the A-ML and the ML detectors in a multiple relay system.

the best performance of the MRC is found in the scenario where $d_{sr}/d_{sd} = 0.1$. For both the A-PL and the PL detectors, their best performance is always found in the scenario where $d_{sr}/d_{sd} = 0.5$, and this can be explained as follows. To both the detectors, the contribution of the $s - r - d$ link is jointly determined by the quality of the $s - r$ and the $r - d$ links. Therefore, to achieve a good performance, the relay needs to be located at some point that balances the quality of the two sublinks in the long term. For ease of analysis, the best location of the relay is commonly assumed to be at the midpoint between the source and the destination, i.e., $d_{sr}/d_{sd} = 0.5$. It is note that in [95], it shows a graphical way of determining the best location of the relay that would generate the minimum end-to-end error probability in a DF single relay system with DBPSK. Here, we can also graphically determine the best location of the relay for different destination detectors, by evaluating their ABEP

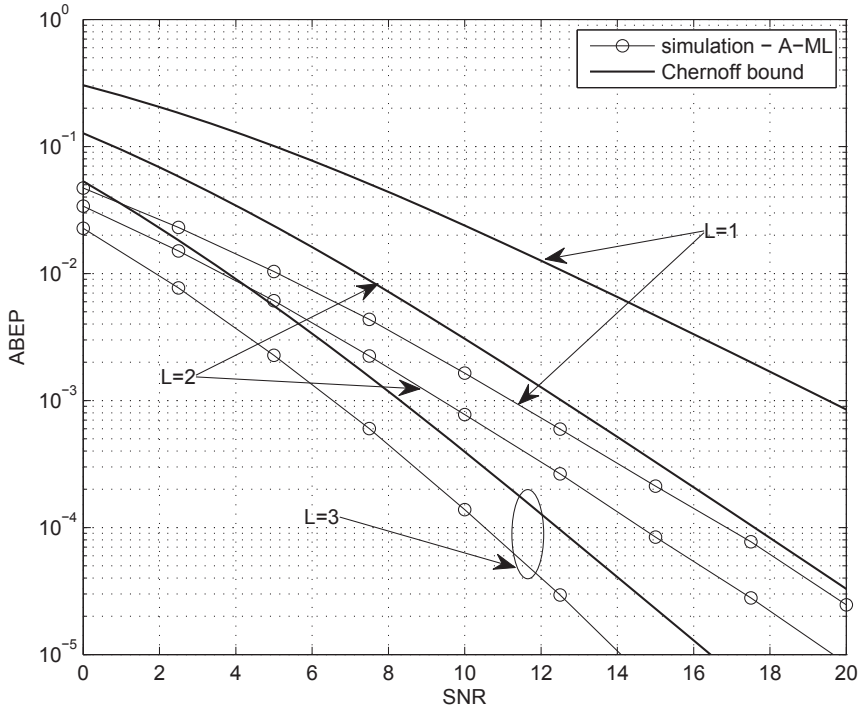

Figure 5.6: Chernoff bound on the ABEP of the A-PL detector in a multiple relay system.

performance for different locations of the relay. However, it should be noted that the best location of the relay cannot be a general suggestion, since the end-to-end error probability also depends on the power allocation between the source node and the relay node. The joint design of power allocation and relay locating for a DF relay system is a new topic, and is beyond the scope of this chapter.

5.5.2 Performance of A Multiple Relay System

In this subsection, we examine the performance of a multiple relay system.

In Fig. 5.5, we show the ABEP performance of the A-ML and the ML detectors in multiple relay system. For simplicity, we assume that all the relay nodes locate at $d_{sr}/d_{sd} = d_{rd}/d_{sd} = 0.5$. All the curves here are drawn from simulations. It is clearly seen that for either the A-ML or the ML detector, as the number of relays increases,

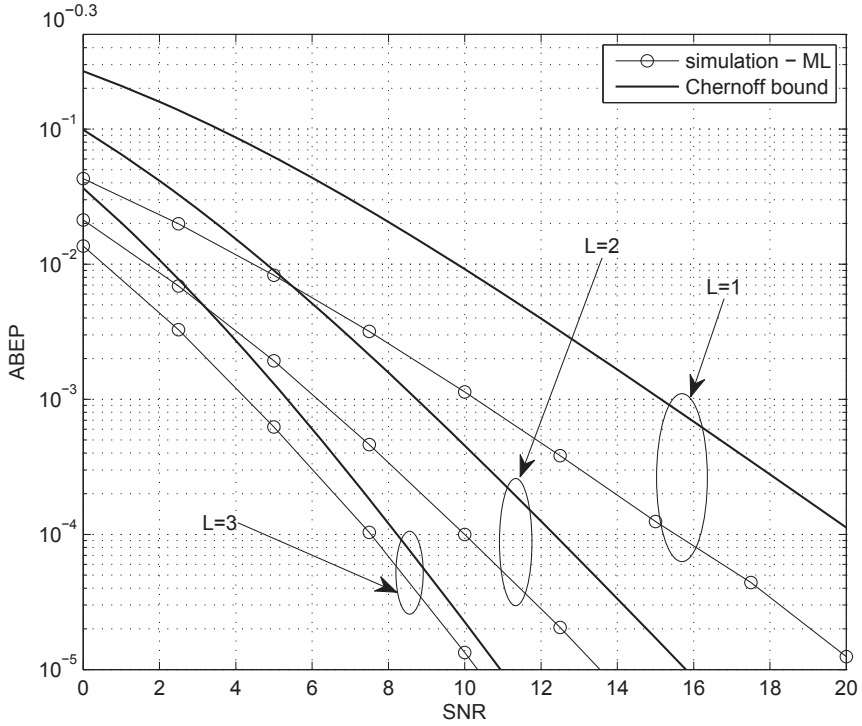

Figure 5.7: Chernoff bound on the ABEP of the PL detector in a multiple relay system.

the achievable diversity increases. It is important to note that, similar to that in a single relay system, in a multiple relay system (in Fig. 5.5, it refers to the case where $L = 2$ or $L = 3$), the A-ML detector suffers a loss in the diversity, compared with the ML detector. This loss is caused by the use of the ABEP at the relay in the A-ML detector. The ML detector shows a substantially better performance than the A-ML detector. For example, in the cases where $L = 2$ and $L = 3$, respectively, the performance gains achieved by the ML detector over the A-ML detector are approximately 6dB and 4dB, at the probability level of 10^{-5}.

In Figs. 5.6 and 5.7, we show, respectively, the partially optimized Chernoff bounds on the ABEPs of the A-PL and the PL detectors, which are given in (5.46) and (5.47), respectively. Since the A-PL and the PL detectors, respectively, closely approximate the A-ML and the ML detectors, the obtained Chernoff bound results

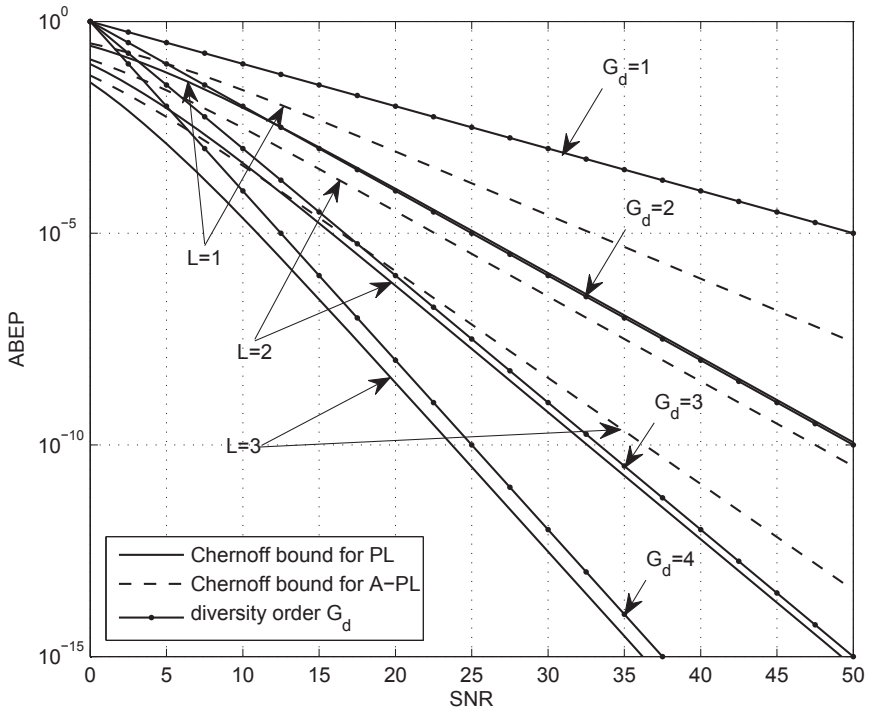

Figure 5.8: Diversity order analysis of a DF multiple relay system.

also apply to the A-ML and the ML detectors. As can be seen in both figures, the Chernoff bound becomes tighter as the the number of relays increases. In the case where $L = 3$, the Chernoff bound bounds the original curves within 2.5dB and 1dB as shown in Fig. 5.6 and Fig. 5.7, respectively. The tight Chernoff bound enables us to use it to analyze the diversity order of a general, uncoded DF multiple relay system. The diversity order refers to the increase in the slope of the curve for BEP versus SNR [49]. In the limit of large SNR, the diversity order is simply denoted by $-\lim_{\mathrm{SNR}\to\infty}(\ln \mathrm{BEP})/(\ln \mathrm{SNR})$. The diversity order can be graphically represented by a BEP curve drawn from $\mathrm{BEP} = \mathrm{SNR}^{-G_d}$ and evaluating at large SNR. The G_d denotes the diversity order. In Fig. 5.8, we plot the Chernoff bounds and compare them with the graphically visualized G_d. As can be seen, the PL detector using the IBEP the relay achieves the full diversity of $L + 1$, where L denotes the number of relays. For example, for $L = 1$, the PL detector achieves a diversity order of 2, since

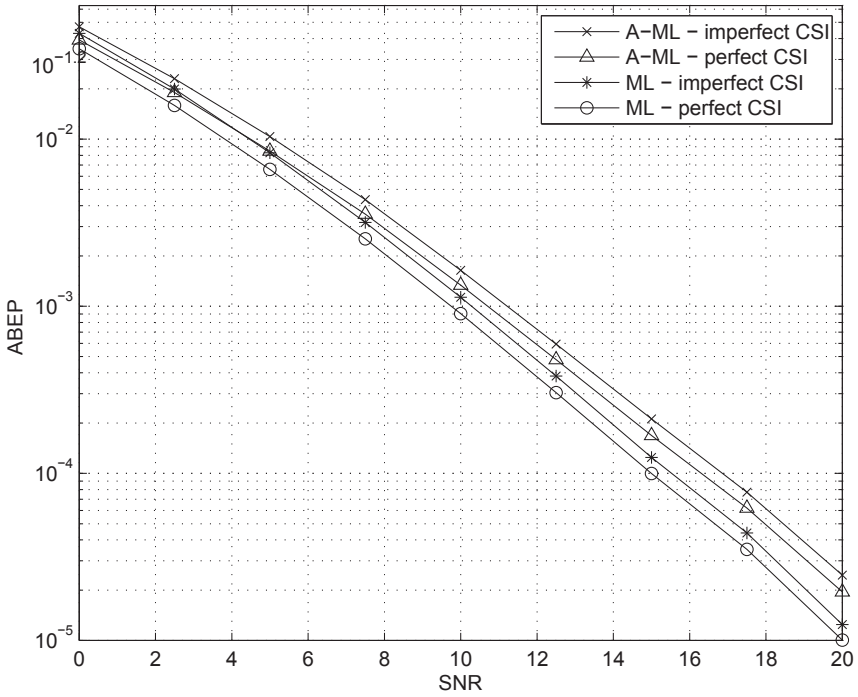

Figure 5.9: ABEP performance of the A-ML and the ML detectors in a single relay system with perfect and imperfect CSI, respectively.

the slope of the ABEP curve for the PL detector is the same as the slope of the BEP curve for $G_d = 2$. The A-PL detector, however, suffers a loss in the diversity order. These observations from Fig. 5.8 show that in the destination receiver design of a DF relay system, the IBEP at the relay instead of its average should be used, to maintain full diversity.

5.5.3 Performance of the Perfect CSI Scenario

Figs. 5.1-5.8 have shown the performance of a DF relay system with imperfect CSI. For analytical purpose, it is also useful to examine the system performance with the assumption of perfect CSI, as it provides a benchmark for performance evaluation. It is noted that all our results in Chapters 4 and 5 are generalized for both perfect and imperfect CSI scenarios. To obtain the results for the perfect CSI scenario,

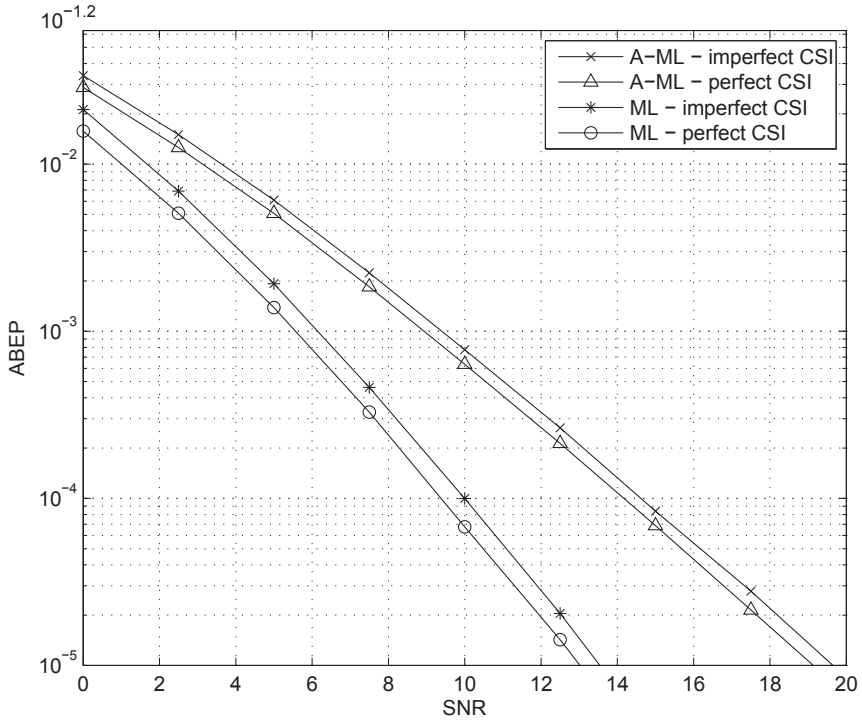

Figure 5.10: ABEP performance of the A-ML and the ML detectors in a two-relay system with perfect and imperfect CSI, respectively.

we simply set the variances of the estimation errors defined in (4.5) to zeros. In Figs. 5.9 and 5.10, we show the simulated ABEP performance of the A-ML and the ML detectors in a single and a two-relay systems, respectively, with either perfect or imperfect CSI. In the perfect CSI case, we maintain a packet length of $N = 500$ bits, and use all of them to carry data information. The other settings remain the same as those in the imperfect CSI case. For simplicity, all the relay nodes are assumed to be located at $d_{sr}/d_{sd} = d_{rd}/d_{sd} = 0.5$. As can be seen from both figures, in either perfect or imperfect CSI case, the ML detector performs better than the A-ML detector. It is also seen that for either the ML or the A-ML detector, with the same number of relays, the ABEP curve for the perfect CSI case has the same slope as the ABEP curve for the imperfect CSI case. The gap between these two ABEP curves is determined by the variance of the channel estimation errors. This equal-slope

property indicates that the diversity order of a DF relay system is irrelevant to the channel estimation errors.

5.5.4 Performance of the ML Detector in A Practical DF Relay System

In this subsection, we deal with the last issue to complete our simulations on a DF relay system. Our effort here is driven by the above observation that the destination detector using the IBEP at the relay achieves full diversity. In Section 4.4, we have briefly introduced an 8-bit-overhead scheme for carrying the IBEP information from the relay to the destination, for practical use. It should be noted that the 8 bits information is sent to the destination along with a data packet, and therefore, it may be decoded wrongly. As this information is critical for the detection at the destination, it needs to be treated carefully, e.g., error correction codes can be used. In our simulations, we do not assume any error control coding on the 8 bits information, and only suggest a straightforward error control strategy at the destination, i.e., if the destination decodes the 8 bits information wrongly to generate an IBEP greater than 0.5, it sets the IBEP to 0.5. From (4.24), (4.33) and (4.35), we note that when $\varepsilon_{sr} = 0.5$, the values of those functions are all zeros, i.e., the contribution of the $s - r - d$ link to those destination detectors is zero. Therefore, this error control strategy also says that once the destination fails to decode a reasonable IBEP, the whole relayed packet that carries the wrong IBEP information is discarded at the destination. To examine the performance of the 8-bit-overhead scheme, we assume perfect CSI for simplicity.

We first consider the same blockwise static channel used in the previous subsections, which affords 500bits/packet and is used with a maximum allowable BEF of 1.021. We mention that in practice where imperfect CSI applies, the maximum allowable BEF is always much larger than our defined value here, and therefore, both the IBEP information and the pilots for channel estimation purpose can be tolerated in one packet. Here, we use a packet which consists of 492 data

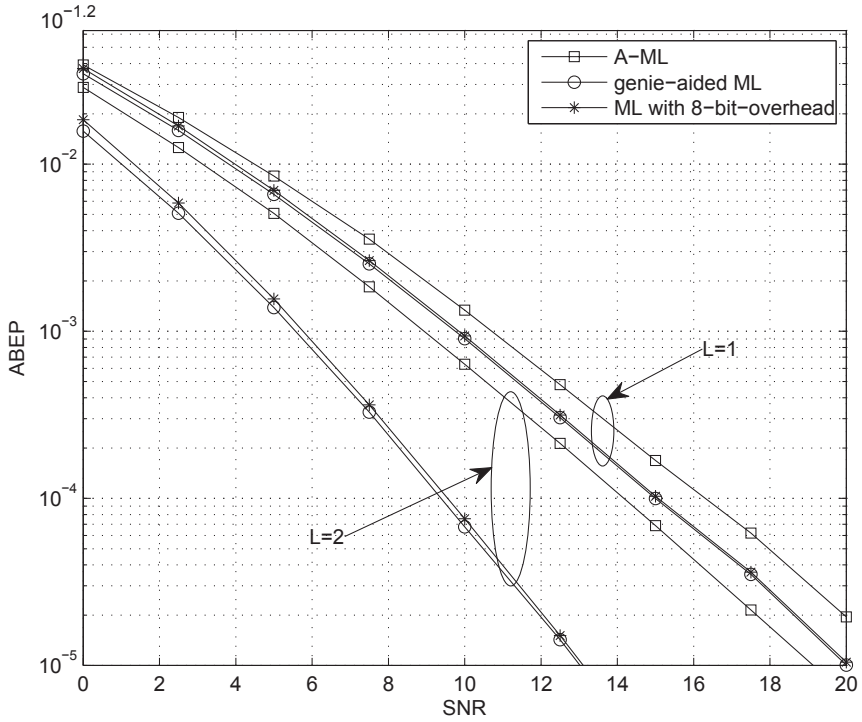

Figure 5.11: ABEP performance of the ML detector in a practical DF relay system, in the case where the blockwise static channel affords 500**bits/packet.**

bits and an additional 8-bit overhead for carrying the IBEP information. The other system settings remain the same as those in the previous subsections. We term the destination detector that has the perfect IBEP information as the *genie-aided* detector. In Fig. 5.11, we show the ABEP of the ML detector in a practical system using the 8-bit-overhead scheme. The performance of the A-ML and the *genie-aided* ML detectors is also included for comparison. We note that for the A-ML detector, only the ABEP at the relay is required, which can be obtained at the destination in advance using the statistical information of the $s - r$ link. As can be seen from Fig. 5.11, the ML detector with the 8-bit-overhead scheme performs very close to the *genie-aided* one. In the low SNR regime, the performance loss of the former compared with the latter is less than 0.5dB, and in the high SNR regime, this loss is negligible. Clearly, the efficiency of the 8-bit-overhead scheme is affected by the

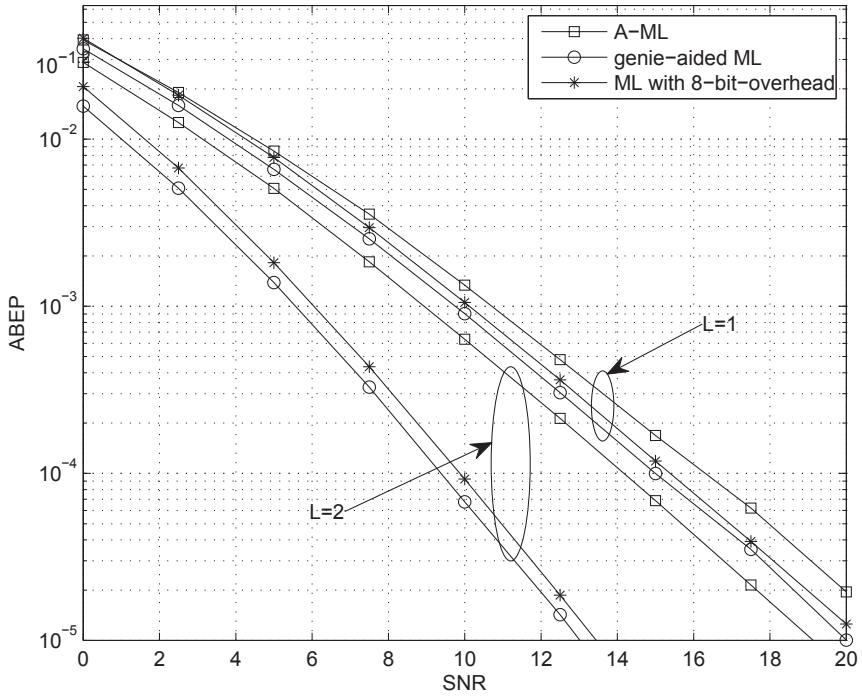

Figure 5.12: ABEP performance of the ML detector in a practical DF relay system, in the case where the blockwise static channel affords 100**bits/packet.**

packet length. We consider in below a more stringent scenario, where the blockwise static channel only affords 100bits/packet. The maximal BEF is assumed to be 1.09 to support the 8-bit overhead. As can be seen from Fig. 5.12, the loss of the ML detector with the 8-bit-overhead scheme compared with the *genie-aided* ML detector is always less than 1dB. Both of these two detectors perform much better than the A-ML detector which only uses the ABEP at the relay. From the above observations, we conclude that the 8-bit-overhead scheme is effective in communicating the IBEP information from the relay to the destination. Again, the results in this subsection show the importance of using the IBEP at the relay for detection at the destination, i.e., even the IBEP information is partially known to the destination receiver, it offers a substantial gain over the receiver using only the ABEP at the relay.

5.6 Conclusions

In this chapter, we analyzed the ABEP performance of a DF relay system. For a single relay case, we derived closed-form ABEP results for different destination detectors introduced in Chapter 4. Among those results, the closed-form, approximate ABEP result for the PL detector is of the greatest interest to us, since it is simple and also closely approximates the ABEP of the ML detector. We emphasize that the PL detector in our work uses the IBEP at the relay. This distinguishes our work from those that only examine the A-PL detector which uses the ABEP at the relay. For a multiple relay system, we derived closed-form Chernoff upper bounds on the ABEPs of the A-PL and the PL detectors, respectively. Numerical and simulation results show that the loss of the instantaneous information of the $s - r$ link at the destination significantly degrades the system performance. The instantaneous information of the $s - r$ link, which is summarized as the IBEP at the relay, is indeed a crucial information for detection at the destination. Our Chernoff bound results prove that for a DF relay system, the destination detector using the IBEP at the relay achieves full diversity. In contrast, the destination detector using the ABEP at the relay suffers a loss of diversity.

Chapter 6

An Efficient Adaptive Algorithm and An Application to Channel Estimation

As has been noted in our works on the feedback power control and the DF relay systems, the CSI is a critical information that affects the system performance. Therefore, in this chapter, we devote some effort to CSI acquisition. Particularly, we propose the ASSA algorithm for the tap-weight coefficients adaptation of an LMS adaptive filter. The LMS adaptive filter can be used for efficient CSI acquisition in a completely unknown wireless environment. The most significant feature that distinguishes the ASSA algorithm from any other existing variable step-size algorithms is that the ASSA algorithm does not require any preset control parameters. When applied to channel estimation, simulation results show the performance advantage of the ASSA algorithm over the existing step-size adjustment algorithms under different wireless channel environments. The ASSA algorithm also serves as a fundamental contribution to the step-size adjustment for the tap-weight coefficients adaptation of LMS adaptive filters.

6.1 Introduction

In coherent detection of wireless communications, an accurate estimate of the instantaneous CSI is a crucial requirement. In many works involving theoretical analysis of transmission over fading channels, the perfect CSI is a common assumption. This assumption greatly simplifies the analysis and helps develop an insightful view of those promising techniques. However, in practice, the perfect CSI is of course, unknown to the receiver, and therefore, channel estimation must be used to provide a degraded version of the perfect CSI, i.e., the imperfect CSI. Channel estimation is a mature technology that has been well-studied in the literature. To obtain the CSI, either decision feedback [93] or pilot tone signalling [96] can be used. One of the most popular pilot-assisted channel estimation schemes is the pilot symbol assisted modulation (PSAM) [15]. In [15], it proposes to use a Wiener filter to extract the pilot information, and form the MMSE estimate of the CSI. By appropriately deploying the pilots, [15] shows that the performance degradation in coherent detection due to channel estimation errors is controllable, and can be very small. The Wiener filtering is a classic topic in linear adaptive signal processing. As it is known, to implement a Wiener filter with optimum filter tap-weight coefficients, the statistics of the input signals and the desired signals are required. In the context of channel estimation in wireless communications applications, if the channel statistics are known, e.g., in [15], the PSAM scheme can be implemented directly. However, more often, transmission is carried out in an environment whose statistics are completely unknown. In such a case, we need to rely on iterative adaptive algorithms to approximate the performance of the Wiener filter in an iterative manner.

As one of the most popular iterative algorithms, the LMS algorithm [71] is widely used for its robustness and simplicity. However, the original LMS algorithm always suffers from a low rate of convergence, or a high steady-state MSE, due to the use of an FSS throughout the adaptation process. The step-size is an important parameter that controls the trade-off between the rate of convergence and

the steady-state MSE. To achieve a good compromise for this trade-off, a variable step-size is desired. The basic idea of using a variable step-size comes from the facts that a large step-size at the beginning of the adaptation, is capable of speeding up the convergence; and when the filter coefficients are about to converge, a small step-size is necessary for a low steady-state MSE. The popularity of the LMS algorithm drives the development of many efficient variable step-size schemes. As has been addressed in Section 2.3, a common feature of all the existing step-size adjustment algorithms is that preset control parameters are required, and of course, the choice of these parameters would greatly affect the performance of these algorithms. As has been noted, those control parameters are always chosen from extensive simulations, or from experience. To obviate the tedious process of choosing appropriate parameters, parameter-free algorithms are desired.

In this chapter, we present the complete theoretical development for a parameter-free algorithm for the tap-weight coefficients adaptation of an LMS adaptive filter that we call the ASSA algorithm. The most significant feature that distinguishes the ASSA algorithm from any other existing variable step-size algorithms is that the ASSA algorithm does not require any preset control parameters. At each time point when a new observation of the input signal arrives, we choose a step-size that would minimize the sum of the squares of the measured estimation errors up to that current time point. This desired step-size is, of course, only obtainable through genie-aided feedback. For a real system, we propose a suboptimum realization of the desired step-size, where the past measured values of the estimation errors and the past realizations of the tap-weight vector are used. The obtained suboptimum step-size, after being normalized by the power of the current tapped filter input, is used as the actual step-size to update the current tap-weight vector. The adaptive filter employing this proposed algorithm can update its tap-weight vector online without setting any control parameters in advance. As an application to wireless communications, we apply the adaptive filter to channel estimation and examine the MSE performance of the ASSA algorithm

using simulations. Simulation results show the effectiveness of the new algorithm in rapidly driving the MSE to a smaller value when compared with other existing adaptive filtering algorithms.

A literature survey that includes many of the popular step-size adjustment algorithms has been done in Section 2.3. The rest of this chapter is organized as follows. In Section 6.2, we formulate and discuss the ASSA algorithm. In section 6.3, we examine the performance of the ASSA algorithm through simulations. Finally, Section 6.4 concludes this chapter.

6.2 The ASSA Algorithm

We begin the formulation by studying the first a few rounds of the adaptation process, and then we generalize it to an online algorithm. Without loss of generality, we assume that the adaptation starts at time point 0, where the input vector is $\mathbf{x}(0) = [x(0) \;\; x(-1) \;\; ... \;\; x(-N+1)]^T$, and the weight vector $\mathbf{w}(0)$ is chosen to be the zero vector. The estimation error is given by $e(0) = d(0) - \mathbf{w}^T(0)\mathbf{x}(0)$, and it is noted that $e(0) = d(0)$. At this stage, an arbitrarily chosen initial step-size μ_0 can be used to update the weight vector as $\mathbf{w}(1) = \mathbf{w}(0) + \mu_0 e(0)\mathbf{x}(0)$, as long as μ_0 keeps $\mathbf{w}(1)$ stable, i.e., the *mis-adjustment* [70] by applying $\mathbf{w}(1)$ is finite. At time point 1, a new observation $x(1)$ arrives and the input vector is now $\mathbf{x}(1) = [x(1) \;\; x(0) \;\; ... \;\; x(-N+2)]^T$. The estimation error is

$$\begin{aligned} e(1) &= d(1) - \mathbf{w}^T(1)\mathbf{x}(1) \\ &= d(1) - [\mathbf{w}(0) + \mu_0 e(0)\mathbf{x}(0)]^T\mathbf{x}(1). \end{aligned} \tag{6.1}$$

From the viewpoint of time point 1, looking backwards, we propose that the step-size would have been more suitably chosen at time point 0 if $e^2(1)$ is minimized. Suppose this more suitable step-size is $\tilde{\mu}_1$. If genie-aided feedback enables us to reset the

step-size for time point 0 as $\tilde{\mu}_1$, we would have

$$\begin{aligned} \tilde{\mathbf{w}}_1(1) &= \mathbf{w}(0) + \tilde{\mu}_1 e(0)\mathbf{x}(0) && (6.2) \\ \tilde{e}_1(1) &= d(1) - \tilde{\mathbf{w}}_1^T(1)\mathbf{x}(1) \\ &= d(1) - [\mathbf{w}(0) + \tilde{\mu}_1 e(0)\mathbf{x}(0)]^T\mathbf{x}(1). && (6.3) \end{aligned}$$

from which $\tilde{\mu}_1$ can be analytically determined. Now we take $\mu_1 = \tilde{\mu}_1/\mathbf{x}^T(1)\mathbf{x}(1)$ to be the actual step-size used for updating the current tap-weight vector, i.e.

$$\mathbf{w}(2) = \tilde{\mathbf{w}}_1(1) + \mu_1 \tilde{e}_1(1)\mathbf{x}(1). \quad (6.4)$$

Then, at time point 2, with input vector $\mathbf{x}(2) = [x(2) \;\; x(1) \;\; ... \;\; x(-N+3)]^T$, the estimation error is given by

$$\begin{aligned} e(2) &= d(2) - \mathbf{w}^T(2)\mathbf{x}(2) \\ &= d(2) - [\tilde{\mathbf{w}}_1(1) + \mu_1 \tilde{e}_1(1)\mathbf{x}(1)]^T\mathbf{x}(2). && (6.5) \end{aligned}$$

Now, again from the viewpoint of time point 2, looking backwards, the step-size would have been more suitably chosen for both time points 0 and 1 at the same time, if $e^2(1) + e^2(2)$ is minimized. Suppose this more suitable step-size is $\tilde{\mu}_2$. If genie-aided feedback allows us to reset the step-size for both time points 0 and 1 as $\tilde{\mu}_2$, we would have

$$\begin{aligned} \tilde{\mathbf{w}}_2(1) &= \mathbf{w}(0) + \tilde{\mu}_2 e(0)\mathbf{x}(0) && (6.6) \\ \tilde{e}_2(1) &= d(1) - \tilde{\mathbf{w}}_2^T(1)\mathbf{x}(1) \\ &= d(1) - [\mathbf{w}(0) + \tilde{\mu}_2 e(0)\mathbf{x}(0)]^T\mathbf{x}(1), && (6.7) \end{aligned}$$

and

$$\begin{aligned} \tilde{\mathbf{w}}_2(2) &= \tilde{\mathbf{w}}_2(1) + \tilde{\mu}_2 \tilde{e}_2(1)\mathbf{x}(1) && (6.8) \\ \tilde{e}_2(2) &= d(2) - \tilde{\mathbf{w}}_2^T(2)\mathbf{x}(2) \\ &= d(2) - [\tilde{\mathbf{w}}_2(1) + \tilde{\mu}_2 \tilde{e}_2(1)\mathbf{x}(1)]^T\mathbf{x}(2), && (6.9) \end{aligned}$$

from which $\tilde{\mu}_2$ can be analytically determined. Then, we take $\mu_2 = \tilde{\mu}_2/\mathbf{x}^T(2)\mathbf{x}(2)$ to be the actual step-size used for updating the current tap-weight vector, i.e.

$$\mathbf{w}(3) = \tilde{\mathbf{w}}(2) + \mu_2 \tilde{e}_2(2)\mathbf{x}(2). \tag{6.10}$$

Generalizing the above idea, from the viewpoint of time point n, a step-size $\tilde{\mu}_n$ would have been more suitable for all the past time points if it minimizes $\sum_{i=1}^{n} e^2(i)$. With genie-aided feedback to reset all the past step-sizes as $\tilde{\mu}_n$, $\tilde{\mathbf{w}}_n(i)$ and $\tilde{e}_n(i)$ are expressible recursively in $\tilde{\mu}_n$ as

$$\tilde{\mathbf{w}}_n(i) = \tilde{\mathbf{w}}_n(i-1) + \tilde{\mu}_n \tilde{e}_n(i-1)\mathbf{x}(i-1), n \geq 1, \tag{6.11}$$

and

$$\begin{aligned} \tilde{e}_n(i) &= d(i) - \tilde{\mathbf{w}}_n^T(i)\mathbf{x}(i) \\ &= d(i) - [\tilde{\mathbf{w}}_n(i-1) + \tilde{\mu}_n \tilde{e}_n(i-1)\mathbf{x}(i-1)]^T \mathbf{x}(i), n \geq 1, \end{aligned} \tag{6.12}$$

respectively, where $\tilde{\mathbf{w}}_n(0) = \mathbf{w}(0)$ and $\tilde{e}_n(0) = e(0)$. Therefore, $\tilde{\mu}_n$ can be determined by solving a common minimization problem. Then, we take $\mu_n = \tilde{\mu}_n/\mathbf{x}^T(n)\mathbf{x}(n)$ to be the actual step-size for updating the current tap-weight vector, i.e.

$$\mathbf{w}(n+1) = \tilde{\mathbf{w}}_n(n) + \mu_n \tilde{e}_n(n)\mathbf{x}(n). \tag{6.13}$$

In the above description, we use the overhead $\tilde{}$ and subscript $n, n = 1, 2, ...$ on a term to indicate that the term comes from genie-aided feedback and is only optimized from the viewpoint of time point n. It should be noted that at each time when a new observation of the input signal arrives, the optimum value $\tilde{\mu}_n$ varies. In addition, the actual step-size μ_n is $\tilde{\mu}_n$ normalized by $\mathbf{x}^T(n)\mathbf{x}(n)$ to compensate for the impact of *gradient noise amplification* [70].

The algorithm described above is expected to have a good performance as the chosen $\tilde{\mu}_n$ results in the least sum of the squares of the measured errors. However, as noted, this algorithm is not practically realizable, unless the genie-aided feedback exists. To implement the idea that a step-size can be chosen to minimize the sum of the squares of the measured estimation errors, we propose a suboptimum realization.

We observe from (6.11) and (6.12) that the difficulty lies in the recursive expressions of $\tilde{\mathbf{w}}_n(i)$ and $\tilde{e}_n(i)$ in $\tilde{\mu}_n$. However, for a real system, viewing from the current time point n, all the past tap-weight vectors $\{\mathbf{w}(i)\}_{i=0}^{n}$ and the past errors $\{e(i)\}_{i=0}^{n}$ have already been realized. Therefore, we replace $\tilde{\mathbf{w}}_n(i-1)$ and $\tilde{e}_n(i-1)$ in (6.11) and (6.12), respectively, by the values $\mathbf{w}(i-1)$ and $e(i-1)$ that have been realized, i.e., we approximate $\tilde{\mathbf{w}}_n(i)$ and $\tilde{e}_n(i)$ by

$$\tilde{\mathbf{w}}'_n(i) = \mathbf{w}(i-1) + \tilde{\mu}'_n e(i-1)\mathbf{x}(i-1), n \geq 1, \tag{6.14}$$

and

$$\tilde{e}'_n(i) = d(i) - [\mathbf{w}(i-1) + \tilde{\mu}'_n e(i-1)\mathbf{x}(i-1)]^T \mathbf{x}(i), n \geq 1, \tag{6.15}$$

respectively. Here, $\tilde{\mu}'_n$ denotes the practically realizable approximation to the genie-aided $\tilde{\mu}_n$. Now, $\tilde{\mu}'_n$ can be determined from the approximation (6.15) by minimizing

$$J(n) = \sum_{i=1}^{n} \tilde{e}'^2_n(i). \tag{6.16}$$

Substituting (6.15) into (6.16) and rearranging the terms, we have

$$\begin{aligned} J(n) = \sum_{i=1}^{n} \Big\{ & [d(i) - \mathbf{w}^T(i-1)\mathbf{x}(i)]^2 - \\ & 2\tilde{\mu}'_n [d(i) - \mathbf{w}^T(i-1)\mathbf{x}(i)] e(i-1)\mathbf{x}^T(i-1)\mathbf{x}(i) + \\ & \tilde{\mu}'^2_n e^2(i-1)[\mathbf{x}^T(i-1)\mathbf{x}(i)]^2 \Big\}. \end{aligned} \tag{6.17}$$

Differentiating successively with respect to $\tilde{\mu}'_n$, we have

$$\begin{aligned} \frac{d}{d\tilde{\mu}'_n} J(n) = \sum_{i=1}^{n} \Big\{ & -2[d(i) - \mathbf{w}^T(i-1)\mathbf{x}(i)] e(i-1)\mathbf{x}^T(i-1)\mathbf{x}(i) + \\ & 2\tilde{\mu}'_n e^2(i-1)[\mathbf{x}^T(i-1)\mathbf{x}(i)]^2 \Big\} \end{aligned} \tag{6.18}$$

$$\frac{d^2}{d\tilde{\mu}'^2_n} J(n) = \sum_{i=1}^{n} \Big\{ 2e^2(i-1)[\mathbf{x}^T(i-1)\mathbf{x}(i)]^2 \Big\} \tag{6.19}$$

From (6.19) it is seen that $\frac{d^2}{d\tilde{\mu}'^2_n} J(n) \geq 0$, and therefore $J(n)$ is a convex function of $\tilde{\mu}'_n$, whose minimum is attained for $\frac{d}{d\tilde{\mu}'_n} J(n) = 0$. Rearranging the terms, we obtain

$$\tilde{\mu}'_n = \frac{\sum_{i=1}^{n} [d(i) - \mathbf{w}^T(i-1)\mathbf{x}(i)] e(i-1)\mathbf{x}^T(i-1)\mathbf{x}(i)}{\sum_{i=1}^{n} e^2(i-1)[\mathbf{x}^T(i-1)\mathbf{x}(i)]^2}. \tag{6.20}$$

We emphasize that $\tilde{\mu}'_n$ is a suboptimum realization of the genie-aided $\tilde{\mu}_n$. At each time point when a new observation of the input signal arrives, $\tilde{\mu}'_n$ is recomputed irrespective of its past values at all previous time points.

After obtaining $\tilde{\mu}'_n$, we update $\mathbf{w}(n)$ as

$$\mathbf{w}(n+1) = \mathbf{w}(n) + \frac{\tilde{\mu}'_n}{\mathbf{x}^T(n)\mathbf{x}(n)} e(n)\mathbf{x}(n), \tag{6.21}$$

where the actual step-size is $\mu'_n = \tilde{\mu}'_n / \mathbf{x}^T(n)\mathbf{x}(n)$. Due to the normalization process, we categorize our proposed algorithm into the NLMS-type algorithm. In addition, we propose a time-varying upper bound $\tilde{\mu}_n^{\max} = \mathbf{x}^T(n)\mathbf{x}(n)$ on $\tilde{\mu}'_n$ to avoid the actual step-size μ'_n from becoming too large. Similarly, a lower bound $\tilde{\mu}_n^{\min}$ on $\tilde{\mu}'_n$ is used to avoid μ'_n from becoming zero. The $\tilde{\mu}_n^{\min}$ can be arbitrarily chosen as long as it is a small positive constant, e.g., $\tilde{\mu}_n^{\min} = 10^{-10}$ is a common value that can be used. Equations (6.20) and (6.21) define the core operations of the adaptive filtering process. It is clearly seen that no preset control parameters need to be specified. The algorithm adapts online by itself with each new arrival of the input signal. We name it the ASSA algorithm to reflect its self-adaptation capability. The ASSA algorithm is summarized in Table 6.1.

Remark 6.1 It should be noted that the least-squares cost function defined in (6.16) is used as the objective function to be minimized to adaptively adjust the parameter $\tilde{\mu}'_n$ that is then used to update the filter tap-weight. The idea of this least-squares cost function-aided adaptation approach first appears in [97]. However, in [97], the cost function is used to adjust the filter weight itself, instead of a step-size parameter for adjusting the filter weight. The proposed algorithm also differs from the recursive least-squares (RLS) algorithm [70] in which a weighted sum of squared errors is used directly in arriving at the algorithm for adjusting the filter weights.

Remark 6.2 In the expression determining $\tilde{\mu}'_n$, as shown in (6.20), both the denominator and the numerator are calculated in a running-sum form, which is easy to implement.

In Table 6.2, we list the computational complexity of various algorithms that

Table 6.1: ASSA Algorithm

Initialization:	$\mathbf{w}(0) = \mathbf{0}$
Input:	Current tap-weight vector $\mathbf{w}(n)$
	Input vector $\mathbf{x}(n)$,
	Desired signal $d(n)$,
Output:	Filter output $y(n) = \mathbf{w}^T(n)\mathbf{x}(n)$
	Updated tap-weight vector $\mathbf{w}(n+1)$

1. Estimation error:

$$e(n) = d(n) - y(n)$$

2. Step-size and tap-weight adaptation:

$$\tilde{\mu}'_n = \frac{\sum_{i=1}^{n}[d(i)-\mathbf{w}^T(i-1)\mathbf{x}(i)]e(i-1)\mathbf{x}^T(i-1)\mathbf{x}(i)}{\sum_{i=1}^{n} e^2(i-1)[\mathbf{x}^T(i-1)\mathbf{x}(i)]^2}$$

if $\tilde{\mu}'_n > \tilde{\mu}_n^{\max}$, $\tilde{\mu}'_n = \tilde{\mu}_n^{\max}$, where $\tilde{\mu}_n^{\max} = \mathbf{x}^T(n)\mathbf{x}(n)$
if $\tilde{\mu}'_n < \tilde{\mu}_n^{\min}$, $\tilde{\mu}'_n = \tilde{\mu}_n^{\min}$, where $\tilde{\mu}_n^{\min} = 10^{-10}$

$$\mathbf{w}(n+1) = \mathbf{w}(n) + \frac{\tilde{\mu}'_n}{\mathbf{x}^T(n)\mathbf{x}(n)}e(n)\mathbf{x}(n)$$

have been introduced in Section 2.3. Note that N denotes the filter order, and the ε-NLMS-RR algorithm denotes the ε-NLMS algorithm incorporating the robust regularization [81]. As can be seen, the ASSA algorithm has the most computational complexity. However, it is noted that computational cost of the ASSA algorithm remains reasonable. For example, it only requires N more additions and $N + 2$ more multiplications than the VSS-NLMS algorithm. Moreover, we emphasize that in choosing the step-size, the other algorithms always rely on extensive trials for a good performance. This would in turn, incur more cost in general.

Table 6.2: Computational Complexity of Various Step-Size Adjustment Algorithms for the LMS Adaptive Filter

Algorithms	Additions	Multiplications	Divisions
LMS [71]	2N+1	2N+1	0
GASS [75]	3N+2	3N+4	0
MVSS [77]	2N+3	2N+7	0
NLMS [70]	3N+1	3N+1	1
VSS-NLMS [79]	4N+2	4N+4	2
ε-NLMS-RR [81]	4N+3	4N+4	1
ASSA	5N+2	5N+6	2

6.3 Simulation Results

In this section, we apply an adaptive filter to channel estimation in wireless communications applications, and examine the performance of different step-size adjustment algorithms. Specifically, we consider a one-step prediction, i.e., given the immediate past N samples $\{x(l)\}_{l=n-N+1}^{n}$ of a random process as the filter input, the filter output $y(n) = \mathbf{w}^T(n)\mathbf{x}(n)$ forms an estimate of $x(n+1)$, where $x(n+1)$ is viewed as the desired signal. The performance metric of concern is MSE versus number of iterations, from which the rate of convergence of an algorithm and the MSE achieved by that algorithm are clearly shown. The MSE at each time point is measured by averaging over a sufficiently large number of runs for a smooth curve.

The two channel models used are the first-order Butterworth process [98] which is useful in modeling the ionospheric skywave and the tropospheric scatter channel, and the Jakes process [1] which is used to model the signal propagation in street microcells and in-building micro, nano and pico cells. Their power spectra are given by

$$S_p(\omega) = \frac{2\sigma_p^2/\omega_d T}{1 + (\omega T/\omega_d T)^2}, \tag{6.22}$$

and

$$S_p(\omega) = \begin{cases} \frac{2\sigma_p^2}{\omega_d T\sqrt{1-(\omega T/\omega_d T)^2}}, & |\omega| \leq \omega_d, \\ 0, & |\omega| > \omega_d, \end{cases} \tag{6.23}$$

respectively. Here, σ_p^2 is the variance of the process, T is the sampling interval, and ω_d is the 3-dB spectral bandwidth. In simulations, the first-order Butterworth sequence is generated by feeding a white Gaussian noise sequence into a first-order Butterworth filter, and the Method of Equal Areas (MEA) [99] is used to generate the Jakes sequence. We use $\{p(n)\}$ to denote the generated random sequence. Without loss of generality, we assume that all pilot symbols are equal to 1. Therefore, each sample of the random sequence is recognized as a sample of the channel at that time point. We consider both a non-noisy environment and a noisy environment. In the non-noisy case, the filter input sequence $\{x(n)\}$ is exactly the generated random sequence $\{p(n)\}$. In the noisy case, a corrupted version of $\{p(n)\}$ is fed into the filter, i.e., the input signal becomes

$$x(n) = p(n) + v(n), \tag{6.24}$$

where $v(n)$ is a white noise with mean zero and variance σ_v^2. The SNR is defined as

$$\text{SNR} = 10\log_{10}(\sigma_p^2/\sigma_v^2). \tag{6.25}$$

In our simulations, we assume a fixed SNR at 10dB.

6.3.1 Comparison of the ASSA algorithm and the LMS-type Algorithms

Although as has been mentioned, the NLMS-type algorithms are usually not compared with the LMS-type algorithms, it would be useful to show the performance gain of the ASSA algorithm over the LMS-type algorithms with variable step-size, and demonstrate the better performance of the former one. To illustrate, we generate a first-order Butterworth sequence with $\sigma_p^2 = 0.25$ and $\omega_d T = 0.01$, and a Jakes sequence with $\sigma_p^2 = 0.25$ and $\omega_d T = 0.05$, respectively. These statistics are of

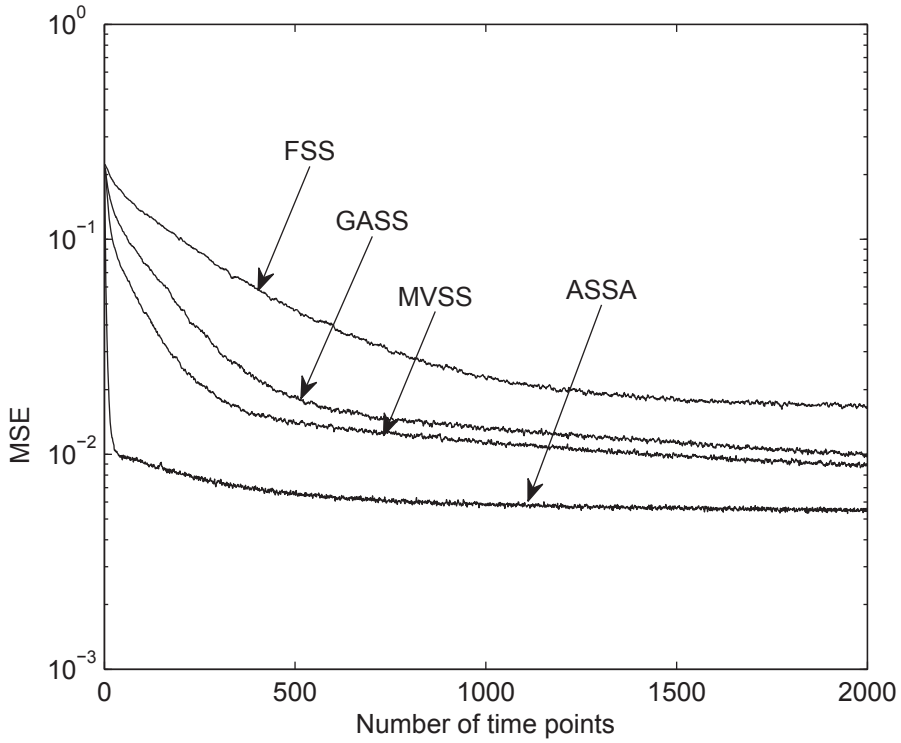

Figure 6.1: MSE comparison of the ASSA, the FSS LMS, the GASS and the MVSS algorithms in predicting the first-order Butterworth process for the non-noisy case.

course, unknown to the receiver. We assume an adaptive filter of order 10 at the receiver for prediction. For fair comparison, the filter tap-weight coefficients are initialized to zeros for each test. We compare the ASSA algorithm with the other two well-known variable step-size algorithms, i.e., the GASS algorithm [75] and the MVSS algorithm [77]. The original FSS LMS algorithm is also included for comparison. We first consider the non-noisy case. To predict the first-order Butterworth sequence, the FSS LMS algorithm is used with step-size being fixed at $\mu = 1 \times 10^{-3}$. For the GASS algorithm, the parameters are chosen to be $\mu(0) = 0$ and $\rho = 1 \times 10^{-4}$. For the MVSS algorithm, the parameters are chosen to be $\alpha = 0.9999$, $\beta = 0.5$ and $\gamma = 5 \times 10^{-3}$. For both the GASS and the MVSS algorithms, their step-sizes are bounded by $\mu_{\max} = 0.034$ and $\mu_{\min} = 1 \times 10^{-10}$. To

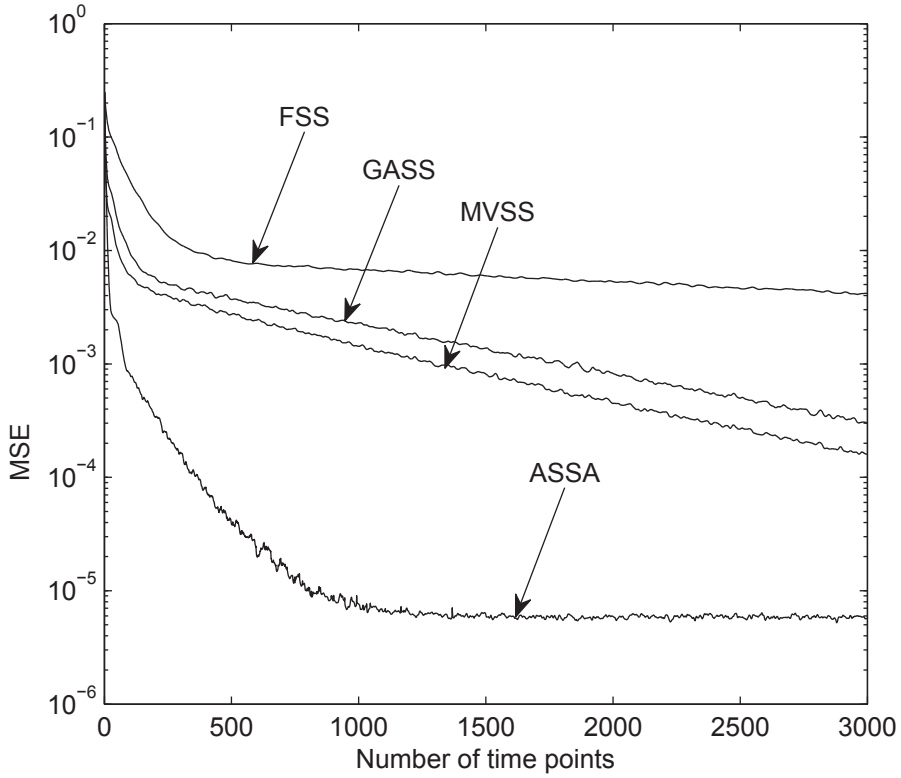

Figure 6.2: MSE comparison of the ASSA, the FSS LMS, the GASS and the MVSS algorithms in predicting the Jakes process for the non-noisy case.

predict the Jakes sequence, we choose $\mu = 5 \times 10^{-3}$ for the FSS LMS algorithm, and $\mu(0) = 0.02$, $\rho = 1 \times 10^{-3}$ for the GASS algorithm, and $\alpha = 0.9999$, $\beta = 0.97$, $\gamma = 1 \times 10^{-3}$ for the MVSS algorithm. For both the GASS and the MVSS algorithms, their step-sizes are bounded by $\mu_{\max} = 0.045$ and $\mu_{\min} = 1 \times 10^{-10}$. Here, $\mu_{\max}$ denotes the maximum allowable step-size for an algorithm to remain stable, and $\mu_{\min}$ denotes the lower bound that can be arbitrarily chosen as long as it is a small, positive constant. We emphasize that all the control parameters used in the above for the GASS and the MVSS algorithms are chosen through extensive trials, for a good performance. Figs. 6.1 and 6.2 show the MSE curves of different algorithms in predicting the first-order Butterworth process and the Jakes process, respectively, under the non-noisy environment. As can be seen in both figures, the

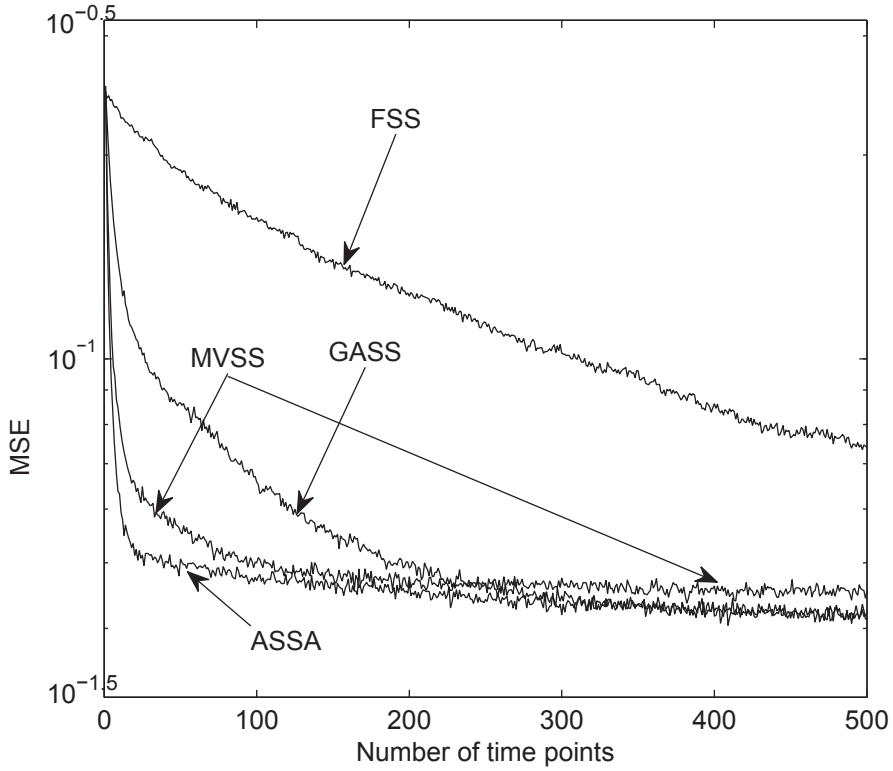

Figure 6.3: MSE comparison of the ASSA, the FSS LMS, the GASS and the MVSS algorithms in predicting the first-order Butterworth process for the noisy case.

ASSA algorithm performs much better than the other ones. It converges the fastest and arrives at the smallest MSE.

Figs. 6.3 and 6.4 show the comparison of different algorithms under the noisy environment. First, it is noted that, reasonably, the MSEs of these algorithms under the noisy environment are larger than those under the non-noisy environment. We mention that for the GASS and the MVSS algorithms, their control parameters for the noisy case are chosen differently from those for the non-noisy case. These control parameters for the noisy case are, again, chosen through extensive trials for a good performance. Specifically, the GASS algorithm is used with $\mu(0) = 0$, $\rho = 1 \times 10^{-3}$ and $\mu_{\max} = 0.03$ for predicting the first-order Butterworth process, and

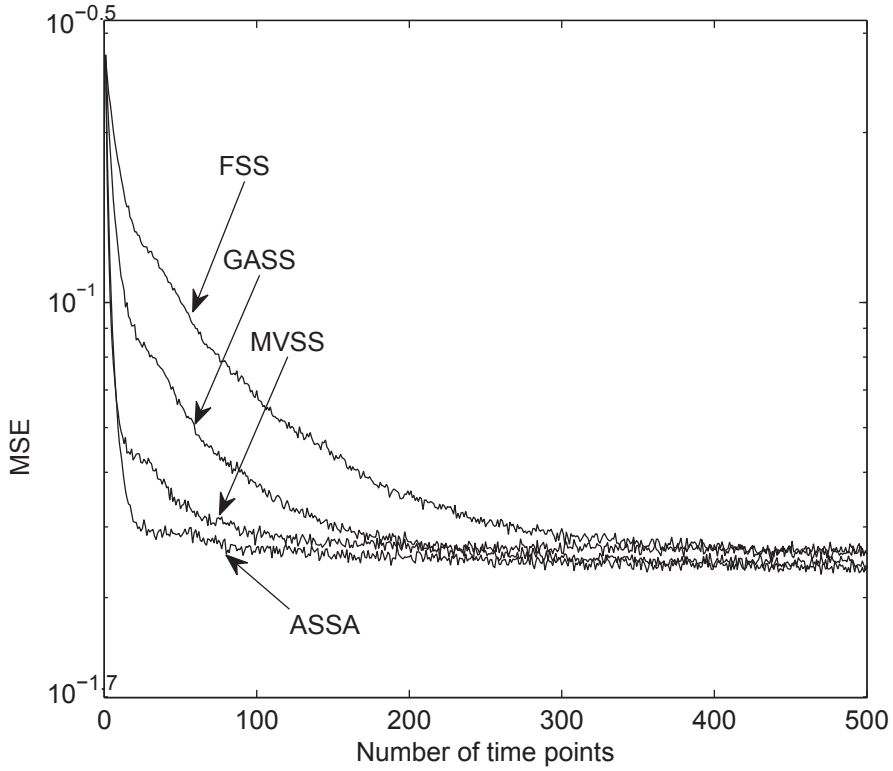

Figure 6.4: MSE comparison of the ASSA, the FSS LMS, the GASS and the MVSS algorithms in predicting the Jakes process for the noisy case.

with $\mu(0) = 0.01$, $\rho = 1 \times 10^{-4}$ and $\mu_{\max} = 0.04$ for predicting the Jakes process. The MVSS algorithm is used with $\alpha = 0.99$, $\beta = 0.6$, $\gamma = 1 \times 10^{-3}$ and $\mu_{\max} = 0.03$ for predicting the first-order Butterworth process, and with $\alpha = 0.99$, $\beta = 0.97$, $\gamma = 1 \times 10^{-4}$ and $\mu_{\max} = 0.04$ for predicting the Jakes process. The lower bound $\mu_{\min} = 1 \times 10^{-10}$ applies to all the cases in the above. As can be seen from Figs. 6.3 and 6.4, the ASSA algorithm still performs the best under the noisy environment. We emphasize that the better performance of the ASSA algorithm is achieved with no preset control parameters.

We conclude that in all the scenarios considered above, the ASSA algorithm performs better than these LMS-type algorithms, and its performance advantage is significant.

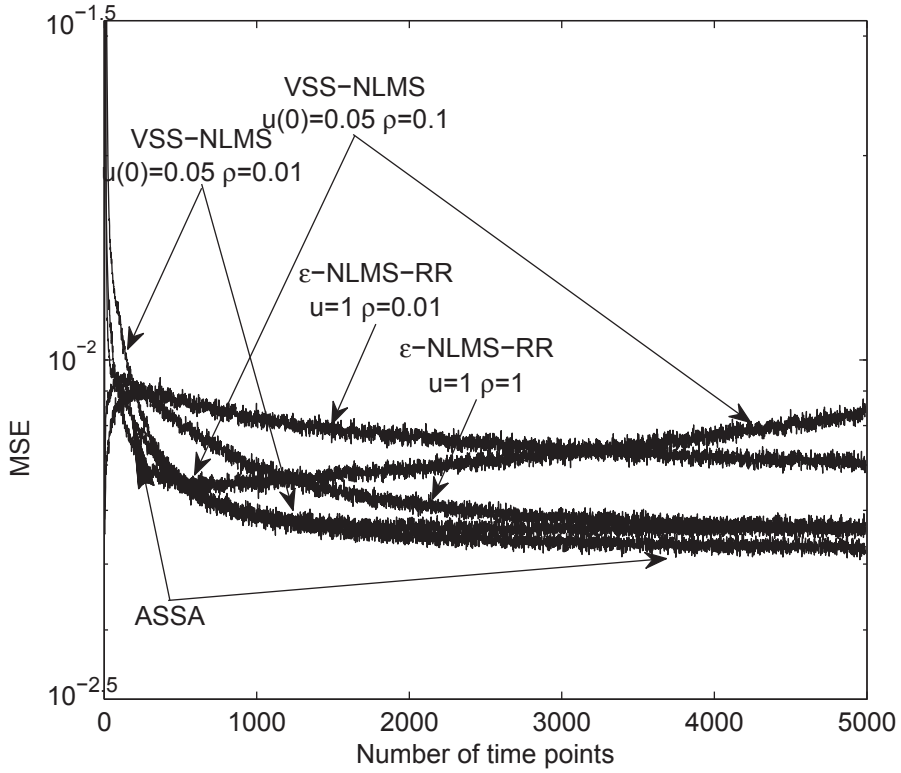

Figure 6.5: MSE comparison of the ASSA, the VSS-NLMS and the ε-NLMS-RR algorithms in predicting the first-order Butterworth process for the non-noisy case; the input sequence is with $\sigma_p^2 = 0.25$ and $\omega_d T = 0.01$; the filter order is $N = 10$.

6.3.2 Comparison of the ASSA algorithm and the NLMS-type Algorithms

To demonstrate the effectiveness of the ASSA algorithm, we are more concerned about the comparison of the ASSA algorithm and the NLMS-type algorithms. In the following, we compare the ASSA algorithm with the VSS-NLMS algorithm [79] and the ε-NLMS-RR algorithm [81]. These two algorithms are typical NLMS-type algorithms with variable step-size. Similar to that in the previous subsection, for fair comparison, all the algorithms start with filter tap-weight coefficients being set to zeros.

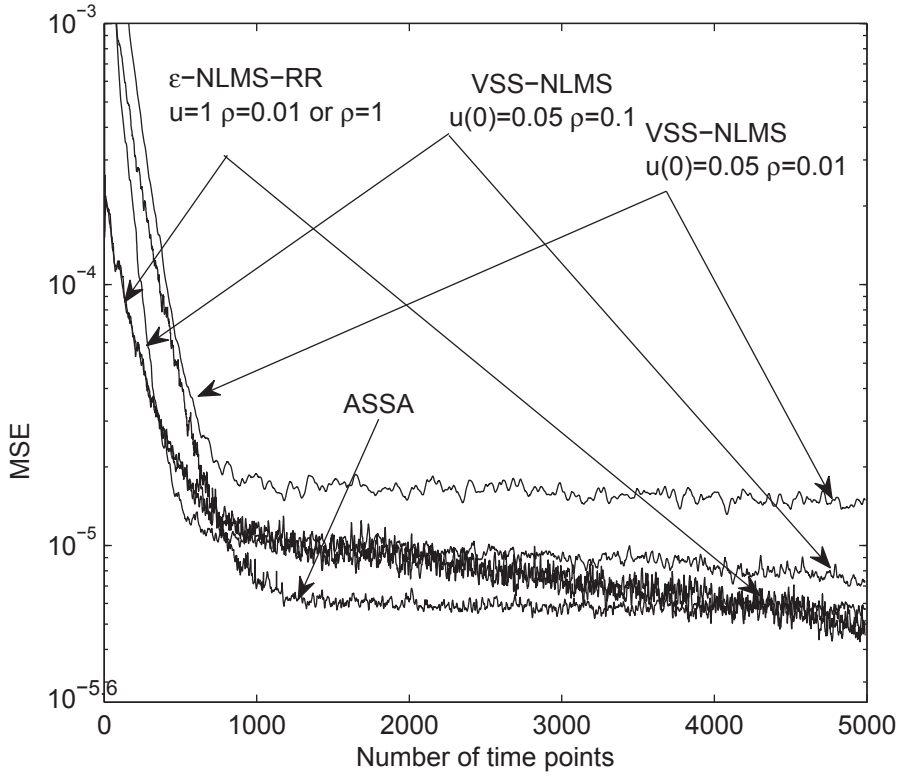

Figure 6.6: MSE comparison of the ASSA, the VSS-NLMS and the ε-NLMS-RR algorithms in predicting the Jakes process for the non-noisy case; the input sequence is with $\sigma_p^2 = 0.25$ and $\omega_d T = 0.05$; the filter order is $N = 10$.

In Figs. 6.5 and 6.6, we plot the MSE curves for the ASSA, the VSS-NLMS and the ε-NLMS-RR algorithms in predicting the first-order Butterworth process and the Jakes process, respectively. The first-order Butterworth sequence is generated with $\sigma_p^2 = 0.25$ and $\omega_d T = 0.01$, and the Jakes sequence is generated with $\sigma_p^2 = 0.25$ and $\omega_d T = 0.05$. For the VSS-NLMS algorithm, its parameter $\mu(0)$ is fixed at 0.05, and ρ is set to 0.01 and 0.1, respectively. Here, $\mu(0)$ is the initial value of the time-varying step-size defined in [79]. For the ε-NLMS-RR algorithm, its parameter μ is fixed at 1, and ρ is set to 0.01 and 1, respectively. As can be seen from Figs. 6.5 and 6.6, by carefully choosing the control parameters, the VSS-NLMS and the ε-NLMS-RR algorithms can perform close to the ASSA algorithm. In Fig. 6.6, it is seen that

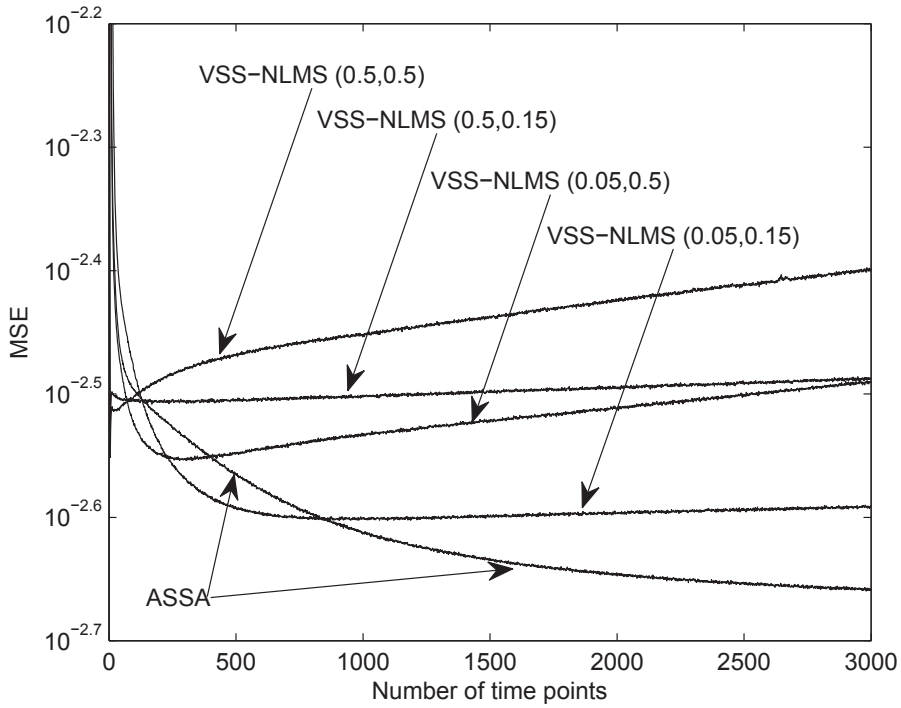

Figure 6.7: MSE comparison of the ASSA and the VSS-NLMS algorithms in predicting the first-order Butterworth process for the non-noisy case; the input sequence is with $\sigma_p^2 = 0.2$ and $\omega_d T = 0.005$; the filter order is $N = 6$.

the ε-NLMS-RR algorithm outperforms the ASSA algorithm from about the 4500th time point onwards in predicting the Jakes process. However, we note that when the same parameters are used for predicting the first-order Butterworth process, the ε-NLMS-RR algorithm shows a poorer performance than the ASSA algorithm at all time points, as shown in Fig. 6.5. It is not surprising that by carefully choosing the control parameters, some of the parameter-controlled algorithms can outperform the ASSA algorithm. However, the ASSA algorithm is undoubtedly more flexible, due to its parameter-free nature. To further demonstrate the performance advantage of the ASSA algorithm, in the following, we change the statistics of those input sequences, and show the performance of those algorithms.

We generate a new first-order Butterworth sequence with $\sigma_p^2 = 0.2$, $\omega_d T =$

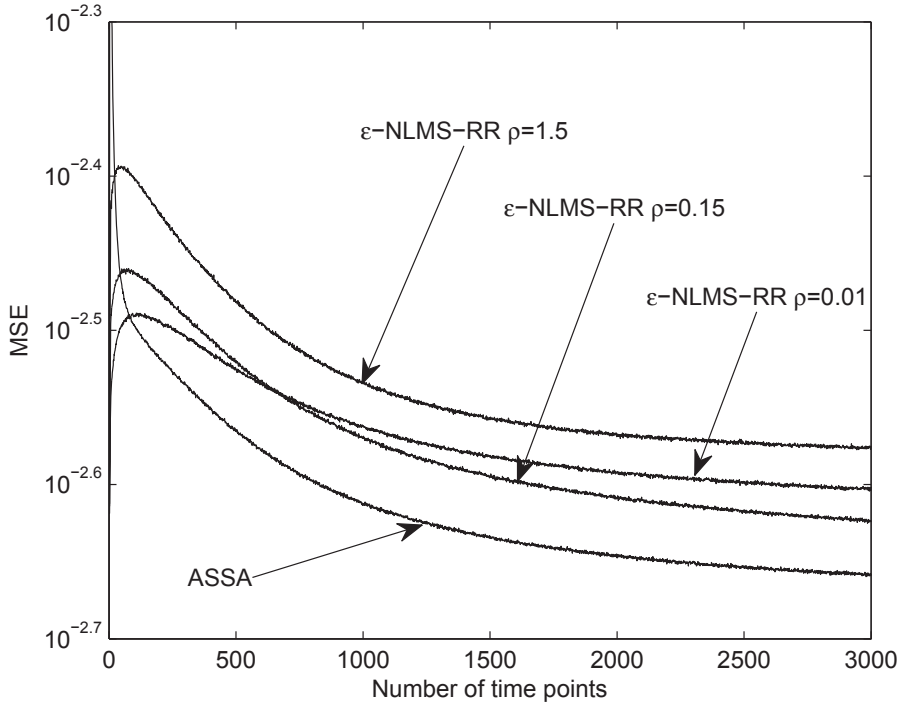

Figure 6.8: MSE comparison of the ASSA and the ε-NLMS-RR algorithms in predicting the first-order Butterworth process for the non-noisy case; the input sequence is with $\sigma_p^2 = 0.2$ and $\omega_d T = 0.005$; the filter order is $N = 6$.

0.005, and a new Jakes sequence with $\sigma_p^2 = 0.2$, $\omega_d T = 0.03$, and we use the filters with order $N = 6$ and $N = 12$, respectively, to predict the first-order Butterworth process and the Jakes process. For the VSS-NLMS and the ε-NLMS-RR algorithms, to assess their performance fairly, we have simulated them with many different choices of parameters to determine the optimum parameters for each of them. Here, we present a few typical results including the best performance achieved by using the optimum control parameters. For the VSS-NLMS algorithm, we show its performance with four different sets of $(\mu(0), \rho)$, given by $(0.05, 0.15)$, $(0.05, 0.5)$, $(0.5, 0.15)$ and $(0.5, 0.5)$. For the ε-NLMS-RR algorithm, μ is fixed at 1 and results for $\rho = 0.01, 0.15$ and 1.5 are shown.

Figs. 6.7 and 6.8 compare the ASSA algorithm with the VSS-NLMS

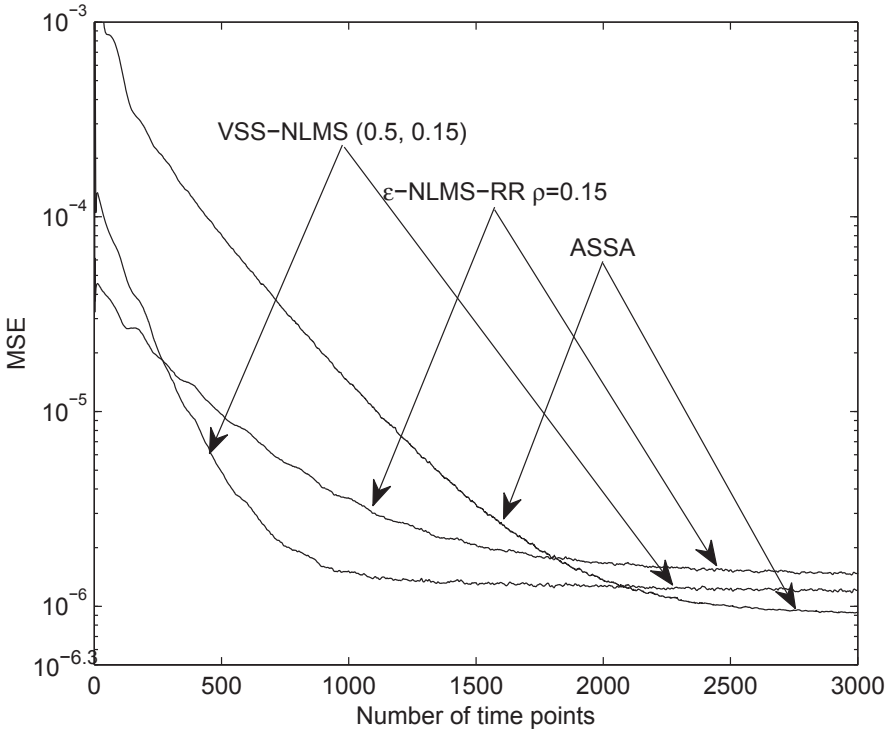

Figure 6.9: MSE comparison of the ASSA, the VSS-NLMS and the ε-NLMS-RR algorithms in predicting the Jakes process for the non-noisy case; the input sequence is with $\sigma_p^2 = 0.2$ and $\omega_d T = 0.03$; the filter order is $N = 12$.

algorithm and the ε-NLMS-RR algorithm, respectively, in predicting the first-order Butterworth process for the non-noisy case. In Fig. 6.7, it is noted that the control parameters for the VSS-NLMS algorithm have to be carefully chosen, otherwise, the MSE may not converge, e.g., when the second parameter ρ is chosen to be 0.5, as iteration goes on, the MSE increases. The VSS-NLMS algorithm with the best choice of parameter, i.e., $(\mu(0) = 0.05, \rho = 0.15)$, converges faster than the ASSA algorithm at the beginning. However, when the VSS-NLMS algorithm stops learning at about the 600th time point, the ASSA algorithm is still learning from the random process and arrives at a smaller MSE from about the 800th time point onwards. In Fig. 6.8, we observe that $\rho = 0.15$ is the best choice for the ε-NLMS-RR algorithm. When further decreasing ρ, the MSE is increased. The performance advantage of

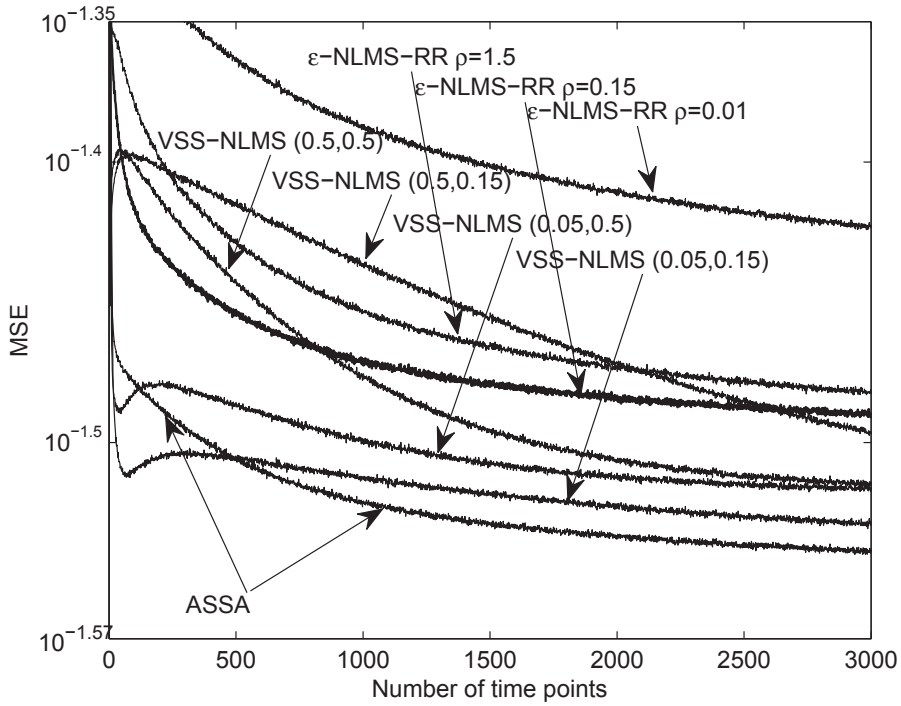

Figure 6.10: MSE comparison of the ASSA, the VSS-NLMS and the ε-NLMS-RR algorithms in predicting the first-order Butterworth process for the noisy case; the input sequence is with $\sigma_p^2 = 0.2$ and $\omega_d T = 0.005$; the filter order is $N = 6$.

the ASSA algorithm is quite clear in Fig. 6.8.

In Fig. 6.9, we compare the three algorithms in predicting the Jakes process in the non-noisy case. For the VSS-NLMS and the ε-NLMS-RR algorithms, we only show the curves with the best choice of their parameters, as for either of the algorithms, the curves with different parameters are very close to one another. This phenomenon also indicates that in predicting the given Jakes process, the MSE of the VSS-NLMS and the ε-NLMS-RR algorithms is not sensitive to the variations of the control parameters, which is in contrast to that in predicting the non-noisy first-order Butterworth process. As can be seen in Fig. 6.9, the ASSA algorithm converges slower than the other two algorithms. The better performance of the ASSA algorithm in terms of the MSE value can only be observed after

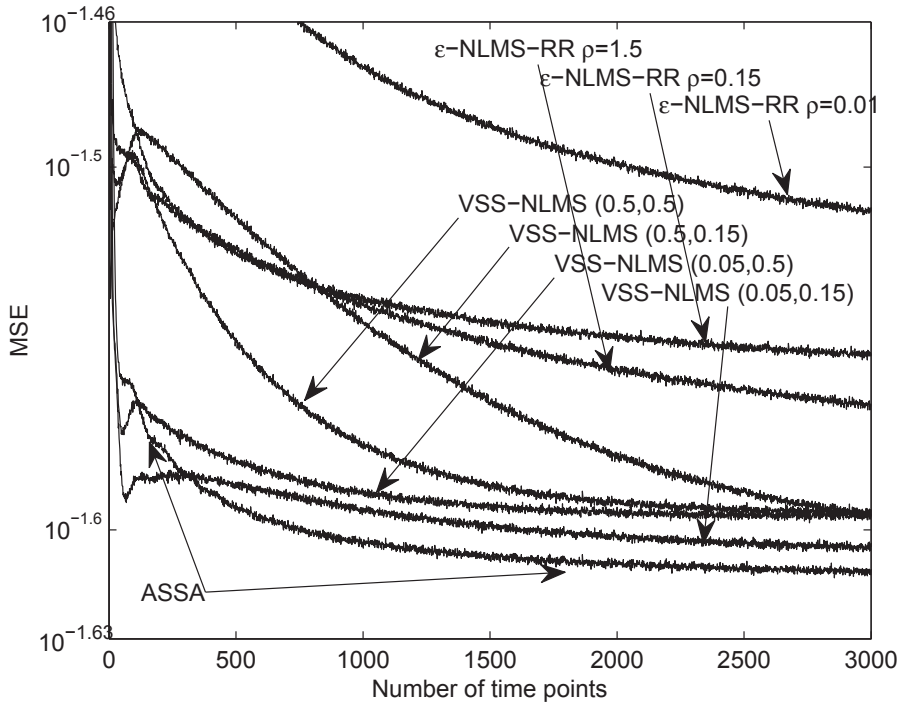

Figure 6.11: MSE comparison of the ASSA, the VSS-NLMS and the ε-NLMS-RR algorithms in predicting the Jakes process for the noisy case; the input sequence is with $\sigma_p^2 = 0.2$ and $\omega_d T = 0.03$; the filter order is $N = 12$.

about the 2100th time point. However, we again emphasize that the best choice of the parameters for the VSS-NLMS and the ε-NLMS-RR algorithms are only obtainable through extensive trials. In practice, to predict an unknown source, it is impossible to experimentally realize an extensive search for the optimum parameters for those parameter-controlled algorithms, as it would be very time-consuming and waste a large amount of energy. Therefore, the ASSA algorithm is a promising approach, as it can be immediately and directly implemented without pre-adjusting any parameters or requiring any knowledge of the environment.

Figs. 6.10 and 6.11 compare the three algorithms in predicting the first-order Butterworth process and the Jakes process, respectively, under the noisy environment. Comparing Fig. 6.10 with Figs. 6.7 and 6.8, and comparing Fig.

6.11 with Fig. 6.9, respectively, it is noted that, as expected, the MSEs of all the algorithms under the noisy environment are larger than those under the non-noisy environment. For example, in predicting the Jakes process, the ASSA algorithm can achieve an MSE of about 10^{-6} at the 3000th time point under the non-noisy environment, as shown in Fig. 6.9. However, this value increases to about $10^{-1.61}$ under the noisy environment, as shown in Fig. 6.11. It has been noted that for the VSS-NLMS algorithm in predicting the first-order Butterworth process under the non-noisy environment, when the second parameter ρ is chosen to be 0.5, the MSE curve does not converge. However, as can be seen from Fig. 6.10, this choice of ρ results in a fairly good performance especially for the choice of $(\mu(0) = 0.05, \rho = 0.5)$. For the ε-NLMS-RR algorithm, from Fig. 6.10, we observe that $\rho = 0.15$ is the best choice, while in Fig. 6.11, $\rho = 1.5$ becomes the best choice. These findings indicate that when the disturbance or the environment changes, the optimum control parameters may also change for those parameter-controlled algorithms. However, in practice, it is impossible to rechoose the control parameters every time when the statistics of the input varies. We have also examined those algorithms at SNR= 20dB and SNR= 30dB, respectively. It is commonly found that when SNR goes higher, the final MSE that those algorithms can achieve becomes smaller, and the SNR has little effect on the rate of convergence of those algorithms. At different SNR values, the ASSA algorithm always shows the smallest final MSE.

Generally, the three algorithms show a comparable rate of convergence, except that in predicting the noiseless Jakes process, the ASSA algorithm converges slower than the other two algorithms, as shown in Fig. 6.9. Figs. 6.7-6.11 show that the ASSA algorithm consistently leads to a smaller MSE when compared with the VSS-NLMS and the ε-NLMS-RR algorithms, no matter what parameters have been chosen for the latter two parameter-controlled algorithms. We emphasize that the better performance of the ASSA algorithm is achieved with no preset control parameters. The other two algorithms require preset control parameters whose optimum values can only be determined through extensive trials, which as has been

mentioned, is not easy to implement in practice. In contrast, the ASSA algorithm can be immediately deployed in any environment.

6.4 Conclusions

In this chapter, we proposed a novel step-size adjustment algorithm, i.e., the ASSA algorithm, for the tap-weight coefficients adaptation of an LMS adaptive filter. Unlike all the existing step-size algorithms that require preset control parameters, the ASSA algorithm is truly control parameter-free. The LMS adaptive filter employing the ASSA algorithm can be used for effective CSI acquisition, when the optimum Wiener filter is not applicable. When applied to channel estimation, we have shown the performance advantage of the ASSA algorithm over the existing step-size adjustment algorithms under different wireless channel environments. The ASSA algorithm serves as a fundamental contribution to the step-size adjustment for the tap-weight coefficients adaptation of LMS adaptive filters. It can be applied to other situations where LMS adaptive filters are employed, e.g., system identification, channel equalization.

Chapter 7

Conclusions and Suggestions for Future Work

7.1 Conclusions

In wireless communications, a severe channel impairment caused by signal fading has become the key challenge for fast and reliable transmission. A straightforward way to mitigate signal fading is to transmit channel-adaptive signals. The design of channel-adaptive communication systems deals with the modification of some transmitter parameters according to the CSIT, which is usually obtained through CSI feedback. In particular, a power-adaptive transmission system for fading channels is designed to adapt the transmitted power to match the current state of the channel. It has been shown that by employing channel-adaptive signaling, a system yields large improvements in almost any performance metric. Another efficient approach to reliable transmission is known as space diversity, and it can be readily combined with time or frequency diversity. By exploiting the broadcast nature of a wireless medium and allowing terminals to cooperatively transmit information through relaying, cooperative relay communication systems achieve space diversity through relay cooperation. Moreover, relay systems realize many benefits over traditional MIMO systems, such as adaptability, coverage and cost-efficiency.

In the design of a power-adaptive transmission system, a common way is to adapt the power to optimize some performance metric, subject to some systematic constraints. Considering the design of a practically realizable feedback power control system for specific modulation formats, the ABEP is commonly used as the performance metric. However, we noted that ABEP is not a good performance measure for high data-rate transmissions. Since the ABEP is obtained by averaging the IBEP over the distribution of the fading, it cannot reflect the instantaneous depth of fade experienced by the user. In high data-rate transmission, a short duration of deep fade may cause thousands of erroneous received data bits. In such a case, the BEOP is a more meaningful measure, and it reflects the instantaneous QoS experienced by the user. We proposed a BEOP-based power control law to compete with the traditional ABEP-based power control law. In all the previous works studying the ABEP-based law, it is assumed that perfect CSI for each bit is immediately available at the transmitter through a genie-aided feedback. However, this is impossible for real transmissions. We developed both the traditional ABEP-based law and the new BEOP-based law for the imperfect CSI scenario, which takes into consideration of feedback delay as well as channel estimation errors. In addition, we generalized the two power laws for both BPSK and QPSK modulations. We explicitly analyzed the ABEP and BEOP results for both laws. Through numerical results, we showed that each law suffers a significant loss in the ABEP or the BEOP performance when imperfect CSIT is applied instead of perfect CSIT. This demonstrates the importance of an accurate estimate of the CSIT. Under both perfect and imperfect CSI scenarios, the BEOP-based law shows a remarkable gain over the ABEP-based law in terms of BEOP, and sacrifices only a little in the ABEP performance.

A large number of works on the multiple relay communication systems has been developed during the past decade. Those works cover a wide range of topics on both information theoretic research and practical systems. However, there remains some unsolved problems regarding to some fundamental issues. In our work, we considered

the receiver design of a DF multiple relay system (without selection) and derived the ML detector at the destination with an arbitrary M-QAM, under imperfect CSI. It is noted that the true ML detector has only been shown in [20] for a single relay system with BPSK, under the assumption of perfect CSI. It is important to note that our receiver result clearly shows that for optimum detection at the destination, the instantaneous information of the $s - r$ link is required, and this information is summarized as the decoding error probability at the relay. This crucial point has been overlooked in many previous works on DF relay systems. We specialized the derived ML detector to BPSK case, and proposed the WSD and the CWSD to approximate the ML detector. These two detectors can be viewed as improvements on the traditional MRC and the PL detector, respectively.

In the performance analysis of the ML detector in a general DF relay system (without selection), all the previous works actually analyzed the suboptimum A-PL detector which uses the ABEP at the relay. In our work, we obtained the ABEP results for several different destination detectors in a single relay system. Among them, we highlight the closed-form, approximate ABEP of the PL detector, and we emphasize that this PL detector uses the IBEP at the relay. This distinguishes our work from those who analyze the A-PL detector which uses the ABEP at the relay. When considering a DF multiple relay system, no exact ABEP performance analysis of the ML or the PL detector has been conducted in previous works. Reference [23] has noted the importance of using the instantaneous information of the $s - r$ link for detection at the destination, and it considers a multiple relay system. However, in [23], the ABEP is only analyzed from the diversity point of view, where extremely high SNR is assumed. In our work, we derived closed-form Chernoff upper bounds on the ABEPs of the A-PL detector and the PL detector, respectively, in a DF multiple relay system with an arbitrary number of relays. The obtained Chernoff upper bound becomes tighter as the number of relays increases. All our theoretical results have been validated using simulations. We made many important and useful observations from the analysis of those derived ABEP results. For example, to

achieve a good performance in a single relay system, the relay needs to be located at some point that balances the quality of both the $s - r$ and the $r - d$ links in the long term; the detectors retain using the IBEP at the relay offers a substantial gain over the averaged-detectors which only use the ABEP at the relay; the channel estimation errors do not affect the diversity order. Our Chernoff bound results prove that in a DF relay system, the detector using the IBEP at the relay achieves full diversity. In contrast, the averaged detector using the ABEP at the relay suffers a loss of diversity, which is quite undesired for the receiver design of spatial diversity systems.

Our works on the feedback power control and the DF relay communications alerted us the importance of CSI. Therefore, we devoted some effort to CSI acquisition. For analytical purpose, a Wiener-filter based channel acquisition model is popular for its simplicity, accuracy and tractability. However, in wireless communication systems, especially when the communication terminals are mobile, the statistics of the environment may change from time to time. In addition, the communication equipments are sometimes required to work in a completely unknown environment. Under such cases, we need to rely on adaptive filters to approximate the performance of the Wiener filter in an iterative manner. We proposed a novel ASSA algorithm for the weights adaptation of an LMS adaptive filter. The most significant feature that distinguishes the ASSA algorithm from any other existing variable step-size adjustment algorithms is that the ASSA algorithm does not require any preset control parameters. When applied to channel estimation, simulation results show the performance advantage of the ASSA algorithm over the existing step-size adjustment algorithms under different wireless channel environments. The ASSA algorithm is a fundamental contribution to the step-size adjustment for the tap-weight coefficients adaptation of LMS adaptive filters. It can be applied to other situations where LMS adaptive filters are employed, e.g., system identification, channel equalization.

7.2 Future Work

7.2.1 Rate Control of A Practical System with CSI Feedback

In Chapter 3, we considered the power control using feedback CSI. Practically, another common transmitter parameter that can be adjusted is the transmitted rate. Some early works on rate control for an actual system, propose to adjust the bit duration to realize the control on the transmitted rate [7, 8, 100]. In those works, the bit duration is assumed to be able to change continuously according to the channel variations. The assumption of a continuous change of bit duration is impractical. Actually, the idea of rate control is more attractive in the context of coded transmission. Instead of keep changing the bit duration, we can tend to change the code rate. When the channel is detected strong, a larger code rate can be used to reduce redundancy. On the contrary, when the channel is weak, a smaller code rate is required for reliable receptions. For rate control, either the ABEP or the BEOP can be used as the performance measure in the design of rate control laws.

7.2.2 Feedback Power Control for Practical SIMO, MISO and MIMO transmissions

Feedback power control in SIMO, MISO and MIMO systems has been widely studied from the information theoretic point of view. However, it remains unaddressed in practical MISO or MIMO system with specific modulation formats. We note that either the ABEP-based or the BEOP-based power control law can be extended to SIMO, MISO or MIMO transmission. The extension to SIMO transmission is straightforward. Since in SIMO transmission, the received SNR is the sum of the SNR of each transmit-receive path, the power of the transmit antenna can be easily adjusted according to this received SNR. The formulation of both power control laws

in SIMO case is the same as that in SISO case, except that the squared magnitude of the single channel fading gain in the SISO case is replaced by a sum of squared magnitude of each transmit-receive channel fading gain. For the power control to be effective in MISO or MIMO transmission, each transmit antenna is expected to gather its own CSI. Thus, power control needs to be performed on each transmit antenna, subject to constraints on the total transmitted power and/or the peak transmitted power of each antenna.

7.2.3 Performance Analysis of A DF Relay System with the BEOP Performance Measure; with Higher Order Modulations

In Chapter 1, we have introduced the BEOP as a new performance measure for transmissions over fading channels. The BEOP reflects the instantaneous QoS experienced by the user, and is extremely useful for high-data rate transmission over time-varying fading. As a new dimension in performance evaluation of wireless communication systems, many of the existing technologies can be relooked at from the viewpoint of the BEOP. Due to lack of time, we did not extend our analysis on the DF relay system to the BEOP performance measure. Rather, we put it here as a future work. It is noted that the examination of the BEOP for a DF relay system is complicated, as it covers the joint of the instantaneous QoS of all the source-relay and relay-destination links. From our experience of analyzing the ABEP, the BEOP is expected to be analyzable with appropriate approximations.

It is also noted that most of the current works on the performance analysis of a DF relay system confine to BPSK modulation. From the general ML detector structure derived in Chapter 4, the performance with higher order modulations can be examined.

7.2.4 Relay Communications with CRC at the Relay

It is known that relay transmissions incorporating error control codes can significantly improve the overall performance. Many current works have assumed the use of CRC at the relay to improve the reliability of the relaying path. A common assumption that has been made in many of these works is that with CRC, the decoding error probability at the relay is zero. However, as it is known, even with CRC and appropriate retransmission schemes, the received packet still suffers from an undetectable error [101]. The probability of the undetectable error is computable and therefore can be used to adjust the weight of the contribution of the relay to the detection at the destination. The undetectable error of CRC has been an overlooked issue in the development of relay communication systems, and needs to be addressed.

7.2.5 Integration of Feedback Power Control and Relay Communications

Another possible extension of our work is the combination of feedback power control and relay communications. This issue needs to be carefully considered as a relay system contains more than one independent transmitting nodes. The power control strategy at the source node highly depends on the availability of the CSI. For example, if all the CSIs of the $s-d$, $s-r$ and $r-d$ links are known to the source node, the source node may employ a comprehensive power control law imposing on all the links. This comprehensive power control law may improve the overall system performance. If only the CSIs of the $s-r$ links are available, the source node has to decide to do power control with respect to which $s-r$ link. Or, it might be better that the source node keeps a constant transmitted power, as it does not know what will happen on the $r-d$ links. The power control at a relay node is also possible. However, it must firstly ensure that the decoded information at the relay is correct. Otherwise, the power control at the relay with respect to the $r-d$ link, would significantly reduce the overall reliability of that relaying path. To that

reason, error control codes are desired to guarantee reliable receptions at the relay. It should also be noted that if the source node chooses to do power control with respect to a certain link, a potential risk is the loss of space diversity. All these issues need to be comprehensively considered for the design of a practical power control strategy for relay communication systems.

Bibliography

[1] T. S. Rappaport, *Wireless Communications: Principles and Practice*, Englewood Cliffs, NJ: Prentice Hall, 1996.

[2] A. J. Goldsmith and P. P. Varaiya, "Capacity of fading channels with channel side information," *IEEE Trans. Inf. Theory*, vol. 43, no. 6, pp. 1986-1992, Nov. 1997.

[3] G. Caire, G. Taricco and E. Biglieri, "Optimum power control over fading channels", *IEEE Trans. on Inf. Theory*, vol. 45, July 1999, pp. 1468-1489.

[4] E. Biglieri, G. Caire and G. Taricco "Limiting performance of block-fading channels with multiple antennas," *IEEE Trans. Inf. Theory*, vol. 47, no. 4, pp. 1273-1289, May 2001.

[5] D. J. Love, R. W. Heath, V. K. N. Lau, D. Gesbert, B. D. Rao and M. Andrews., " An Overview of Limited Feedback in Wireless Communication Systems," *IEEE J. Sel. Areas in Commun.*, vol. 26, no. 8, pp. 1341-1365, Oct. 2008.

[6] J. F. Hayes, "Adaptive feedback communications," *IEEE Trans. Commun. Tech.*, vol. 16, no. 1, pp. 29-34, Feb. 1968.

[7] R. Srinivasan and R. L. Brewster, "Feedback communications in fading channels," *IEEE Trans. Commun.*, vol. 22, no. 1, pp. 93-95, Jan. 1974.

[8] V. O. Hentinen, "Error performance for adaptive transmission on fading channels," *IEEE Trans. Commun.*, vol. 22, no. 9, pp. 1331-1337, Sep. 1974.

[9] R. Srinivasan, "Feedback communications over fading channels," *IEEE Trans. Commun.*, vol. 29, no. 1, pp. 50-57, Jan. 1981.

[10] Y. H. Lee and Y. B-Ness, "Power adaptation for BPSK signalling with average and peak power constraints in Rayleigh fading channels," *IEEE Trans. Commun.*, vol. 51, no. 11, pp. 1871-1876, Nov. 2003.

[11] J. N. Laneman, D. N. C. Tse, and G. W. Wornell, "Cooperative diversity in wireless networks: Efficient protocols and outage behavior" *IEEE Trans. Inf. Theory*, vol. 50, no. 12, pp. 3062-3080, Dec. 2004.

[12] J. G. Proakis, *Digital Communications*, 4th edition, New York: McGraw-Hill, 2001.

[13] M. Wu and P.-Y. Kam, "Instantanesous symbol error outage probability over fading channels with imperfect channel state inforamtion," in *Proc. IEEE VTC 2010-Spring*, pp. 1-5, Taipei, May 2010.

[14] M. Wu and P.-Y. Kam, "ARQ with packet-error-outage-probability QoS measure", in *Proc. IEEE Int. Conf. Commun. (ICC2011)*, Kyoto, Jun. 2011, pp. 1-5. (Best Paper Award)

[15] J. K. Cavers, "An analysis of pilot symbol assisted modulation for Rayleigh fading channels," *IEEE Trans. Veh. Tech.*, vol. 40, pp. 686-693, Nov. 1991.

[16] P. Ligdas and N. Farvardin, "Optimizing the transmit power for slow fading channels," *IEEE Trans. Inf. Theory*, vol. 46, no. 2, pp. 565-576, Mar. 2000.

[17] S. Bahashyam, A. Sabharwal and B. Aazhang, "Feedback gain in multiple antenna systems," *IEEE Trans. Commun.*, vol. 50, no. 5, pp. 785-798, May 2002.

[18] A. Khoshnevis and A. Sabharwal, "On the asymptotic performance of multiple antenna channels with quantized feedback," *IEEE Trans. Wireless Commun.*, vol. 7, no. 10, pp. 3869-3877, Oct. 2008.

[19] S. Ekbatani, F. Etemadi and H. Jafarkhani "Outage behavior of slow fading channels with power control using partial and erroneous CSIT," *IEEE Trans. Inf. Theory*, vol. 56, no. 12, pp. 6097-6102, Dec. 2010.

[20] J. N. Laneman and G. W. Wornell, "Energy-efficient antenna sharing and relaying for wireless networks," in *Proc. IEEE Wireless Communications and Networking Conference (WCNC)*, 2000.

[21] A. Sendonaris, E. Erkip and B. Aazhang, "User cooperation diversity-Part I: System description," *IEEE Trans. Commun.*, vol. 51, no. 11, pp. 1927-1938, Nov. 2003.

[22] A. Sendonaris, E. Erkip and B. Aazhang, "User cooperation diversity-Part II: Implementation aspects and performance analysis," *IEEE Trans. Commun.*, vol. 51, no. 11, pp. 1939-1948, Nov. 2003.

[23] T. Wang, A. Cano, G. B. Giannakis, and J. N. Laneman, "High-performance cooperative demodulation with decode-and-forward relays," *IEEE Trans. Commun.*, vol. 55, no. 7, pp. 1427-1438, Jul. 2007.

[24] M. Ju and I.-M. Kim, "ML performance analysis of the decode-and-forward protocol in cooperative diversity networks," *IEEE Trans. Wireless Commun.*, vol. 8, no. 7, pp. 3855-3867, Jul. 2009.

[25] D. Chen and J. N. Laneman, "Modulation and demodulation for cooperative diversity in wireless systems," *IEEE Trans. Wireless Commun.*, vol. 5, no. 7, pp. 1785-1794, Jul. 2006.

[26] G. V. V. Sharma, V. Ganwani, U. B. Desai and S. N. Merchant, "Performance analysis of maximum likelihood decode and forward cooperative systems in Rayleigh fading" in *Proc. IEEE ICC*, pp. 1-5, 2009.

[27] V. Lau, Y. Liu and T.-A. Chen, "On the Design of MIMO Block-Fading Channels With Feedback-Link Capacity Constraint," *IEEE Trans. Commun.*, vol. 52, no. 1, pp. 62-70, Jan. 2004.

[28] I. Saarinen and A. M*ä*mmel*ä*, "Power Control and Diversity in Feedback Communications Over a Fading Channel" *IEEE Trans. Commun.*, vol. 52, no. 11, pp. 1857-1861, Nov. 2004.

[29] N. Ahmed, M. A. Khojastepour, A. Sabharwal and B. Aazhang, "Outage Minimization With Limited Feedback for the Fading Relay Channel," *IEEE Trans. Commun.*, vol. 54, no. 4, pp. 659-669, Apr. 2006.

[30] T. T. Kim and M. Skoglund, "On the Expected Rate of Slowly Fading Channels With Quantized Side Information," *IEEE Trans. Commun.*, vol. 55, no. 4, pp. 820-829, Apr. 2007.

[31] P. Herhold, E. Zimmermann and G. Fettweis, "A simple cooperative extension to wireless relaying", in *Proc. of Int. Zurich Seminar on Commun.*, Feb. 2004.

[32] A. Bletsas, A.Khisti, D. P. Reed and A. Lippman, "A simple cooperative diversity method based on network path selection", *IEEE J. Sel. Areas in Commun.*, vol. 24, no. 3, pp. 659-672, Mar. 2006.

[33] F. A. Onat, A. Adinoyi, Y. Fan, H. Yanikomeroglu and J. S. Thompson, "Optimum threshold for SNR-based selective digital relaying schemes in cooperative wireless networks," in *Proc. of IEEE WCNC*, 2007.

[34] E. Beres and R. Adve, "Selection cooperation in multi-source cooperative networks," *IEEE Trans. Wireless Commun.*, vol. 7, no. 1, pp. 118-127, 2008.

[35] Z. Yi and I.-M. Kim, "Diversity order analysis of the decode-and-forward cooperative networks with relay selection," *IEEE Trans. Wireless Commun.*, vol. 7, no. 5, pp. 1792-1799, May 2008.

[36] M. M. Fareed and M. Uysal, "On Relay Selection for Decode-and-Forward Relaying," *IEEE Trans. Wireless Commun.*, vol. 8, no. 7, pp. 3341-3346, Jul. 2009.

[37] T. M. Cover and A. A. E. Gamal, "Capacity theorems for relay channel," *IEEE Trans. Inf. Theory*, vol. IT-25, no. 5, pp. 572-584, Sep. 1979.

[38] M. Gastpar, "The Wyner-Ziv problem with multiple sources," *IEEE Trans. Inf. Theory*, vol. 50, no. 11, pp. 2762-2768, Nov. 2004.

[39] G. Kramer, M. Gastpar, and P. Gupta, "Cooperative strategies and capacity theorems for relay networks," *IEEE Trans. Inf. Theory*, vol. 51, no. 9, pp. 3037-3063, Sep. 2005.

[40] A. Høst-Madsen and J. Zhang, "Capacity bounds and power allocation for wireless relay channels," *IEEE Trans. Inf. Theory*, vol. 51, no. 6, pp. 2020-2040, Jun. 2005.

[41] P. Gupta and P. R. Kumar, "Towards an information theory of large networks: An achievable rate region," *IEEE Trans. Inf. Theory*, vol. 49, no. 8, pp. 1877-1894, Aug. 2003.

[42] L. L. Xie and P. R. Kumar, "An achievable rate for multipe-level relay channel," *IEEE Trans. Inf. Theory*, vol. 51, no. 4, pp. 1348-1358, Apr. 2005.

[43] B. Wang, J. Zhang, and A. Høst-Madsen, "On the capacity of MIMO relay channels," *IEEE Trans. Inf. Theory*, vol. 51, no. 1, pp. 29-43, Jan. 2005.

[44] J. N. Laneman and G. W. Wornell, "Distributed space-time coded protocols for exploiting cooperative diversity in wireless networks," *IEEE Trans. Inf. Theory*, vol. 49, no. 10, pp. 2415-2525, Oct. 2003.

[45] G. Scutari and S. Barbarossa, "Distributed space-time coding for regenerative relays networks," *IEEE Trans. Wireless Commun.*, vol. 4, no. 5, pp. 2387-2399, Sep. 2005.

[46] P. A. Anghel, G. Leus, and M. Kaveh, "Distributed space-time cooperative systems with regenerative relays," *IEEE Trans. Wireless Commun.*, vol. 5, no. 11, pp. 3130-3141, Nov. 2006.

[47] Y. Jing and B. Hassibi, "Distributed space-time block coding in wireless relay networks," *IEEE Trans. Wireless Commun.*, vol. 5, no. 12, pp. 3524-3536, Dec. 2006.

[48] M. O. Hasna and M. S. Alouini, "End-to-end preformance of transmission systems with relays over Rayleigh fading channels," *IEEE Trans. Wireless Commun.*, vol. 2, no. 6, pp. 1126-1132, Nov. 2003.

[49] M. K. Simon and M.-S. Alouini, *Digital Communication over Fading Channels*, 2nd edition, John Wiley & Sons, Inc., 2005.

[50] P. A. Anghel and M. Kaveh, "Exact symbol error probability of a cooperative network in a Rayleigh-fading environment," *IEEE Trans. Wireless Commun.*, vol. 3, no. 5, pp. 1416-1421, Sep. 2004.

[51] A. Ribeiro, X. Cai, and G. B. Giannakis, "Symbol error probabilities for general cooperative links," *IEEE Trans. Wireless Commun.*, vol. 4, no. 3, pp. 1264-1273, May. 2005.

[52] P. Liu and I.-M. Kim, "Average BER analysis for binary signallings in decode-and-forward dissimilar cooperative diversity networks", *IEEE Trans. Commun.*, vol. 8, no. 8, pp. 3961-3968, Aug. 2009.

[53] B. M. Hochwald and S. T. Brink, "Achieving near-capacity on a multiple-antenna channel," *IEEE Trans. Commun.*, vol. 51, pp. 389-399, Mar. 2003.

[54] X. Liu and W. Su "BER performance analysis of the optimum ML receiver for decode-and-forward cooperative protocol," in *Proc. IEEE Acoustics, Speech and Signal Process. (ICASSP)*, pp. III-485 - III-488, 2007.

[55] W. Su, "Performance analysis for a suboptimum ML receiver in decode-and-forward communications," in *Proc. IEEE GLOBECOM*, pp. 2962-2966 2007.

[56] G. V. V. Sharma, V. Ganwani, U. B. Desai and S. N. Merchant, "Performance analysis of maximum likelihood detection for decode and forward MIMO relay channels in Rayleigh fading" *IEEE Trans. Wireless Commun.*, vol. 9, no. 9, pp. 2880-2889, Sep. 2010.

[57] A. Jain, G. V. V. Sharma, S. N. Merchant and U. B. Desai, "Exact error analysis for the piecewise linear combiner for decode and forward cooperation with two relays," in *Proc. NCC*, 2011.

[58] J. Gil-Pelaez, "Note on the inversion theorem," Biometrika, vol. 38, pp. 481-482, 1951.

[59] H. Mheidat and M. Uysal, "Non-coherent and mismatched-coherent receivers for distributed STBCs with amplify-and-forward relaying," *IEEE Trans. Wireless Commun.*, vol. 6, no. 11, pp. 4060C4070, Nov. 2007.

[60] C. Patel and G. Stuber, "Channel estimation for amplify and forward relay based cooperation diversity systems," *IEEE Trans. Wireless Commun.*, vol. 6, no. 6, pp. 2348C2356, Jun. 2007.

[61] F. Gao, T. Cui, and A. Nallanathan, "On channel estimation and optimal training design for amplify and forward relay networks," *IEEE Trans. Wireless Commun.*, vol. 7, no. 5, pp. 1907C1916, May 2008.

[62] Y. Wu, and M. Pätzold, "Performance analysis of amplify-and-forward cooperative communication systems with channel estimation errors," in *Proc. IEEE ICCS*, 2008.

[63] S. Han, S. Ahn, E. Oh and D. Hong, "Effect of channel-estimation error on BER performance in cooperative transmission," *IEEE Trans. Veh. Tech.*, vol. 58, no. 4, pp. 2083-2088, May. 2009.

[64] B. Gedik and M. Uysal, "Impact of imperfect channel estimation on the performance of amplify-and-forward relaying," *IEEE Trans. Wireless Commun.*, vol. 8, no. 3, pp. 1468-1479, Mar. 2009.

[65] O. Amin, B. Gedik, and M. Uysal, "Channel estimation for amplify-and-forward relaying: Cascaded against disintegrated estimators," *IET Commun.*, vol. 4, no. 10, pp. 1207C1216, Jul. 2010.

[66] O. Amin, S. S. Ikki and M. Uysal, "On the performance analysis of multirelay cooperative diversity systems with channel estimation errors", *IEEE Trans. Veh. Tech.*, vol. 60, no. 5, pp. 2050-2059, Jun. 2011.

[67] A. S. Ibrahim and K. J. R. Liu, "Mitigating channel estimation error via cooperative communications," in *Proc. IEEE ICC*, 2009.

[68] S. S. Ikki, S. I. A.-Dharrab and M. Uysal, "Exact closed-form error probability expression for cooperative diversity networks with channel estimation errors in time selective Rayleigh fading channels," in *Proc. IEEE ICC*, 2010.

[69] C. Yang, W. Wang, S. Zhao and M. Peng, "Performance of decode-and-forward opportunistic cooperation with channel estimation errors," in *Proc. IEEE PIMRC*, 2010.

[70] S. Haykin, *Adaptive Filter Theory*, Chs. 5-6, 9, 4th edition, Upper Saddle River, N.J.: Prentice Hall, c2002.

[71] B. Widrow and S. D. Stearns, *Adaptive Signal Processing*, Englewood Cliffs, NJ: Prentice-Hall, 1985.

[72] S. C. Douglas and T. H.-Y. Meng, "Normalized data nonlinearities for LMS adaptation," *IEEE Trans. Signal Process.*, vol. 42, issue 6, pp. 1352-1365, Jun. 1994.

[73] J. I. Nagumo and A. Noda, "A learning method for system identification," *IEEE Trans. Autom. Control*, vol. AC-12, pp. 282-287, Jun. 1967.

[74] R. W. Harris, D. M. Chabries, and F. A. Bishop, "A variable step (VS) adaptive filter algorithm," *IEEE Trans. Acoust., Speech and Signal Process.*, vol. ASSP-34, pp. 309-316, Apr. 1986.

[75] V. J. Mathews and Z. Xie, "A stochastic gradient adaptive filter with gradient adaptive step size," *IEEE Trans. Signal Process.*, vol. 41, pp. 2075-2087, Jun. 1993.

[76] R. H. Kwong and E. W. Johnston, "A variable step size LMS algorithm," *IEEE Trans. Signal Process.*, vol. 40, no. 7, pp. 1633-1642, Jul. 1992.

[77] T. Aboulnasr and K. Mayyas, "A robust variable step-size LMS-type algorithm: analysis and simulations," *IEEE Trans. Signal Process.*, vol. 45, issue 3, pp. 631-639, Mar. 1997.

[78] D. I. Pazaitis and A. G. Constantinides, "A novel kurtosis driven variable step-size adaptive algorithm," *IEEE Trans. Signal Process.*, vol. 47, no 3, pp. 864-872, Mar. 1999.

[79] A. I. Sulyman and A. Zerguine "Convergence and steady-state analysis of a variable step-size NLMS algorithm," *Signal Process. EURASIP*, vol. 83, no. 6, pp. 1255-1273, Jun. 2003.

[80] D. P. Mandic, "A generalized normalized gradient descent algorithm," *IEEE Signal Process. Lett.*, vol. 11, no. 2, pp. 115-118, Feb. 2004.

[81] Y. S. Choi, H. C. Shin and W. J. Song, "Robust regularization for normalized LMS algorithms," *IEEE Trans. Circuits and Systems*, vol. 53, no. 8, pp. 627-631, Aug. 2006.

[82] K. Ozeki and T. Umeda, "An adaptive filtering algorithm using an orthogonal projection to an affine subspace and its properties," *Eletron. Commun. Jpn.*, vol. 67-A, no. 5, pp. 19-27, 1984.

[83] B. Hassibi, A. H. Sayed, and T. Kailath, "H^∞ optimality of the LMS algorithm," *IEEE Trans. signal process.*, vol. 44, no. 2, Feb. 1996.

[84] J. E. Greenberg, "Modified LMS algorithms for speech processing with an adaptive noise canceller," *IEEE Trans. Speech and Audio Process.*, vol. 6, no. 4, Jul. 1998.

[85] W. Ang and B. Farhang-Boroujeny, "A new class of gradient adaptive step-szie LMS algorithms", *IEEE Trans. Signal Process.*, vol. 49, no. 4, pp. 805-810, Apr. 2001.

[86] V. Myllylä and G. Schmidt, "Pseudo-optimal regulariztion for affine projection algorithms," in *Proc. IEEE Int. Conf. Accoust., Speech, Signal Process.* (ICASSP'02), Orlando, FL, pp. 1917-1920, May 2002.

[87] A. I. Hanna, I. Yates, and D. P. Mandic, "Analysis of the class of complex-valued error adaptive normalized nonlinear gradient descent algorithms," in *Proc. IEEE Int. Conf. Accoust., Speech, Signal Process.* (ICASSP'03), Hong Kong, Apr. 2003.

[88] S. C. Ng, C. C. Cheung, C. Y. Chung and S. H. Leung, "Variable step-size LMS algorithm using regulated least square error criterion," *IEEE Electronics Lett.*, vol. 39, no. 1, pp. 160-162, Jan. 2003.

[89] S. Zhao, Z. Man and S. Khoo, "Modified LMS and NLMS algorithms with a new variable step size," in *Proc. 9th Int. Conf. Control, Automation, Robotics and Vision.* (ICARCV'06), pp. 1-6, 2006.

[90] J. Benesty, H. Rey, L. R. Vega and S. Tressens, "A nonparametric VSS NLMS algorithm," *IEEE Signal Process. Lett.*, vol. 13, no. 10, Oct. 2006.

[91] L. Cao and P.-Y. Kam, "Goodput-optimal rate adaptation with imperfect channel state information," in *Proc. IEEE VTC*, Fall-2007.

[92] P. Y. Kam, "Optimal detection of digital data over the nonselective Rayleigh fading channel with diversity reception," *IEEE Trans. Commun.*, vol. 39, no. 2, pp. 214-219, Feb. 1991.

[93] P. Y. Kam and C. H. Teh, "Reception of PSK signals over fading channels via quadrature amplitude estimation," *IEEE Trans. Commun.*, vol. 31, no. 8, pp. 1024-1027, Aug. 1983.

[94] I. S. Gradshteyn and I. M. Ryzhik, *Table of Integrals, Series, and Products*, 7th edition, Academic Press, 2007.

[95] Y. Zhu, P.-Y. Kam and Yan. X., "Differential modulation for decode-and-forward multiple relay systems," *IEEE Trans. Commun.*, vol. 58, no. 1, Jan. 2010.

[96] J. P. McGeehan and A. J. Bateman, "Phase locked transparent tone-in-band (TTIB): A new spectrum configuration particularly suited to the transmission of data over SSB mobile radio networks," *IEEE Trans. Commun.*, vol. COM-32, pp. 81-87, Jan. 1984.

[97] P. Y. Kam, K. H. Chua and X. Yu, "Adaptive symbol-by-symbol reception of MPSK on the Gaussian channel with unknown carrier phase characteristics," *IEEE Trans. Commun.*, vol. 46, no. 10, pp. 1275-1279, Oct. 1998.

[98] A. Papoulis, *Probability, Random Variables and Stochastic Processes*, McGraw-Hill, 3rd edition, Feb. 1991.

[99] M. Patzold, U. Killat and F. Laue, "A deterministic digital simulation model for Suzuki Processes with application to a shadowed Rayleigh land mobile radio channel," *IEEE Trans. Veh. Tech.*, vol. 45, no. 2, pp. 318-331, May 1996.

[100] J. K. Cavers, "Variable-rate transmission for Rayleigh fading channels," *IEEE Trans. Commun.*, vol. COM-20, no. 1, pp. 15-22, Feb. 1972.

[101] S. B. Wicker, *Error Control System for Digital Communication and Storage*, 1st edtion, Upper Saddle River, New Jersey: Prentice-Hall, 1995.

List of Publications

1. Peijie Wang and Pooi-Yuen Kam, "Receiver Design and Performance Analysis of DF Relay Communication Systems," to be submitted to *IEEE Trans. Commun.*.

2. Peijie Wang and Pooi-Yuen Kam, "Feedback Power Control for the Rayleigh Channel," submitted to *IEEE Trans. Commun.*, Feb. 2012.

3. Peijie Wang and Pooi-Yuen Kam, "An Automatic Step-Size Adjustment Algorithm for LMS Adaptive Filters, and An Application to Channel Estimation," accepted by *Phy. Commun.*, Apr. 2012.

4. Peijie Wang, Pooi-Yuen Kam and Meng Wah Chia, "A novel automatic step-size adjustment approach in the LMS algorithm," in *Proc. of 1st Intl. Conf. WirelessVitae'09*, pp. 867-871, Aalborg, Denmark, May 2009.

5. [1] Shirazi Ghasem Naddaf, Peijie Wang, Xiangxu Dong, Zhi Ang Eu and Chen-Khong Tham, "A QoS network architecture for multi-hop, multi-sink target tracking WSNs," in *Proc. of 11th IEEE Singapore Intl. Conf. Commun. Systems*, pp.17-21, Singapore, 2008.

6. [1] Mingding Han, Shirazi Ghasem Naddaf, Peijie Wang and Chen-Khong Tham, "Mobile target tracking for healthcare applications: Trade-off between accuracy and energy," in *Proc. of 10th Intl. Conf. e-health Networking, Applications and Services (HealthCom)*, pp. 206-211, 2008.

[1]Papers 5 and 6 are produced from term papers during coursework at NUS.